



**Politecnico  
di Torino**

**POLITECNICO DI TORINO**

**DIPARTIMENTO DI INGEGNERIA MECCANICA E AEROSPAZIALE  
(DIMEAS)**

Master's degree course in Biomedical Engineering

Master's Degree Thesis

**On optimization of an embedded  
ATC-FES system for synergic  
muscles actions execution**

**Supervisors**

Prof. Danilo Demarchi  
Ph.D. Paolo Motto Ros  
M.Sc. Fabio Rossi  
M.Sc. Andrea Mongardi

**Candidate**

Nicolò LANDRA

TORINO, DECEMBER 2021

## Abstract

The Functional Electrical Stimulation (FES) exploits low-energy electrical pulses to retrain, or even restore, the functional mobility in patient affected by neuromuscular disorders. The FES effectiveness can be increased modulating the stimulation delivery using the activation pattern of muscles. The ATC is an event-driven processing technique which can be applied to the Surface ElectroMyoGraphy (sEMG) to estimate the muscle contraction force with a low-power approach, representing an effective solution for controlling the FES therapy.

The aim of this project is the optimization of an embedded ATC-controlled FES system, which was developed using Python programming language. The application of the system relies on two calibration phases: the first calibration determines the maximum ATC value expressed during the muscle contraction, whereas in the second phase stimulation parameters are tuned to induce the execution of functional movements. In the previous version of the system, the two calibrations could not manage more than a single channel at a time and the stimulation profile used for setting FES parameter did not represent the physiological muscle activation. In this project the Profile Extraction algorithm (PE) has been proposed to extend the calibration to functional movements based on the synergic activation of multiple muscles. Specifically, the PE allows the system to extract a multichannel ATC profile from the repetitive execution of a specific movement, representing a statistical information of the voluntary muscle activity. The resulting activation profile can be used to calibrate the maximum ATC value of each channel and to produce a biomimetic stimulation of the patient even during the FES parameters calibration. Moreover, extracted profiles can be stored and used to deliver fully automated FES therapies.

In the first part of the project the PE algorithm has been developed using Python programming language: the processing pipeline receives the sequence of ATC values from each acquisition channel and computes the segmentation of movements in real-time. When the acquisition is terminated, segmented movements undergo the final processing phase, which firstly selects the most correlated movements and secondarily aligns selected data maximizing their correlation. Statistical ATC profiles are eventually extracted for each acquisition channel, performing the median among aligned movements.

In the second part the ATC-controlled FES system is applied to the stimulation of a multichannel functional task, named drinking task. Initially, a feasibility

study has been conducted breaking down the task in the rotation of the glenohumeral joint and the elbow joint, controlled by the contraction of anterior deltoid (AD) and biceps brachii (BB) respectively. An experimental protocol has been designed to validate the multichannel application of the ATC-FES system: eight therapist-patient couples are involved in structured experimental sessions, in which movement trajectories are collected using a motion tracking system. Sessions are performed testing different functional tasks (single channel, multichannel) and stimulation types (biomimetic profile, general pyramidal pattern) delivered during FES calibration. For each couple the validation is performed comparing movement trajectories in different experimental conditions.

# Acknowledgements

Desidero ringraziare Fabio Rossi, Andrea Mongardi ed Andrea Prestia per avermi guidato durante lo svolgimento del progetto di tesi. Rivolgo inoltre i miei ringraziamenti a Danilo Demarchi e Paolo Motto Ros per avermi concesso l'opportunità di lavorare a questa tesi. Infine, desidero dedicare questa tesi alla mia famiglia e a Irene, a cui sono grato per essermi stati accanto, supportandomi nei momenti di difficoltà.

# Contents

<b>List of Figures</b>	VI
<b>1 Introduction</b>	1
1.1 Skeletal Muscle	1
1.1.1 Muscle architecture	2
1.1.2 Nervous stimulation and contraction mechanism	5
1.1.3 Contraction types	6
1.1.4 Muscle force generation	7
1.1.5 Fiber types	8
1.2 Surface electromyography (sEMG)	10
1.2.1 Signal properties	11
1.2.2 Electrodes	11
1.2.3 Noise sources	13
1.2.4 Signal acquisition and conditioning	14
1.2.5 Features extraction	16
1.3 Average Threshold Crossing	20
1.4 Functional Electrical Stimulation	22
1.4.1 Technology	22
1.4.2 Stimulation parameters	24
1.4.3 FES Intensity Calibration	25
1.4.4 Muscle fatigue	25
<b>2 State of Art</b>	27
2.1 sEMG wearable acquisition systems	27
2.2 ATC technique	30
2.3 FES control strategies based on sEMG	34
2.4 ATC-FES System description	36
2.4.1 Wearable acquisition device	36
2.4.2 Control platform	38
2.4.3 Electrical stimulator	40
2.4.4 FES Calibration	43

<b>3</b>	<b>Profile extraction algorithm</b>	45
3.1	Processing pipeline . . . . .	46
3.1.1	Smoothing . . . . .	46
3.1.2	Movements Segmentation . . . . .	49
3.1.3	Irregular Movements Detection (IMD) . . . . .	51
3.1.4	Movements alignment and Profile extraction . . . . .	56
3.2	Algorithm development and system integration . . . . .	59
3.2.1	<i>ProfileGenerator</i> . . . . .	59
3.2.2	<i>MovementSegmentation</i> . . . . .	61
3.3	Preliminary tests . . . . .	63
<b>4</b>	<b>Multichannel ATC-FES: Calibration validation</b>	67
4.1	Materials . . . . .	68
4.2	Methods . . . . .	69
4.3	Results . . . . .	71
<b>5</b>	<b>Conclusion</b>	77
	<b>Bibliography</b>	79

# List of Figures

1.1	Skeletal Muscle . . . . .	1
1.2	Muscle architecture . . . . .	2
1.3	The Muscle fiber . . . . .	3
1.4	The sarcomere . . . . .	5
1.5	The contraction mechanism . . . . .	6
1.6	Muscle contraction types . . . . .	7
1.7	Twitch summation . . . . .	7
1.8	Fibers recruitment strategy . . . . .	8
1.9	Surface EMG signal . . . . .	10
1.10	MUAPS summation . . . . .	11
1.11	Surface electrode model . . . . .	12
1.12	EMG acquisition configurations . . . . .	15
1.13	Instrumentation Amplifier circuit . . . . .	16
1.14	Muscle fatigue effect on frequency spectrum and signal amplitude . . . . .	19
1.15	Average Threshold Crossing . . . . .	20
1.16	FES principle . . . . .	23
2.1	State of the Art wireless sEMG acquisition devices . . . . .	28
2.2	ATC-based force estimation . . . . .	30
2.3	ATC-Force correlation in different noise conditions . . . . .	31
2.5	Schematic diagram of an EMG-FES system . . . . .	35
2.6	Wireless ATC acquisition device . . . . .	36
2.7	Analog Front-End digram . . . . .	37
2.8	RehaStim2 electrical stimulator . . . . .	41
2.9	Biphasic current pulse . . . . .	41
2.10	Continuous Channel List Mode . . . . .	43
2.11	FES Calibration . . . . .	44
3.1	Profile Extraction Pipeline . . . . .	46
3.2	ATC smoothing . . . . .	47
3.3	ATC smoothing example . . . . .	48
3.4	Acquisition channel activation . . . . .	49

3.5	Movements Segmentation . . . . .	50
3.6	Movements Segmentation example . . . . .	51
3.7	Irregular Movements Detection . . . . .	51
3.8	Movements pairing . . . . .	52
3.9	Channels Cross-Correlation . . . . .	53
3.10	Average correlation . . . . .	54
3.11	Correlation and Displacement matrices . . . . .	55
3.12	IMD example . . . . .	56
3.13	Movements Alignment . . . . .	57
3.14	Movements Alignment and Profile Extraction . . . . .	58
3.15	Profile Extraction: Python objects . . . . .	62
3.16	g.HIAMP: high performance biosignal amplifier . . . . .	63
3.17	Preliminary tests: sEMG Electrodes placement configurations . . . . .	64
3.18	Profile Extraction validation: Segmentation Lags . . . . .	65
3.19	Profile Extraction validation: Median Correlations . . . . .	66
3.20	Profile Extraction validation: Movements Difference . . . . .	66
4.1	Multichannel task: <i>Drinking</i> . . . . .	68
4.2	Validation setup: Electrodes placement . . . . .	69
4.3	Elbow Flexion angle: Multichannel task . . . . .	72
4.4	Elbow vertical elevation: Multichannel task . . . . .	72
4.5	Similarity analysis boxplots: Multichannel task . . . . .	73
4.6	Movement delays boxplots: Multichannel task . . . . .	74
4.7	Single channel boxplots: Analysis of the similarity and delays . . . . .	75

# Chapter 1

## Introduction

### 1.1 Skeletal Muscle

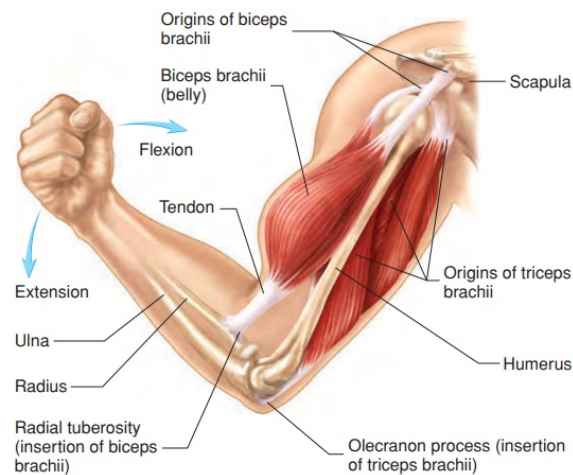


Figure 1.1: The skeletal muscle connects different bone segments, enabling body movements. The joint rotation results from the competitive action of agonist and antagonist muscles [4].

The muscle is an composed of contractile tissue, which can shorten after nervous stimulation converting chemical energy into mechanical work. Muscles are organized into the muscular system responsible for many essential physiological functions, such as voluntary movements, posture maintenance, blood circulations, digestion, and breathing control. Skeletal muscle is a class of muscles that connects bone segments and is voluntarily controlled, allowing body movements. Skeletal muscle also plays a crucial role in human metabolism, storing essential substrates such as amino acids and carbohydrates [29]. Skeletal muscle can connect two bone

segments crossing one or two joints. In the former case, muscle is called mono-articular, whereas it is bi-articular if it crosses two joints connecting separated bones.

Complex movements are often performed by the synergic activation of different muscle groups, which work together, maximizing the action efficiency. Inside groups, each muscle can be classified according to its function: Agonist muscles, also known as primary movers, works to produce joint motion, whereas antagonists are located on the opposite side of the joint and contrast agonist action. Besides these two main classes, other muscles assist the movement execution: Among them, synergists sustain the agonist action, guiding the movement, stabilizers fix the agonist muscle origin, and neutralizers limit the action of other muscles preventing undesired motions.

### 1.1.1 Muscle architecture

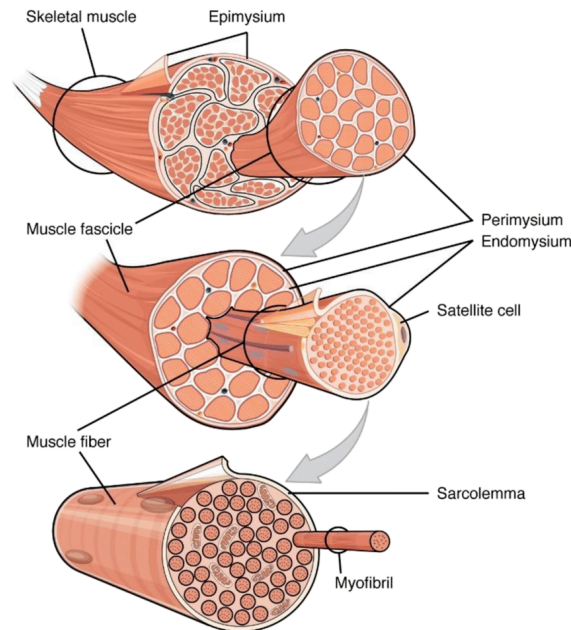


Figure 1.2: The skeletal muscle architecture [77].

Skeletal muscle consists of a contractile body, called muscle belly, attached to different bone segments by fibrous connective structures, called tendons. The proximal attachment point is called origin, and it is often the less movable, whereas the distal one is called insertion, and it transmits the force from the muscle to the bone producing the joint movement. As shown in the figure 1.2, the muscle belly consists of a fibrous structure with multiple levels of organization: the skeletal muscle is firstly surrounded by an outer layer of connective tissue called epimysium. Within the outer layer of connective tissue, muscle fibers are grouped

in bundles and surrounded by a further layer of connective tissue called perimysium. The muscle fiber is also known as myocyte and is a multinucleated tubular cell with approximate dimensions of 100  $\mu\text{m}$  in diameter and 1 cm in length [29]. Thanks to its multinuclear structure, the myocyte can diversify protein expression across different regions of the cell [29]. The myocyte consists of a cellular membrane called sarcolemma, which surrounds the intracellular environment, including many organelles, such as the transverse tubular system (T tubule), the sarcoplasmic reticulum, mitochondrial network, and a bundle of myofibrils. Myofibril is a rod-like organelle that consists of the repetition of the fundamental contractile unit of skeletal muscles called sarcomere.

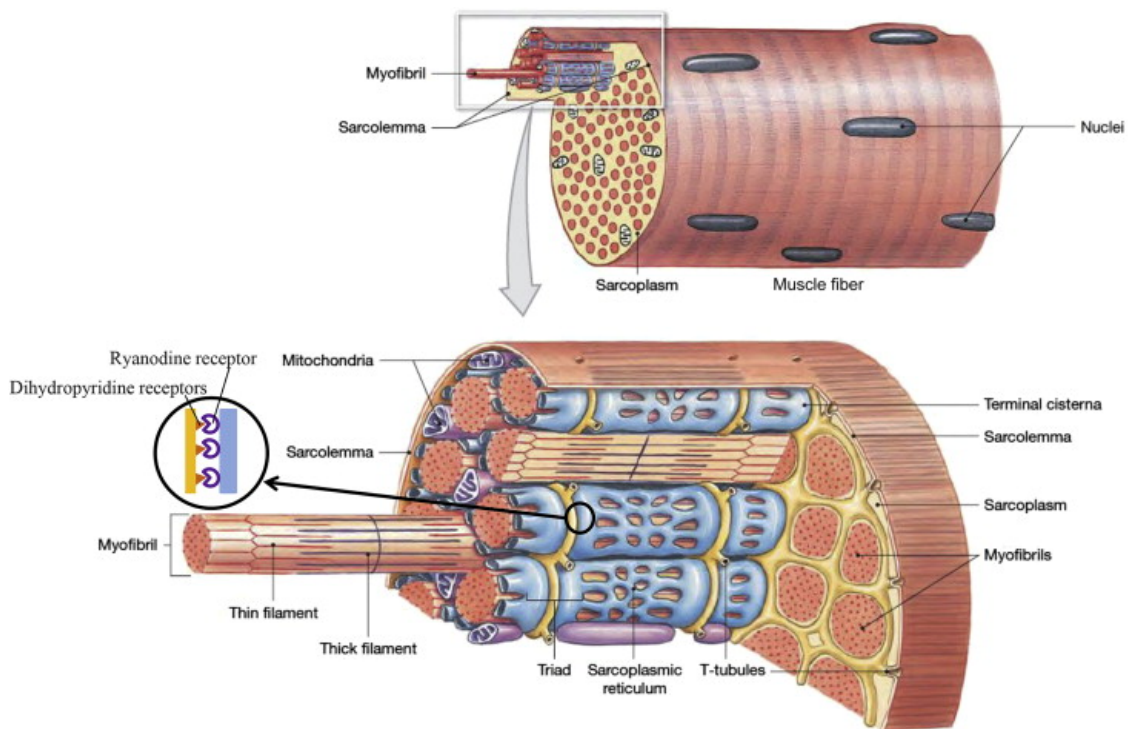


Figure 1.3: The internal structure of a muscle fiber [48].

The sarcomere consists of the combination of two types of protein-based filaments organized in a multiple bands structure (Figure 1.4): The sarcomere is delimited by two external I-bands, where each one is composed of thin actin filaments, anchored to a high protein density disk, called Z-disk or Z-line. The A-band is located in the middle region of the sarcomere and is mainly composed of thick myosin filaments bound to a protein structure called M-line. The two filament types are aligned and partially overlapped, interacting and producing the structure contraction: The thin actin filaments disposed in a hexagonal arrangement surround a bundle of myosin stalks, which forms the thick filament.

The thin filament consists of a central F-actin strand formed from the polymerization of G-actin monomers around a structural protein called nebulin [30]. Actin monomers exhibit the binding site for the actin-myosin interactions, giving structural and functional polarity to the thin filament and orienting the direction of the contractile force. A secondary filamentous structure formed by the head-to-tail polymerization of coiled-coil dimers of tropomyosin (Tm) runs helically along the actin filament [30]. The troponin (Tn) is a protein complex made up of three individual subunits, and it is bound to each Tm molecule. The Tm-Tn complex is sensitive to the presence of  $\text{Ca}^{2+}$  ions, which induce a morphological rearrangement of the complex along the actin filament. At low  $\text{Ca}^{2+}$  concentrations, the Tm filament physically blocks the myosin-binding sites, whereas higher concentrations of  $\text{Ca}^{2+}$  produce a cascade of allosteric changes within the Tn-Tm complex, resulting in the active sites exposition [30].

The thick filament comprises myosin-II molecules, which are hexameric proteins consisting of four light chains and two heavy chains (MHC). Each MHC consists of two main parts: the globular head and the long coiled-coil tail connected via the hinge region. The Coiled-coil tail region has an  $\alpha$ -helical structure 1500 Å long and 20 Å in diameter and polymerizes with the other chains forming the thick filament [70]. The globular head regions protrude from the thick filament at regular intervals and contain an ATPase site and an actin-binding site allowing the interaction with actin to form cross-bridges [30]. The orientation of MHC molecules is crucial for directing force toward the center of the sarcomere during a contraction: The globular heads are oriented toward the Z-line, while the coiled-coil tails are directed toward the M-line [30].

Each thick filament is also connected to the Z-disk via an elastic element made of titin, which improves filament stabilization [44]. Inside the sarcomere titin elements are passive force generators, whereas the myosin motors along the thick filament behave as active force generators [44].

The sarcolemma presents many surface invaginations which connect the extracellular environment to the interior of the cell. Such connections are called T-tubules and are responsible for the conduction of the nervous excitation throughout the myocyte. The sarcoplasmic reticulum surrounds myofibril chains and controls calcium homeostasis, which plays a fundamental role in the contraction mechanism. The ends of the sarcoplasmic reticulum, called terminal cisternae, store calcium ions and are in close contact with the T tubule system. Mitochondria are arranged in a three-dimensional network and are responsible for the aerobic production of adenosine triphosphate (ATP). The number and the size of mitochondria can be both increased with proper training programs based on aerobic exercises [29].

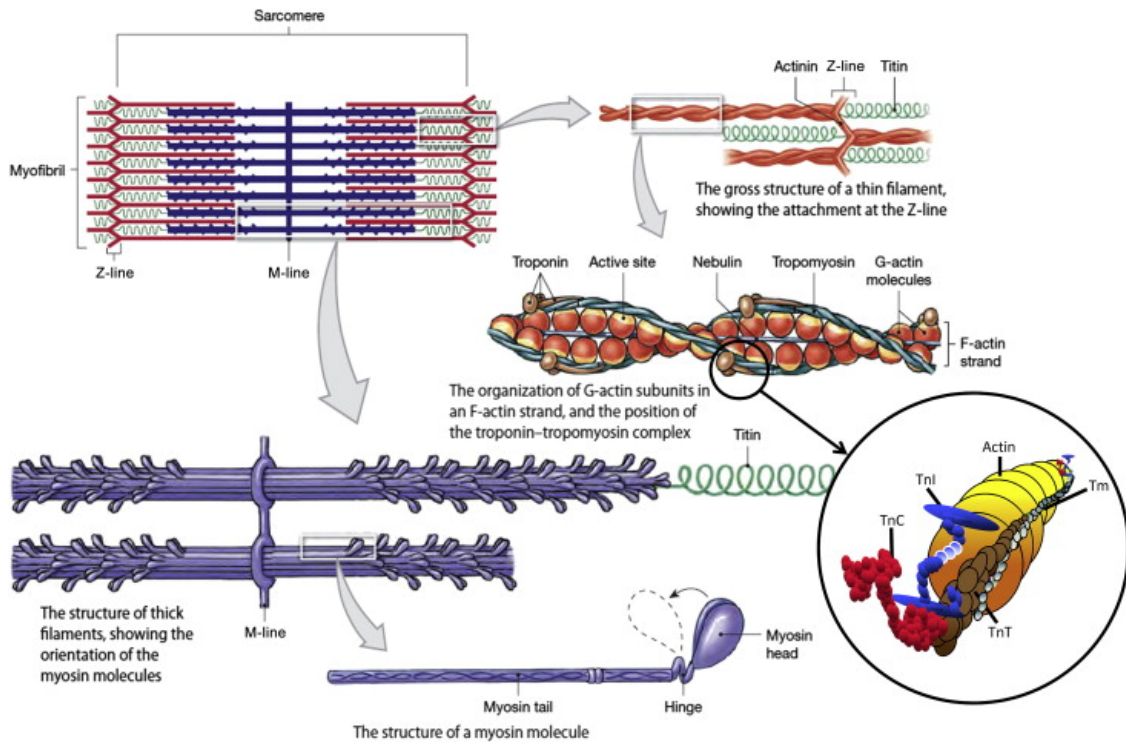


Figure 1.4: The sarcomere [30].

### 1.1.2 Nervous stimulation and contraction mechanism

Skeletal muscle contraction is a complex mechanism carried out by myocytes and results in mechanical force generation. The muscle action starts in the brain motor cortex, where the voluntary movement is elaborated and coded into action potential (AP) trains delivered from the brain to the target muscle through efferent neurons, called motor neurons. The dendrites of the inferior motor neuron are connected to a group of myocytes through specific chemical synapses called neuromuscular junctions, forming the motor unit. At the neuromuscular junction, the acetylcholine neurotransmitter is released into the motor plate by the motor neuron [15]. Then, it starts the AP in muscle fibres causing the membrane depolarization from the resting transmembrane potential of about  $-85$  mV to reach values of up to  $100$  mV [15]. The AP propagates along the sarcolemma and transversally inside the cell body along the T-tubules system. When the nervous signal reaches specific T-tubules dihydropyridine receptors, it induces their allosteric interaction with the neighboring sarcoplasmic reticulum (SR) ryanodine receptors. After receptors activation, the SR releases  $\text{Ca}^{2+}$  ions from the terminal cisternae into the sarcoplasm. The resting cytoplasmatic concentration of  $\text{Ca}^{2+}$  ions increases from  $100$  nM up to  $20$   $\mu\text{M}$ , with a release rate over  $200$   $\mu\text{moles/ms}$  in fast-twitch mammalian fibres [15]. The  $\text{Ca}^{2+}$  ions bind to troponin, triggering the Tm-Tn complex structural modification and

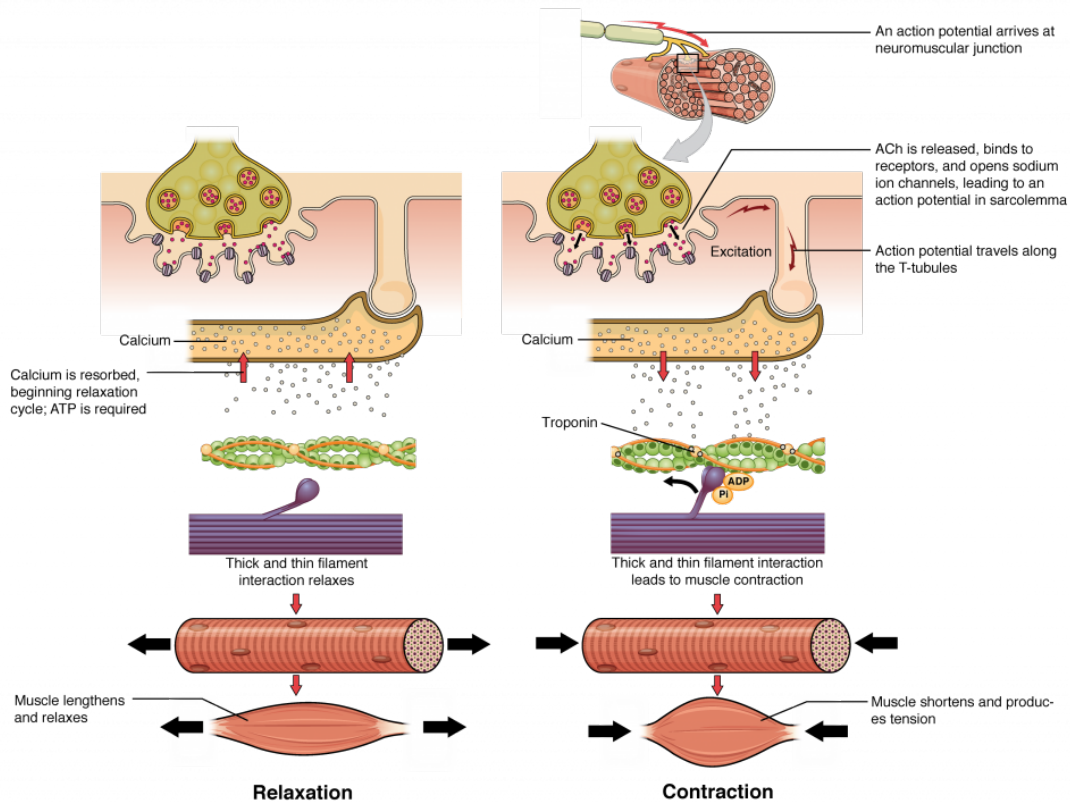


Figure 1.5: The skeletal muscle contraction mechanism [7].

the thin filament activation. Myosin heads of the thick filaments can now interact with the F-actin filaments forming the cross-bridge bindings. ATP molecules in the sarcoplasm interact with myosin heads, and their hydrolysis releases energy and induces the structural rotation of myosin heads, producing the thick filaments sliding over thin filaments and generating tension in the sarcomere structure. The  $\text{Ca}^{2+}$  is constantly taken back to the SR buffered by soluble cytoplasmic proteins with a removal rate of  $50 \mu\text{moles/ms}$  [15]. This process is energy-consuming, requiring ATP molecules, and prevents the formation of new actin-myosin bonds in the absence of neuronal stimulations [42]. A single contraction cycle followed by relaxation is called twitch [42].

### 1.1.3 Contraction types

The muscle contractions can be classified according to the movement induced: The contraction is defined as isometric or static when the muscle tension generates no action. In this case, the muscle tension equals the resistive force, which can be external or internally produced by antagonist muscles. The muscle contraction is isotonic when it produces a joint movement and occurs when the muscle generates a

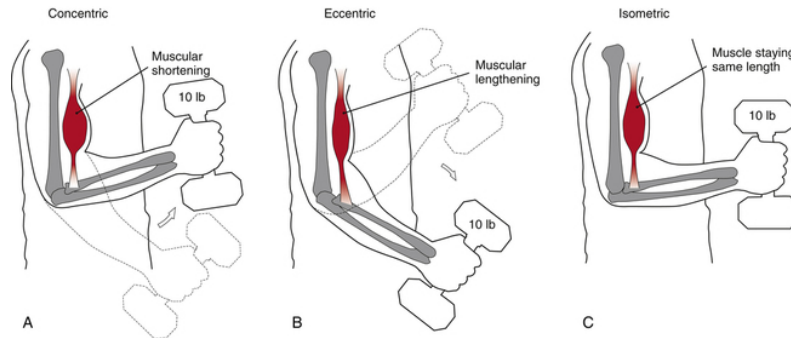


Figure 1.6: Muscle contraction types [46].

force level different from the resistance, and it can be either concentric or eccentric. In the former case, the isotonic contraction develops tension, overcoming resistance and producing muscle shortening and positive work on the joint. On the other hand, the contraction is considered eccentric when the tension is lower than the resistance, resulting in a controlled movement towards the resistive force direction. During the eccentric contraction, the muscle lengthens although it develops tension, performing a negative work. The eccentric contraction has gained a growing interest in rehabilitation for its physiological properties: This contraction type can generate greater forces activating less motor unit and consuming less oxygen and energy than concentric contractions [36].

### 1.1.4 Muscle force generation

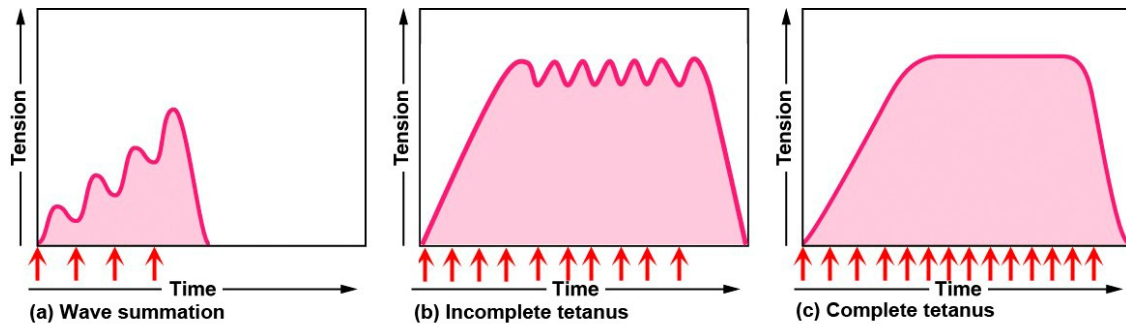


Figure 1.7: The temporal summation of consecutive twitch events produces an increase of the contraction force [8].

The muscle force results from different regulation mechanisms, which range from the control of a single myocyte’s force level to the recruitment of motor units. The stimulation frequency represents a key mechanism in the muscle force generation [42]. Since the duration of a single twitch is higher than the AP period, it is possible to induce new  $\text{Ca}^{2+}$  releases before the intracellular concentration reaches

the resting value. AP trains with time intervals lower than  $1/3$  of twitch periods produce a cumulative increase of the  $\text{Ca}^{2+}$  concentration until it reaches a plateau in which no more  $\text{Ca}^{2+}$  ions can be released from the SR [42]. In these conditions, the myocytes produce a tetanic contraction. After stimulation cessation, the  $\text{Ca}^{2+}$  concentration is taken back to the resting value, thanks to the ATP molecules consuming [42]. Besides the APs temporal summation, the selective recruitment of MU represents a fundamental mechanism for controlling force levels during delicate movements [42]. Motor units generally differ for the number of controlled muscle fibers, typically ranging from few myocytes in motor units responsible for the execution of precision movements to thousands of elements in units that must deal with high efforts. The recruitment of different MUs is both sequential, and additive [42]. When a movement starts requiring precise fine-tuning, smaller units are generally recruited first. The largest units are recruited last as the requirement for force increases. For providing even force distribution inside the muscle during the whole movement execution, fibers of individual MUs are evenly distributed within the muscle [42].

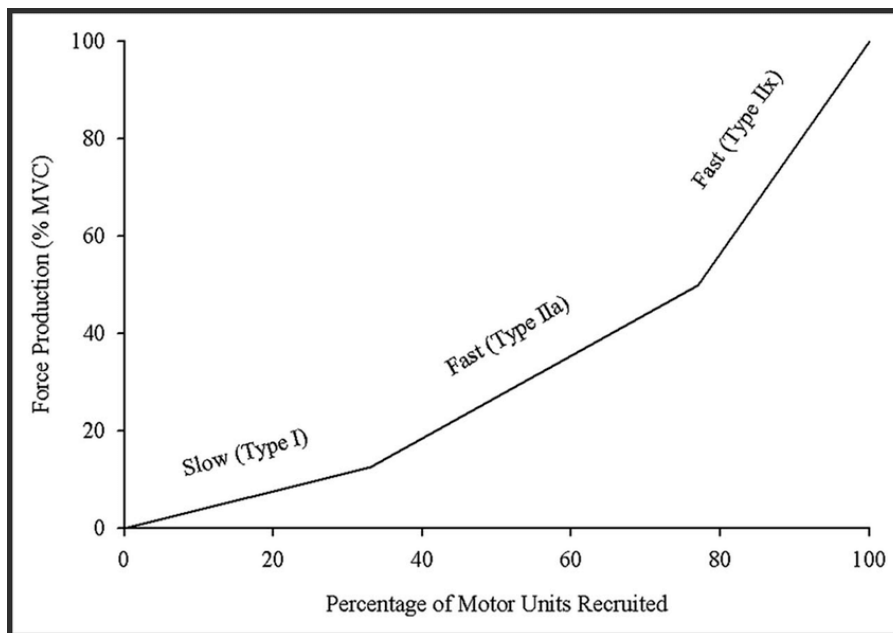


Figure 1.8: The muscle fibers recruitment strategy [31].

### 1.1.5 Fiber types

The skeletal muscle structure consists of a heterogenic composition of fiber types to adapt to different activities, demanding specific mechanical and metabolic performances. Fibers can be distinguished according to their contractile and metabolic

properties [51]. The contraction speed of a muscle fiber is mainly related to its protein expression, such as differences in the myosin heavy chain structure [51] and SR development [29]. Muscle fibers can be classified as fast-twitch or slow-twitch fibers, according to the contractile speed. The metabolic pathway of the muscle fiber characterizes its tolerance to fatigue and the energy production rate. Muscle fibers with high mitochondrial content and well-vascularized can use oxidative metabolism, exhibiting a lower fatigability and a reduced ability to quickly satisfy high energy demand. On the other hand, Muscle fibers can follow the glycolytic pathway to produce ATP molecules, increasing the energy production rate but lowering the tolerance to fatigue due to the lactic acid production [29]. According to the previous properties, muscles can include three fiber types in proportions that reflect their typical usage: Type I fibers have a slow contractile response but are less susceptible to fatigue, rely on aerobic metabolism, and are predominant in muscles that must perform long-lasting activities. Type IIA fibers produce fast contractions with intermediate resistance to fatigue since their metabolism results from the overlap between aerobic and anaerobic pathways. Type IIB fibers produce fast contractions demanding rapid energy supplies. They are subjected to rapid fatigability and are suited for activities that involve explosive efforts.

## 1.2 Surface electromyography (sEMG)

Electromyography (EMG) is an instrumental technique for measuring muscle activity, recording the electric signal generated during contractions. The resulting time-dependent bio-signal is called electromyogram and provides information about neuromuscular system properties, such as the force level developed during a contraction [24], and the muscular fatigue state [18]. The EMG signal can be recorded by either inserting needle electrodes inside the muscle or placing a set of surface electrodes externally on the skin, close to the target muscle. The former methodology is known as intramuscular EMG and allows to perform high precision recordings, focusing on small muscle regions and reducing external interferences. On the other hand, the needle insertion results uncomfortable for the patient, and for this reason, this technique is limited to the evaluation of peripheral neuromuscular disorders [20]. The latter methodology is known as surface electromyography (sEMG), and it is widely used in many application fields, thanks to its non-invasive approach, such as rehabilitation medicine, ergonomics, sports medicine, physiotherapy, neurophysiology, and kinesiology [53]. One of the main drawbacks of the sEMG recording is the low spatial selectivity and the source location uncertainty inside the detection volume [53].

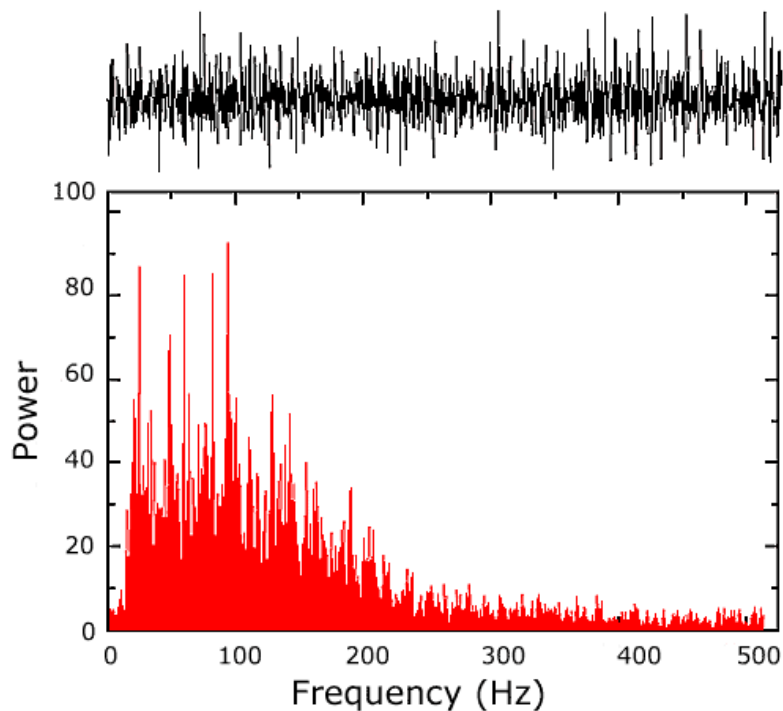


Figure 1.9: sEMG signal detected from the Tibialis Anterior during an isometric contraction and the respective Power Spectral Density (PSD) function [21].

### 1.2.1 Signal properties

Each muscle consists of multiple motor units, which are selectively stimulated through motor unit action potentials (MUAPs). MUAPs reaches the neuromuscular junction of each myocyte, eliciting the membrane depolarization, which propagates in opposite directions until it reaches the muscle fiber endings [68]. The membrane depolarization induces potential changes in the extracellular environment, which can be detected employing invasive or external electrodes[68]. The EMG signal is the result of the algebraic summation of these electrical events (Figure 1.10), which can be constructive or destructive because depolarization waves can be bi-phasic or tri-phasic [68]. Since the MU firing rate is a random process, with a low level of synchronization, the EMG signal appears as a Gaussian stochastic process [21], with significant variability in the signal morphology and less proportionality between the signal amplitude and the number of firing MUs [68]. The sEMG signal has a peak-to-peak amplitude which can range from 0 to 10 mV, and a frequency bandwidth that typically spans from 0 to 500 Hz (Figure 1.9), with a high energy content in the 50-150 Hz range [21].

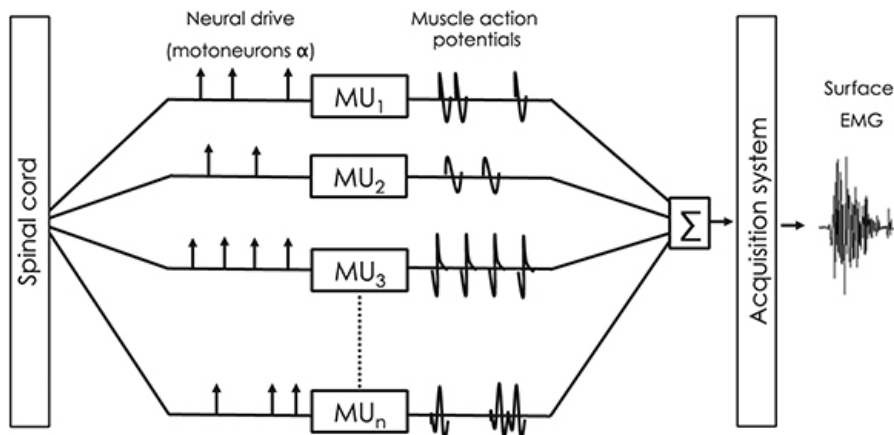


Figure 1.10: The EMG signal is the result of the algebraic summation of MUAPS trains [47].

### 1.2.2 Electrodes

Electrodes for biopotentials are electrochemical transducers that convert ions currents, generated by electrophysiological events inside the tissue, into the electric current conducted by metal wires and measured using proper instrumentations [53].

Electrodes are generally organized in a multilayer architecture, composed of a series of metal plates and an electrolytic layer, which is in contact with the biological tissue. The electrolyte exchanges ions with the tissue and produces redox reactions at the interface with the metal. Ions and charges produced by the redox reactions

may form a double layer distribution, polarizing the interface and generating a DC offset voltage, called half-cell potential. Generated electrons can be conveyed through a metal wire connected to the conductive plate.

The electrode-skin interface can be modeled by a non-linear RC circuit organized in the series of two impedances (Figure 1.11), which represent the electrode-electrolyte interface and electrolyte-skin interface [53]: the metal-electrolyte interface is represented by an RC parallel, which takes into account the polarizability and the capacitive behavior of the junction, in series to a DC voltage generator and a resistor, which model the half-cell potential and the electrolyte gel respectively. A similar model describes the electrolyte-skin interface with the respective half-cell potential and interface impedance. The global impedance depends on many operation parameters, such as the electrode size and materials, the electrolyte composition, and the skin properties, and range from a few  $k\Omega$  to  $M\Omega$  [53]. The previous electrode features are generally variable in time, involving significant variations of model impedances during long term recordings.

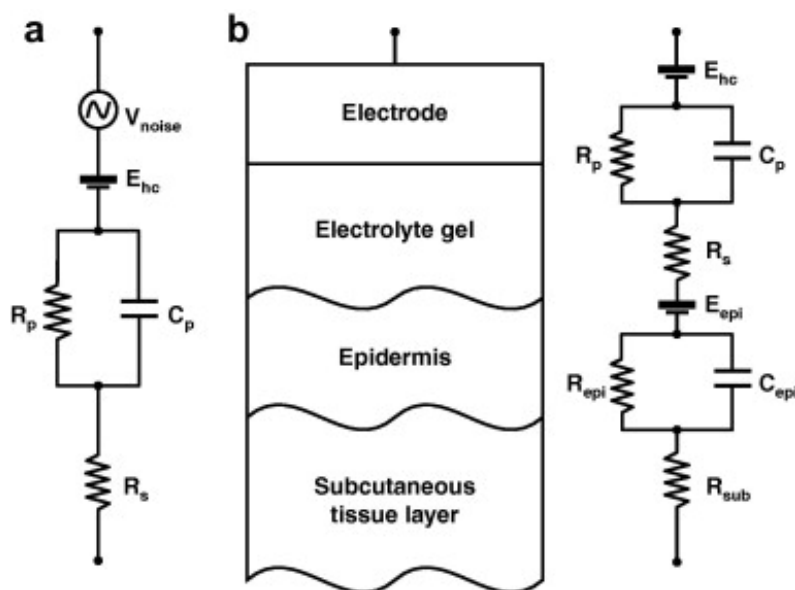


Figure 1.11: Electrical model of the electrode-skin interface [53]

Electrodes used for sEMG applications can be classified in dry and wet electrodes, according to their building materials and manufacturing technologies [53]:

- Dry electrodes are composed only by the conductive layer, which directly contacts the skin, exploiting the sweated skin as an electrolytic layer. For this class of electrodes, manufacturing materials include noble metals, carbon, sintered silver, and silver chloride.
- Wet electrodes consist of a metal component in contact with a soft layer,

saturated with an electrolyte solution. This type of electrode often exhibits an adhesive surface which increases the application stability and allows to perform sEMG recordings in dynamic conditions.

A further classification criterion is represented by the electrochemical behavior, which distinguishes electrodes in polarizable and non-polarizable [53]:

- The polarizable electrode exhibits primarily a capacitive nature producing a double charges layer distribution at the metal-electrolyte interface and limiting the current transmission. These electrodes have higher half-cell potentials and are particularly susceptible to motion artifacts since the electrode movement produces a perturbation in the charges distribution.
- The non-polarizable electrode exhibits mainly an ohmic behavior, producing a direct ionic current at the interface between the electrode and tissue in the presence of an applied voltage. This latter type is currently preferred for sEMG applications, mainly the Ag–AgCl electrode is highly stable and exhibits a lower noise level at the metal-gel junction with respect to other metallic electrodes [53].

### 1.2.3 Noise sources

Multiple noise sources can alter the surface EMG signal, which affects the signal information content and leads to misinterpretation. Using filtering techniques, proper electronic design, and electrode configurations can generally reduce signal contamination, preserving its informative content.

- **Electrode noise:** Part of the noise that alters the EMG signal is due to the electrodes in which charge exchanges occur at the metal-electrolyte interface. The electrode noise intensity is frequency-dependent, and it becomes more relevant than the resistive thermal noise at frequencies lower than 100 Hz. Ag–AgCl electrodes are typically recommended for sEMG recordings due to their low noise interface. In addition, a proper skin preparation, consisting of a slight skin abrasion, is recommended for decreasing both the noise and the impedance values. [53]
- **Movement artifact:** Performing sEMG recordings in dynamic conditions implies the movement of electrodes and their connection cables. The relative movement of the metal part of the electrode over the electrolyte solution or the skin can induce a change in the surface potential, producing motion artifacts [53]. The resulting time-varying voltage produced across the two electrodes has a frequency interval that can overlap with the low part of the EMG frequency spectrum [22], ranging from 1 Hz to 10 Hz [17]. While the Cable motion artifact can be almost eliminated by exploiting modern electronic

technologies and performing an appropriate circuit design [22], the movement artifact influence is reduced processing the signal with a Butterworth high-pass filter with a corner frequency of 20 Hz and a slope of 12 dB/oct. This technique offers the best compromise between noise rejection and information content preserving in general uses [22].

- **Muscle crosstalk:** The sEMG technique allows to record the electrical signal generated by muscle fibers inside a detection volume, and their position can be far from recording electrodes[27]. When the detection volume includes different muscles that are close to each other, the sEMG signals can be attributed to non-active muscle, whereas it is produced by a neighboring muscle [27]. This phenomenon, which produces misinterpretation of muscle activity, is known as crosstalk and can be limited using small-sized electrodes[21] and reducing the inter-electrodes distance[27].
- **ECG contamination:** The cardiac activity can interfere with the sEMG recording, especially when investigated muscles are located in the body trunk. This signal alteration is prominent in muscle activity performed in static conditions or below the 25% of maximum voluntary contraction. Since the ECG and sEMG frequency spectra are partially overlapped, it is difficult to filter out the ECG artifact from EMG recordings. [17]
- **External electromagnetic interference:** The human body is constantly surrounded by external electromagnetic fields, which can be transmitted through the body tissues affecting bio-signal recordings. The amplitude of electromagnetic noise can be one to three times greater than the EMG signal [17]. The most relevant electromagnetic interference is produced by power sources, which can interact with the human body through parasitic capacitances. The resulting electromagnetic noise has a constant frequency, either 50 Hz in Europe or 60 Hz in the USA. The power-line interference can be reduced by applying selective filtering techniques, such as the notch filter[17], and properly designing the front-end stage of the recording device in order to increase the common-mode rejection [53].

#### 1.2.4 Signal acquisition and conditioning

The electrodes unit enables the EMG signal acquisition, representing a critical aspect that influences the signal fidelity and the subsequent processing stage [21]. Different electrodes configurations can be employed in order to provide minimal signal distortion and maximal noise suppression:

- The monopolar configuration represents the ideal condition in which a single electrode is placed on the skin close to the signal source, while a reference electrode is located as far as possible on a neutral area. This configuration

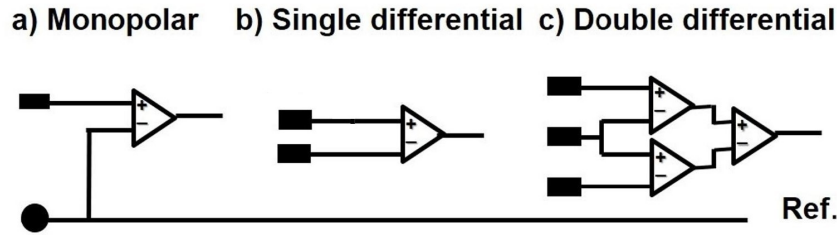


Figure 1.12: Three different configurations of the sEMG acquisition stage [52]

allows collecting the entire information from the detection volume, which may be affected by the background noise. [53]

- The single differential configuration (SD) allows increasing the signal-to-noise ratio removing the common-mode noise influence. The resulting signal is the difference between potentials detected from two different detection sites at a fixed distance along the muscle fiber direction [53]. However, in practice, it is difficult to perform a complete common-mode suppression. Therefore the performance of the differential circuit is determined by the common-mode rejection ratio (CMRR), which is expressed in dB and compares the differential signal amplitude with the residual common-mode noise.
- The double differential configuration (DD) is constituted by a series of three equally spaced electrodes positioned along the longitudinal axis of the muscle [53]. The resulting signal is the difference between two SD signals acquired from two electrodes referred to the middle one. This configuration appertains to the main class of spatial filters, which allow limiting the detection volume, enhancing the spatial selectivity of surface recordings [53]. The enhanced selectivity can be exploited for detecting potential propagations and estimating the muscle fiber conduction velocity (CV) [53]. Moreover, the DD configuration increases the common-mode rejection.

The signal recorded by the electrode unit must be processed in order to amplify the information content and to reduce the signal corruption:

The input stage of sEMG amplifiers is represented by the instrumentation amplifier (IA) (Figure 1.13), which performs the difference between two floating signals, maximizing the CMRR and providing a single-ended signal referred to the reference ground [53]. A CMRR of 90 dB is generally sufficient to suppress extraneous electrical noises [21]. Operational amplifiers in voltage follower configuration may be interposed between the electrodes and the IA in order to increase the input impedance and to reduce the coupling of interfering sources to the EMG wires [53]. Additionally, the common-mode interference can be reduced by exploiting the driven right leg (DRL) circuit: this system is based on a negative feedback circuit

that detects the common-mode voltage and applies it back to the subject after amplification and phase reversal [53].

The conditioning of the signal can be performed either by hardware or digitally. The first method requires the integration of different analogical filters in the amplification chain: An high-pass filter should be implemented in the first stage to remove low-frequency interferences due to movements artifacts and instability of the electrodes contacts [53]. A low-pass filter is placed at the end of the amplification chain to remove the high-frequency noise introduced by all the electronic components and prevent the aliasing occurrence [53]. The offset introduced by the cascaded amplification stages can be removed by placing additional high-pass filters along the processing chain [53].

In the second conditioning, method components are reduced to a low gain amplifier and a low-pass filter before the sampling process. The high-pass filter can be avoided if the A/D converter resolution is large enough. The low-frequency components are removed via digital online filtering.

For both the processing methods, the recommended 3 dB cut-off frequency is 10–20 Hz for the high-pass filter and 400–450 Hz for the low-pass filter [53].

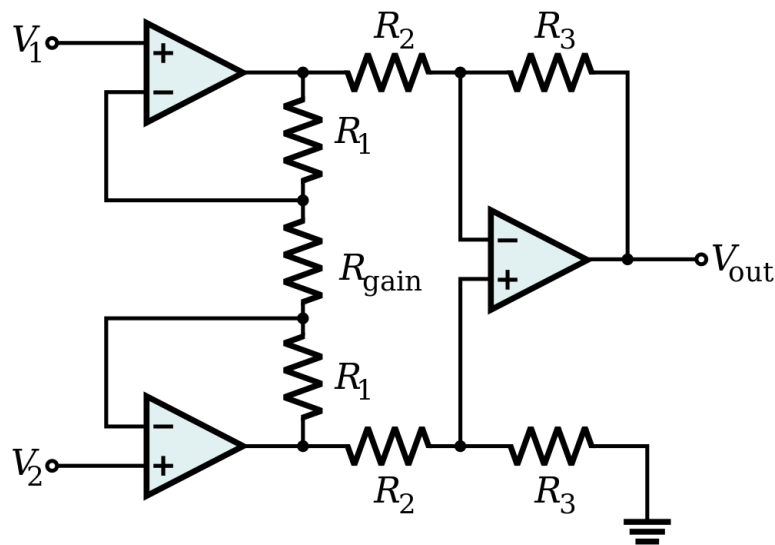


Figure 1.13: Circuit diagram of the instrumentation amplifier (IA) [5]

### 1.2.5 Features extraction

In order to perform quantitative studies on muscle activations and to perform classification tasks, different features can be extracted from raw sEMG signals in time and frequency domain. [67]

Time domain features are easy to calculate and are based upon the EMG signal amplitude. They are computed considering signal segments, in which its length is represented by  $N$  and the general sample by  $x_i$ :

- The integrated EMG (IEMG) is the area under the curve of the rectified EMG signal and is used as a pre-activation index for muscle activity.

$$IEMG = \sum_{i=1}^N |x_i|$$

- The Mean Absolute Value (MAV) is the average value of a rectified EMG signal segment and is used for detecting and muscle contraction levels.

$$MAV = \frac{1}{N} \sum_{i=1}^N |x_i|$$

- The Mean Absolute Value Slope (MAVS) is the estimation of the difference between the MAVs of the adjacent signal segments.

$$MAVS_i = MAV_{i+1} - MAV_i$$

- The Simple Square Integral (SSI) expresses the energy content of a EMG signal segment. It is computed performing the integral of a squared segment.

$$SSI = \sum_{i=1}^N (x_i)^2$$

- The Variance of EMG (VAR) expresses the power of a EMG signal segment. It is computed dividing the SSI by the number of samples inside the segment minus one.

$$VAR = \frac{1}{N-1} \sum_{i=1}^N (x_i)^2$$

- The Root Mean Square (RMS) is calculated square rooting the division between SSI and the number of sample in the considered time segment. This feature allows to estimate the muscle fatigue occurrence, since the fatigue typically implies an EMG amplitude increase [74].

$$RMS = \sqrt{\frac{1}{N} \sum_{i=1}^N (x_i)^2}$$

- The Waveform Length (WL) is the cumulative length of the waveform over the segment. Rapid amplitude variations inside a signal segment increase the WL feature.

$$WL = \sum_{i=1}^{N-1} |x_{i+1} - x_i|$$

- Wilson amplitude (WAMP) is the number of times that the difference between two consecutive amplitudes in a time segment overcome a specific threshold. This feature is an indicator of the motor units firing rate and therefore estimates the muscle contraction level [13].

$$WAMP = \sum_{i=1}^{N-1} f(|x_i - x_{i+1}|)$$

where

$$f(x) = \begin{cases} 1 & \text{if } x \geq \text{threshold} \\ 0 & \text{otherwise} \end{cases}$$

- Zero crossing (ZC) is the number of times that the EMG signal crosses the zero amplitude axes.

$$ZC = \sum_{i=1}^{N-1} \text{sgn}(-x_i \cdot x_{i+1})$$

where

$$\text{sgn}(x) = \begin{cases} 1 & \text{if } x > 0 \\ 0 & \text{otherwise} \end{cases}$$

The features extracted using the frequency domains are generally based on a signal's estimated power spectral density (PSD) [67], demanding more computational resources than the previous class of features. This type of features are usually employed for monitoring the muscle fatigue.

- The Median Frequency (MDF) is the frequency value which divide the PSD in two parts with equal area. The fatigue state occurrence induces the shift of this parameter to lower frequencies.

$$\sum_{f=f_{min}}^{MDF} PSD_f = \sum_{f=MDF}^{f_{max}} PSD_f = \frac{1}{2} \sum_{f=f_{min}}^{f_{max}} PSD_f$$

where the frequency domain range from  $f_{min}$  to  $f_{max}$  and  $PSD_f$  represents the generic sample of the PSD function.

- The Mean Frequency (MNF) is the ratio between spectral moments of order 1 and 0. In case of fatigue onset this feature behave similarly to the MDF.

$$MNF = \frac{\sum_{f=f_{min}}^{f_{max}} f \cdot PSD_f}{\sum_{f=f_{min}}^{f_{max}} PSD_f}$$

- The Dimitrov Spectral Index ( $FI_{nsmk}$ ) is computed as the ratio between spectral moments of order -1 and k, with k value higher than 1. This feature is proposed by Dimitrov et al. [23] as an alternative to MDF and MNF, offering higher sensitivity in the muscle fatigue detection.

$$FI_{nsmk} = \frac{\sum_{f=f_{min}}^{f_{max}} f^{-1} \cdot PSD_f}{\sum_{f=f_{min}}^{f_{max}} f^k \cdot PSD_f}$$

The Conduction Velocity (CV) is computed comparing the EMG signals recorded by two different DD acquisition channels. Knowing the inter-electrode distance is possible to estimate the time lag between the two signals and the conduction velocity. The CV represents a crucial parameter for estimating muscle fatigue: An intensive muscle activity increases the concentration of metabolic products into the intracellular environment causing a CV decrease.

The CV decrease is reflected by the signal power spectrum shift toward lower frequencies, dues to the shape mutation of MUAPs, followed by the increase of sEMG signal amplitude because of a spatial low-pass filtering effect of tissue as a conductor [18].

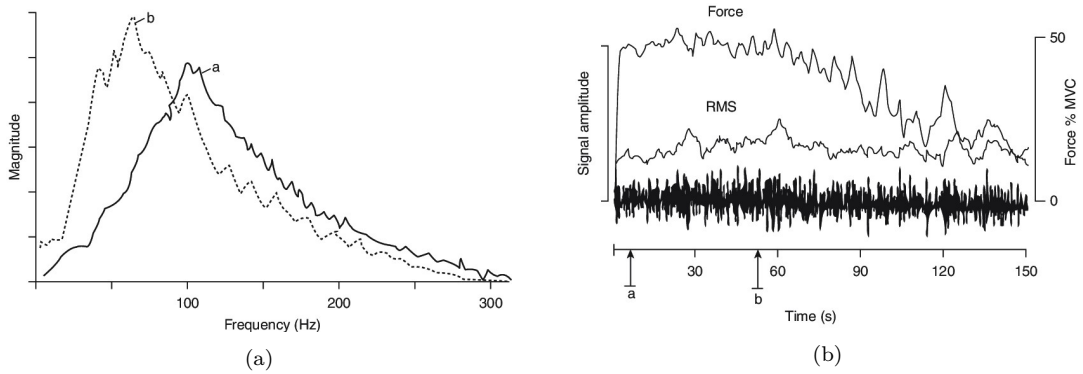


Figure 1.14: Muscle fatigue effect on frequency spectrum (a) and signal amplitude (b). In figure (a), the dashed line represents the sEMG spectrum in the presence of muscle fatigue. The solid line spectrum is referred, on the contrary, to the muscle activity in the absence of fatigue. [14]

### 1.3 Average Threshold Crossing

The Average Threshold Crossing (ATC) is a signal processing technique based on an event-driven approach that reduces the information stored inside an analogical signal into a simple quasi-digital pulses sequence. First, the signal is compared with a static or dynamic threshold, generating a digital pulse whenever the signal overcomes the threshold level. This procedure behaves similarly to the nervous system since it generates potential pulse sequences exploiting time dimension rather than amplitude for storing information. A microcontroller then counts the number of events generated in fixed time windows and computes the ATC value performing the ratio between the number of events and the observation window length.

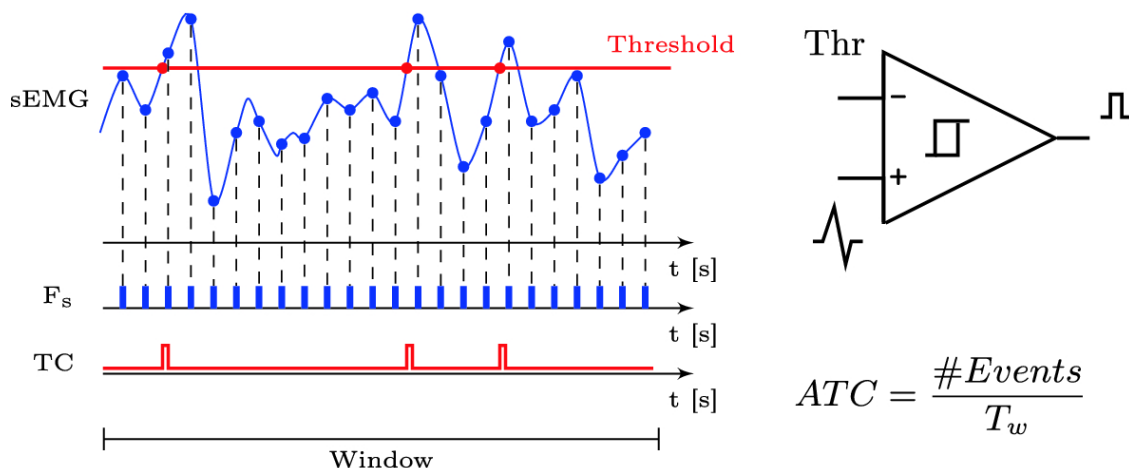


Figure 1.15: ATC signal represents an alternative technique to process EMG signal: It reduces the extracted information to the essential and simplifies the digitalization process, employing a voltage comparator rather than an A/D converter [62].

Typically, the estimation of muscle contraction force requires the acquisition and processing of the EMG signal. Like many biological signals, it has an analogical nature that implies the employment of an A/D converter (ADC) for digitizing its information, impacting power consumption and transmission performances, and limiting wearable applications. The ATC technique can be exploited for extracting quasi-digital information from biological signals, such as the EMG signal: Crepaldi et al. [19] demonstrated that the firing rate of motor units present in a muscle, and consequently the force generated, are highly correlated with the ATC signal obtained. This technique allows extracting essential informative content from the EMG signal, avoiding the ADC employment, improving the information transmission, and reducing the global power consumption. The main drawback of this technique is represented by the morphological information loss, limiting the use

of the ATC technique in specific diagnostic applications. Different technical aspects influence the ATC performances: Firstly, the threshold selection process is particularly crucial for the ATC signal extraction. If the voltage threshold is too high, the EMG signal hardly overcomes this level, reflecting a reduction of generated events and information. On the other hand, low-level thresholds are likely susceptible to environmental noise, generating spurious TC events and corrupting the ATC signal. In order to achieve a compromise between information integrity and noise robustness, a dynamic voltage threshold selection can be implemented [66]. Alternatively, the threshold can be set at a fixed level after a research process, reinforced by hysteresis implementation. Another operational parameter affecting the ATC technique performances is the time window length in which the number of threshold crossings is averaged. With the extension of the window width, a higher number of events can be detected, but the time resolution of the signal is consequently reduced.

## 1.4 Functional Electrical Stimulation

The spinal cord injury (SCI) and stroke represent two classes of injuries which prevent the affected individuals to perform and control voluntary motions. In SCI patients the descendent connection between central and peripheral nervous system is interrupted blocking the nervous signal transmission, whereas in stroke patients cerebral motor areas are damaged affecting the ability to perform motor control functions. However, in these pathological cases muscles innervations, joints and muscle tissue are often intact, allowing the electrical stimulation of muscle and achieving joints actuation. When the stimulation activates the damaged or disabled neuromuscular system producing coordinated body movements it is called Functional electrical stimulation (FES) [34]. This technique can be exploited in two different use cases: Firstly it can artificially induce body movements oriented to carry out daily tasks, resulting suitable for developing neuroprostheses which aims to restore permanently motion functions. Secondly, FES can be also used as short term therapy for supporting and retraining specific movements execution. The latter approach is often preferred since the long period stimulation effectiveness can be limited by the fatigue onset.

The nervous system controls muscle contractions through electrical pulse trains transmitted along with motor neuron connections organized in nerves. External electrical stimulation produces potential changes in nerves, eliciting the action potential generation. Lower motor neurons, which connect the spine to muscles, represent the access point for inducing muscle contractions using electrical stimulation. This process represents the basis of the FES application, and it is possible only if these terminal connections are intact. However, direct muscle stimulation is possible but implies a higher energy consumption [49]. If the stimulation of the motor neuron is sufficient to induce the cell depolarization, the action potentials generated propagates along the axon directed toward both ends. The depolarization wave which travels from the starting point towards the muscle is called *orthodromic* wave, whereas the other wave which is directed towards the CNS is called *antidromic* wave. Typically the former stimulus is used for generating coordinated muscle contractions, whereas the latter is considered an irrelevant side effect of FES [49]. Artificially induced muscle activations are generally limited owing to the decreased contraction efficiency and the tendency to induce neuromuscular fatigue due to the alteration of the normal recruitment order and the unnatural simultaneous activation of MUs [26].

### 1.4.1 Technology

The FES can use different types of stimulation electrodes, either transcutaneous or subcutaneous electrodes: transcutaneous electrodes are placed over the skin surface

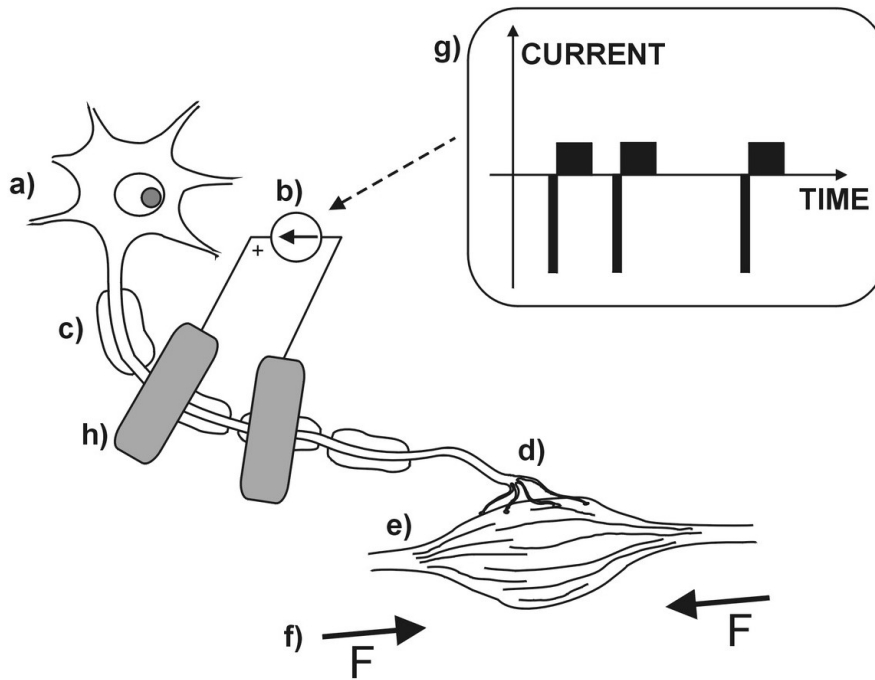


Figure 1.16: Functional Electrical Stimulation (FES) principle:  $\alpha$ -motorneurons (a) are stimulated electrically (b) producing depolarizations which travel along the axons (c) until they reach the neuromuscular junctions (d). Received action potentials induce the activation of multiple motor units in the muscle (e) and force production (f). The biphasic current stimulation (g) prevents the charge accumulation under the stimulating electrodes (h). [3]

above the neuromuscular junction of the muscle that needs to be activated. These electrodes are widely used in rehabilitation therapies since they are non-invasive and generally inexpensive. The two main drawbacks of using surface electrodes are the difficulty to reach deeper innervations and the higher stimulation intensity required for overcoming the skin impedance and eliciting contractions. On the contrary, the subcutaneous stimulation is carried out by invasive electrodes precisely located close to the nerve target. This class of invasive electrodes is further distinguished in percutaneous and implanted electrodes. Percutaneous electrodes are thought for temporary interventions. They consist of thin wires inserted through the skin to reach specific target areas inside the muscle tissue. Implanted electrodes are permanently inserted in the body and aim to sustain patient movements in the long term. The use of percutaneous solutions allow to precisely stimulate nerves with lower current intensities but expose the patient to the risk of infections. The electrical stimulation is delivered as a train of square-shaped impulses, imitating the control strategy exploited by the CNS for transmitting the information. Although both voltage and current pulses are effective in eliciting action potential generation in nerves, current modulation exhibits several advantages if

compared with the voltage modulation [49]. Firstly the use of current-modulated pulses in transcutaneous stimulation systems is not affected by changes in the skin impedance that occur during, which instead represents a problem for pulses based on voltage regulation. Moreover, tuning the current impulse width allows precisely controlling the amount of delivered charge and its removal. Charge accumulation is particularly harmful since it can affect biological functions and damage tissues. Considering the stimulation pulse shape, it can be either monophasic or biphasic. Through monophasic pulse stimulation, the current flows in a single direction from the anode to the cathode electrode, causing the charge accumulation into the tissue. The charge extraction is obtained through the use of balanced biphasic stimulation pulses. If the two stimulation phases are symmetrical, both electrodes result active. Otherwise, the muscle below the anode is mainly stimulated [49].

### 1.4.2 Stimulation parameters

The selection of proper stimulation parameters represents a critical aspect that must precede the FES therapy delivery since it influences stimuli effectiveness and prevents the rapid occurrence of fatigue. Main stimulation parameters are represented by pulse amplitude, duration, and frequency.

#### **Pulse amplitude:**

The pulse amplitude is expressed in mA for current pulses. This parameter directly influences the amount of charge delivered to the patient and, consequently, the number of motor units (MUs) that can be recruited with a stimulus. However, the number of MUs that the stimulation can involve is limited to those in proximity to stimulating electrodes. For this reason, pulse intensity can be increased until the stimulation does not produce a contraction increase. Beyond this point, the electrical stimulation is perceived as uncomfortable. Current amplitudes can typically range from 0 to 140 mA[11]. The right pulse amplitude is highly variable and depends on muscle features, skin impedance, electrodes integrity, and stimulation set-up.

#### **Pulse width:**

The time duration of the stimulation pulse typically ranges from 200  $\mu\text{s}$  to 400  $\mu\text{s}$  [38]. This parameter contributes to controlling the muscle force generation, defining the stimulation intensity. Short pulse widths result in being more comfortable than longer stimulations [11] but need higher pulse amplitude in order to deliver the same amount of charge. Moreover, longer pulse durations can penetrate more deeply into the muscle tissues, recruiting a wider motor units population, including deeper type I muscle fibers, which show better resistance to fatigue [38].

**Stimulation Frequency:**

The stimulation frequency refers to the number of pulses delivered in a second and is expressed in Hertz (Hz). Paralyzed skeletal muscle can be typically activated with a stimulation frequency that ranges from 20 to 50 Hz [39]. Through the variation of this operative parameter, different types of muscle fiber can be recruited, achieving different stimulation responses [11]. Specifically, higher frequencies are responsible for fast contraction fibers recruitment, inducing the rapid onset of muscle fatigue, whereas lower frequencies involve slower fiber types that are generally more resistant to the fatigue phenomenon. However, extended low-frequency stimulation produces a different type of fatigue, which is called *low-frequency fatigue* and consists in a long-lasting effect that reduces the force-generating capabilities of skeletal muscle [40].

**1.4.3 FES Intensity Calibration**

Since the pulse amplitude is highly variable and depends on the muscle investigated and subject's conditions, it must be properly calibrated each time that a new stimulation session is conducted. The typical calibration approach is performed for each muscle individually and consists of the patient stimulation, performed slowly ramping current amplitude values [11]. The intensity is increased until reaches the motor threshold, which represents the minimum stimulation level to induce a motor response of the muscle [69]. When the FES is used for stimulating a full movement similar to a voluntary, the calibration is further extended until the pulse amplitude reaches the functional threshold [16].

**1.4.4 Muscle fatigue**

The FES application benefits in assisting the muscle contraction of the subject with neuromuscular disorders are limited by the muscle fatigue phenomenon, which mainly affects paralyzed muscles [49]. The term fatigue refers to the decline of the expected force generated by muscles due to extended muscular activity. Even though this phenomenon is expressed with visible effects, it is due to complex physiological processes within motor units and Central Nervous System. Muscle fatigue can be classified in *peripheral fatigue*, and *central fatigue* [25], according to the origin site: The peripheral fatigue refers to intracellular events which affect the conversion of action potentials arrived at the neuromuscular junction into contractions of the muscle fiber. On the contrary, central fatigue is due to processes that occur outside muscle fiber, specifically within the CNS, failing in action potential transmission and motor unit recruitment. Considering pathological subjects, in which the transmission of the nervous signal is seriously impaired or interrupted, the central fatigue influence is negligible.

The electrical stimulation produces a non-physiological contraction condition that

enhances muscle fatigue: the primary cause is the inverse MU recruitment strategy. The CNS progressively recruits MU starting from the slow contractile type I MU, which are innervated by small-diameter axons, going to the fast contractile type IIa and IIb MU, which motor neurons axons have larger dimensions, following the effort increase. In addition, the recruited MU are evenly distributed in the muscle belly, and their number increases with contraction tension. On the contrary, the electrical stimulation primary activates larger axons in the proximity of stimulating electrodes, causing the preferential recruiting of type II MU and limiting the contraction endurance. Moreover, repetitive stimulations involve the same group of MU which are more likely to decline force level during extended activity. Pathological subjects are further susceptible to a rapid fatigue onset since their muscles exhibit an altered composition of different MU types [37].

In order to prevent the rapid fatigue onset, a proper modulation of stimulation parameter is fundamental: Considering constant parameters, Kesar *et al.* [41] suggest that the use of lowest frequency and most extended pulse duration may maximize performance. Other studies focused on the employment of time-varying parameters, such as Keabaetse *et al.*[39], which proposed an alternative stimulation strategy based on the switch of pulse frequency from low to high values, improving the stimulation of repetitive contractions and overcoming the effects of low-frequency fatigue.

# Chapter 2

## State of Art

### 2.1 sEMG wearable acquisition systems

The acquisition of sEMG signal is particularly significant in many applications which involve physical activity monitoring. Considering sEMG acquisition systems, they can be distinguished in four different scenarios by differences in instrumentation cost and precision [54]: The first scenario is represented by diagnostic applications, which requires high-quality signal acquisition and processing in order to minimize signal distortions. In such application, the data analysis is mainly performed offline. The required high standard performances are satisfied by the employment of high-cost components. The use of sEMG for prosthesis control represents the second scenario, in which the signal is recorded and processed in real-time, translating the stored information into the desired gestures which the prosthesis has to reproduce. The primary technical constraint is the movement recognition time which must be shorter as possible to ensure a quick prosthesis response. The third scenario is represented by rehabilitative application, in which sEMG devices are designed to be easily deployed, also for at-home uses. The last scenario includes non-medical applications, such as human-machine interfaces, in which the signal quality requirements and the system complexity can be lower than in medical devices.

Thanks to the latest technological development, wearable acquisition systems have started to represent a reliable solution for performing real-time bio-signal recordings in dynamic conditions in the previous application scenarios. This class of devices is meant to be completely wireless, allowing freedom of movement and reducing signal alterations owed to cable connections. This technical approach implies the adoption of a wireless communication system for performing data exchange and an internal power supply provided by a battery. In order to extend the battery life, the power consumption represents a critical factor that must be limited while ensuring solid acquisition and communication performances.

Wearable EMG devices consist of embedded solutions with a miniaturized circuit

board responsible for signal acquisition and conditioning. The acquisition is performed through a single-differential (SD) configuration, involving two surface metal electrodes connected to the instrumentation amplifier (INA) and an additional one as a reference electrode. As reported in the section 1.2.4, the differential signal must be filtered, removing high and DC noise components, and amplified with a programmable gain amplifier in order to adapt the signal amplitude to the input voltage range of the ADC. The digital signal produced by the A/D conversion stage is processed by a micro-controller unit that performs the feature extraction. Micro-controller can also receive and process data from other embedded sensor systems, such as the inertial measurement unit (IMU) [12]. The data transmission is performed by implementing a wireless communication protocol. Among different possible protocol solutions, the Bluetooth Low Energy (BLE) represents an excellent candidate for many applications, combining good performances and ubiquitous diffusion [73].

Different high-performance wireless sEMG acquisition solutions are present on the market:



Figure 2.1: State of the Art wireless sEMG acquisition devices: (a) Biometrics Ltd DataLITE [9]; (b) Cometa srl PicoEMG [2]; (c) Cometa srl Mini Wave Infinity [2].

The DataLITE wireless EMG sensor (Figure 2.1a), made by Biometrics Ltd [9], with a weight of 17 g and a compact size of 42 x 24 x 14 mm, can be easily worn, allowing comfortable muscle activity readings even in dynamic conditions. The amplification stage exhibits an input impedance higher than 100 M $\Omega$ , which allows the user to interface two reusable dry electrodes to the skin without preparation and the need of any conducting gels. The data exchange between the DataLITE sensor and the PC is performed exploiting the DataLITE PIONEER dongle, which enables wireless communication up to a distance of 30 m. The power supply is provided by a rechargeable Li-Ion Polymer, which ensures a battery life of up to 8 hours.

Cometa srl [2] produces high performance wireless sEMG devices, such as the PicoEMG (Figure 2.1b) and the Mini Wave Infinity (Figure 2.1c). The PicoEMG

represents one of the lightest acquisition devices on the market, with a total weight of only 7 grams, while the Mini Wave Infinity provides the longest transmission range on the market, reaching an indoor distance of 50 m. Both devices include an accelerometer and a memory integrated onboard. Considering power consumption performances, the PicoEMG can last more than 12 hours with a single recharge, whereas the battery life of Mini Wave Infinity is limited to 8 hours of operation.

## 2.2 ATC technique

The ATC processing technique can be successfully applied to sEMG recordings to extract information about the muscle contraction force, reducing hardware and transmission complexity.

The work of Crepaldi *et al.* [19] firstly introduced the application of ATC to sEMG recordings, where the force level exerted by a muscle during a contraction activity was compared with the number of TC events generated. Comparison results showed a correlation level of  $0.95 \pm 0.02$ , suggesting that ATC values could be used as a reliable estimator of contraction force (Figure 2.2). Moreover, the adoption of the ATC as a processing method implied the hardware simplification since a voltage threshold comparator is employed instead of the ADC module for extracting the digital information and allowed the transmission of muscle force information through an event-driven wireless approach. Motto Ros *et al.*[58] extended the use of ATC to a multi-channel case, using Address-Event Representation (AER) as means to convey information in the wireless transmission. Additionally, they compared the ATC robustness with the average rectified value (ARV) in three different noise conditions: white noise artificial addition, amplifier distortion, and ATC events loss. In the first condition (Figure 2.3a), the ATC already reached the maximum of correlation at 5-6 dB of SNR, whereas the ARV reached the maximum at 20 dB. The second test condition (Figure 2.3b) demonstrated that the ATC paradigm is nearly independent of the amplifier distortion, relaxing the requirements for the EMG signal amplifier. The third test condition (Figure 2.3c) highlighted the ATC paradigm's robustness to information loss, tolerating almost 70% event losses.

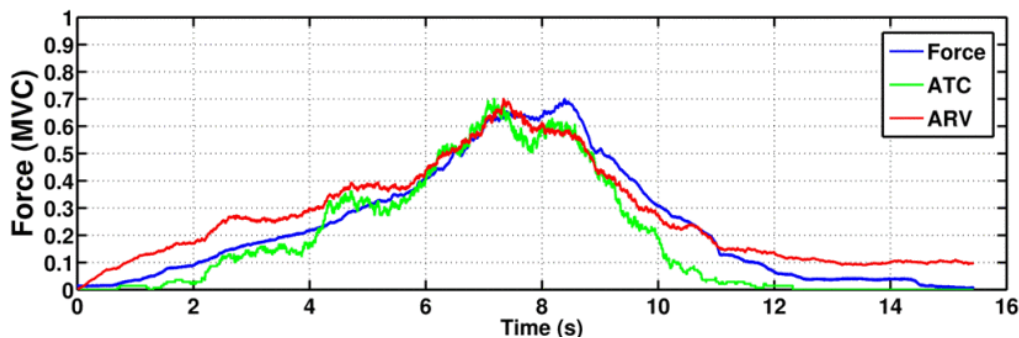


Figure 2.2: The ATC technique applied to the grip force estimation. The ATC values are compared with the Absolute Rectified Values (ARV) extracted from the sEMG signal [19].

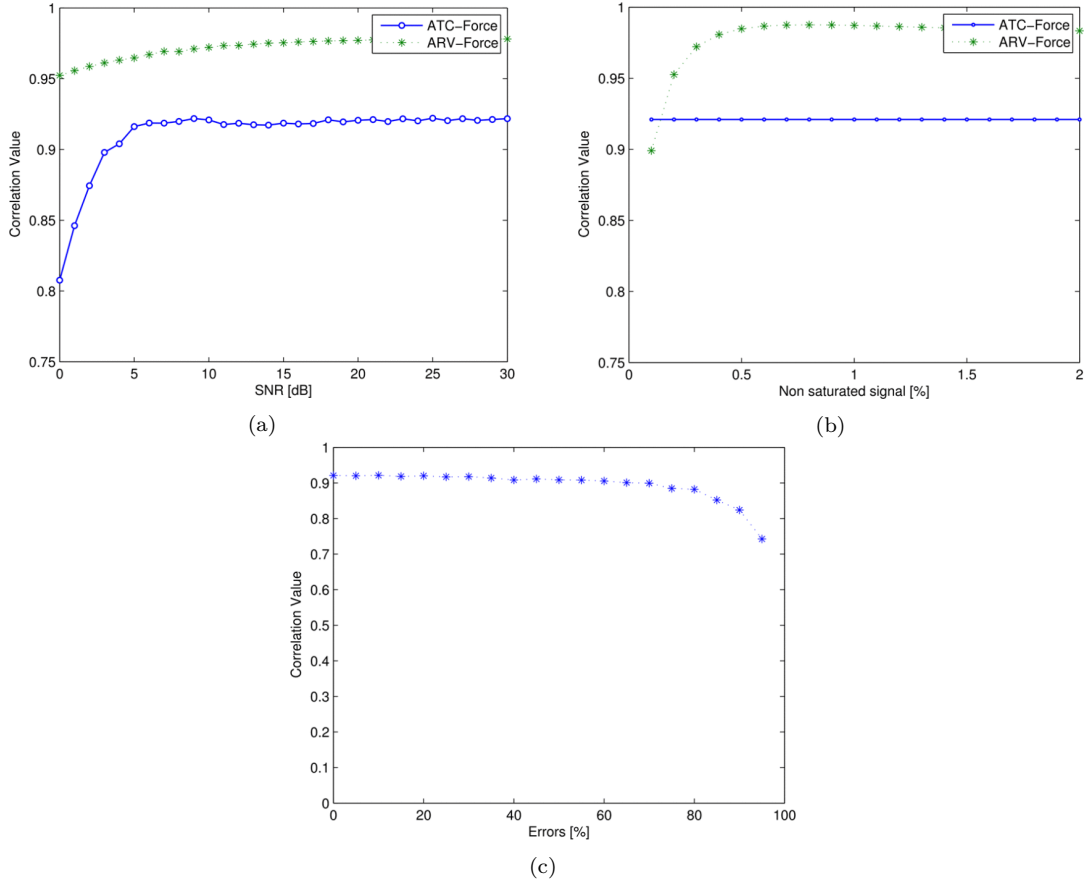


Figure 2.3: ATC-Force correlation in different noise conditions: (a) varying SNR; (b) amplification distortion effect; (c) presence of ATC events losses [58].

Sapienza *et al.*[63] investigated the lowest level of complexity reachable by an ATC system, realizing a miniaturized wearable prototype with a whole systems power consumption of 15.49 mW. The system was capable of performing the differential EMG acquisition, followed by the ATC technique implementation. The wireless transmission of the resulting quasi-digital signal was performed, delivering ultra-wideband (UWB) pulses to an external receiver. Additionally, in-vivo experiments were conducted in order to study the relationship between the muscle activity produced during an isometric and isotonic contraction and the number of TC events generated. The experimental results showed a growth of ATC pulses number as the muscle tension was increased. Later, Guzman *et al.*[33] developed an ATC acquisition system made of Commercial Off-The-Shelf (COTS) components and explored the opportunity of exploiting a static threshold in order to simplify the ATC implementation and to maintain system complexity as low as possible.

The first application of the ATC technique to a movement recognition algorithm

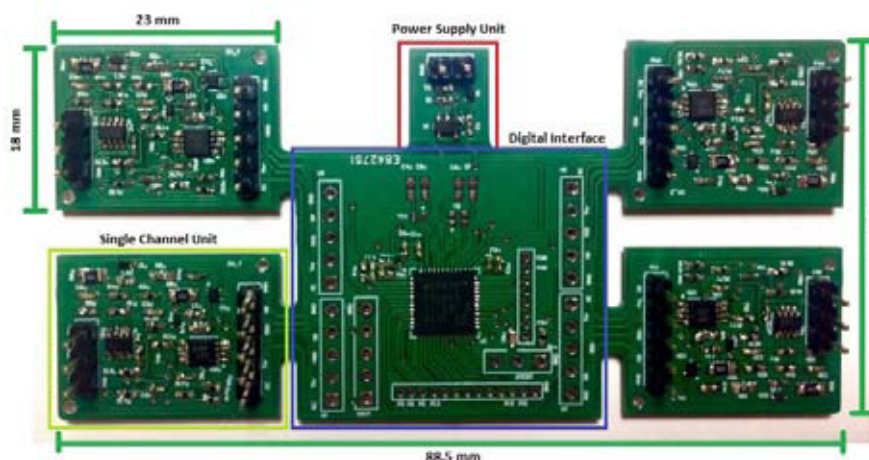


Figure 2.4: [33].

was presented by Sapienza *et al.* [64]. This study used a full-custom acquisition board to extract TC events from sEMG recordings of three different forearm muscles. Then, ATC signals generated from the muscles activation were used for classifying four different wrist movements: flexion, extension, abduction, and grasp. The movement classification was performed employing a Support Vector Machine (SVM) model, which was trained with the signals of repetitive gestures repetitions acquired from ten different subjects. Classification results showed that, from the acquisition of three channels, it is possible to identify four different wrist movements with an accuracy above 92.87% and latencies of only 160 ms. The application of the ATC paradigm, instead of the use of raw sEMG signal, allowed to significantly reduce the data rate from 6.14 kB/s to 30 B/s, and consequently consumption values. In recent work, Mongardi *et al.* [55] implemented a low power system for real-time hand movement recognition. The system exploited the event-driven processing of the sEMG signal for extracting three input features used to classify six different movements. The classification was performed using a fully-connected Neural Network (NN), implemented on an Apollo 2 microcontroller. The system classification performances achieved an accuracy of 96.34%, a system latency of 268.5 ms, and total power consumption of 2.9 mW.

In the work of Rossi *et al.* [62], the ATC processing was applied, for the first time, to the control of Functional Electrical Stimulation (FES), using the ATC parameter generated by a muscle activation to modulate the electrical stimulation in a real-time mode. They employed the acquisition hardware proposed in a previous work [33], composed of 4 analog front-end channels and a microcontroller unit, and implemented the Bluetooth wireless communication protocol in order to exchange data with an external workstation. The management application was implemented in Matlab<sup>®</sup>, coupled with a Simulink<sup>®</sup> model for controlling stimulation parameters.

Considering power consumption, it amounted to 5.125 mW for the acquisition stage, while including the data transmission phase, the power usage reached 20.23mW and 23.47 mW for TC events and sEMG signal transmission, respectively. Then, the system was validated and further evolved, thanks to subsequent works [61][60]. In [61] two stimulation modalities are implemented in order to cover the standard rehabilitation flow: in the former, two subjects were involved, with a therapist figure, from whom the ATC signal was recorded, and a patient figure which was proportionally stimulated based on the therapist activity. The second stimulation mode involved a single subject that was able to perform a self-stimulation. The system was tested, evaluating the reproducibility between the voluntary movement and the stimulated one in the therapist-patient stimulation modality. Experimental results showed the median value of the correlation coefficient, used as similarity measurement, above 0.9 across four benchmark movements. In [60] the system management software was moved from a general-purpose PC to an embedded solution, represented by a Raspberry Pi. The previous Matlab<sup>®</sup> & Simulink<sup>®</sup> software architecture was replaced with a novel and more versatile version programmed in Python, which was able to work with several devices and different operating systems, exploiting the advantages of the object-oriented and multi-threaded approach. Moreover, in this work, the conversion from ATC to FES stimulation parameters values was quickly performed, exploiting a calibrated lookup table.

## 2.3 FES control strategies based on sEMG

In rehabilitation, FES systems are used for assisting the movements of pathological subjects in accomplishing fundamental tasks in daily life, such as reaching and grasping. Such movements involve the contraction of different muscle groups, following specific activation patterns. The use of passive electrical stimulation for supporting patient movements may result in ineffective stimulation since it cannot reproduce the muscle activation complexity, and additionally, it can cause excessive stimulation leading to a quicker muscle fatigue onset [76]. The effectiveness of an FES therapy, in terms of movement reproducibility and muscle fatigue prevention, can be increased by implementing an active control of stimulation parameters capable of adapting to physiological activation patterns to generate effective movement executions. A biomimetic control method for modulating the electrical stimulation is represented by the use of sEMG signal as an indicator of muscle force level, which can be applied in three different scenarios:

- The first scenario consists of the application of signal acquisition and stimulation to contralateral muscles. This case can be applied to severe hemiplegic patients whose affected side can be stimulated based on the muscle activity of the unaffected side. The main advantage of this application is represented by the patient's active participation, which is desired to improve the rehabilitation performances [76].
- In the second scenario, a master-slave approach is implemented: the sEMG signal acquisition is performed on the muscle of a healthy subject, denoted as a therapist, and used as a reference for driving the electrical stimulation of the patient muscle. In addition, the therapist represents a visual reference for the patient. This strong inductive effect will enhance the rehabilitation effectiveness [45].
- The ipsilateral stimulation represents the last scenario, in which the movement intention of the patient triggers the electrical stimulation, and additionally, it is modulated using the voluntary muscle activity, expressed as EMG signal. In such application, active engagement of the patient is fundamental for enhancing the therapeutic effect of FES [56].

Zhou *et al.* [75] proposed a FES closed-loop control system in which the sEMG bias between two bilateral arms is used for driving the electrical stimulation on the affected arm. Firstly, the healthy arm performs a standard rehabilitation gesture, and the sEMG signal generated by the muscle contraction is processed, extracting the root mean square (RMS) feature as an indicator of voluntary contraction force. A second time, the subject performs the same action using the affected arm. The RMS values extracted during the second training are compared with the reference RMS sequence generated by the healthy arm in real-time. The bias between the

RMS values of the two arms represents the input of the FES controller.

In [76], a multichannel FES control system based on the sEMG acquisition is proposed. The implemented algorithm exploits a gaussian mixture regression (GMR) for mapping the relationship between the sEMG and the muscle force, followed by a polynomial fitting (PF), which estimates both stimulation amplitude and pulse width from the muscle force value. The grip movement was selected to validate the effectiveness of the method. Estimated parameters were tested comparing the FES-induced grip force and the originally recorded voluntary grip force, revealing a high correlation index ( $R > 0.9$ ).

Osuagwu *et al.* [56] proposed an active FES system (Figure 2.5), in which the FES intensity is proportionally modulated exploiting the sEMG signal extracted from the ipsilateral muscle voluntary activity. The main challenge they addressed is the removal of the stimulation artifact, which contaminates the voluntary electromyogram (EMG) during FES application: they have implemented an entirely software-based solution that extracts voluntary EMG from muscles under FES in real-time, using an adaptive filtering technique with an optional comb filter. The resulting EMG-FES system was validated among fifteen patients with tetraplegia, demonstrating that the FES intensity modulation produced by the active system was proportional to intentional movement.

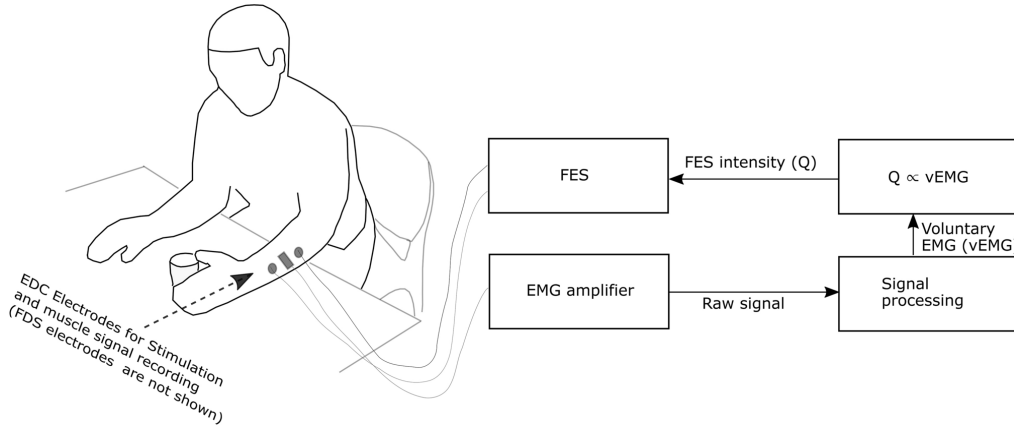


Figure 2.5: Schematic diagram of an EMG-FES system proposed by Osuagwu *et al.* (EDC, Extensor digitorum muscle; FDS, Flexor digitorum muscle) [56].

## 2.4 ATC-FES System description

The aim of this project is the optimization of an embedded ATC-controlled FES system, which has been developed in previous works [62][61][60]. The system exploits sequences of ATC values extracted from the sEMG signal to control the Functional Electrical Stimulation (FES) therapy in real-time. The system has been designed to operate on a maximum of eight channels and is composed of three central communicating units: The acquisition unit is represented by wearable embedded devices which detect the sEMG signal generated during the voluntary contraction and compute the ATC. The control unit is a software environment implemented on PC, which enables the communication with acquisition devices, the processing of ATC values, and the management of the electrical stimulation. This unit provides a Graphical User Interface to allow users to interact with the system through different services. The FES unit is represented by an external stimulator, which communicates with the control unit through a USB interface.

### 2.4.1 Wearable acquisition device



Figure 2.6: Wireless ATC acquisition device [59].

The acquisition unit of the ATC-FES system is organized in multiple channels, which enable the acquisition of the sEMG generated from different muscle groups. Each channel is represented by a wearable device, developed by Rossi *et al.*[59], which consists of an analog front-end, responsible for the sEMG detection and the event-driven hardware processing of the bio-signal, embedded with a digital part, which employs a microcontroller unit for the wireless data transmission and for optionally sampling the sEMG signal. The whole device circuitry is powered with a constant voltage supply of 1.8 V.

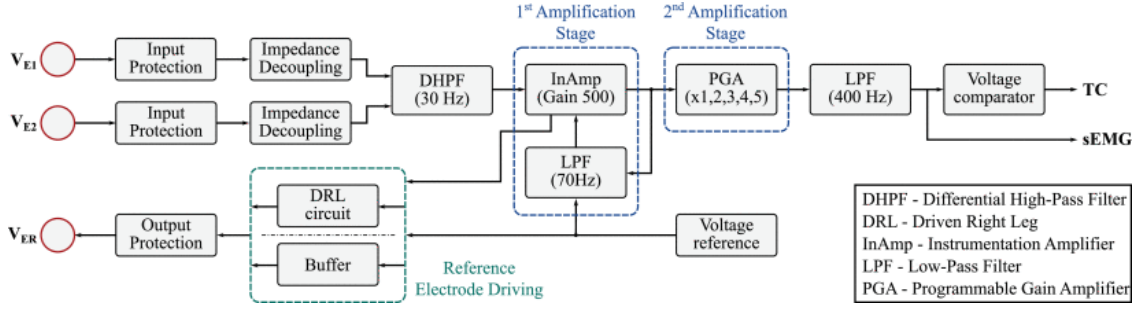


Figure 2.7: Schematic diagram of the Analog Front-End [59].

**Analog Front-End (AFE):** The analogical part of the acquisition channel consists of the sEMG conditioning circuit completely designed using commercial off-the-shelf components. The front-end exploits a single differential configuration, in which two sensing electrodes detect the muscle fibers depolarization, and an additional electrode refers the body potential to an internally-generated voltage. As shown in the figure 2.7, input and reference terminals are connected to protection circuits to preserve the onboard circuitry components from high input voltages that overcome the supply voltage and to ensure the user safety limiting output currents. Before the amplification stage, sensing terminals are decoupled from the electrode-skin impedance employing a couple of voltage followers and then are connected to a first order Differential High-Pass Filter (DHPF), with a cut-off frequency set to 30 Hz. The use of DHPF avoids the amplification of low-frequency noises and movement artifacts, preventing the saturation of consecutive electronic components and limiting the attenuation of the sEMG energy content.

The amplification is carried out in two separated stages in order to relax amplifier constraints and reduce the signal alteration induced by each amplification stage. The first amplification stage is represented by the Instrumentation Amplifier (IA) with negative feedback on the reference. The IA amplifies the difference between the two inputs with a differential amplification  $A_d$ , equal to 500 V/V, and rejects the common-mode noise. The negative feedback takes the output, and after a low pass filtering and a phase, reversion feeds it again to the IA reference, increasing the stability of the amplified signal. The second amplification stage can be programmed, allowing the user to set an additional gain for detecting low muscle activities.

The amplification chain is followed by a low-pass Butterworth filter which limits the signal bandwidth to 400 Hz, also working as an anti-aliasing filter in case of sEMG sampling. At the end of the sEMG-conditioning chain, a voltage comparator is employed, enabling the conversion of the analogical signal into a sequence of Threshold Crossing (TC) events. The threshold can be adequately set through a Digital-to-Analog Converter (DAC), with a hysteresis of 30 mV around the threshold, stabilizing the digital output of the comparator and preventing the generation

of spurious events.

The user susceptibility to external common-mode interference is reduced employing the Driven Right Leg circuit (DRL) as a reference voltage control solution.

**Digital unit and data transmission:** The TC signal, given as output by the AFE, undergoes a digital processing stage to compute the ATC parameter. This process is carried out by the microcontroller unit (MCU) Apollo3 Blue, powered with an ARM Cortex<sup>®</sup>-M4F processor, which has been selected for its technical characteristics:

- Power efficiency:  $6 \mu\text{A MHz}^{-1}$ .
- Clock frequency: Up to 48 MHz.
- Transmission (TX) current: 3 mA TX power transmitting at 0 dBm
- RAM: 384 kB
- Flash/ROM: 1024 kB
- Package sizes:  $4.5 \text{ mm} \times 4.5 \text{ mm}$
- Power supply: 1.8 V
- Transmission standard: Bluetooth 4.2

The use of the ATC technique has led to a complexity reduction of the muscle force information, enabling low-power data transmission. Thus, Bluetooth Low Energy (BLE) 4.2 is adopted as a low-power communication protocol, thanks to its flexible throughput and widespread usage.

The performances of the resulting embedded device were tested, showing high acquisition performances, with a signal-to-noise ratio higher than 15 dB. Moreover, the device allows the user to perform both the sEMG and ATC acquisition. In the former case, the transmission throughput reaches  $2 \text{ kB s}^{-1}$ , supported by a battery life of 80 h. Instead, considering the transmission of ATC values, the throughput is relaxed to  $8 \text{ Bs}^{-1}$ , extending the operating time up to 230 h.

## 2.4.2 Control platform

The control software has been developed in [60] and further updated in [57], using Python programming language, in order to exploit the advantages of the *Object Oriented Programming* (OOP) paradigm: the platform architecture organized in objects facilitates the software maintenance and allows the application to be easily scalable and modular, maintaining its performance independently by the number and type of devices involved. Moreover, exploiting the multithreading function, the real-time simultaneous control of multiple system processes is realized.

The software architecture is organized in a three-layer structure: the bottom layer

is responsible for the communication between the control application and external devices instantiating an object for each physical device involved. The middle layer represents the core of the control platform, consisting of an object called *System*, which manages the communication among the objects of the lower layer. The top layer implements the Graphical User Interface (GUI), which allows the user to interact with the system, specifically with the middle layer. The GUI was developed inheriting from the classes of the *Kivy* Python framework [6], making the application usable on different Operating Systems (OSs), such as Microsoft® Windows®, Linux®, Raspbian. The Bluetooth communication can be implemented in different ways, depending on the OSs of the device: Computers based on Microsoft® Windows® rely on an external USB dongle CC2540 [1], from Texas Instrument, for communicating with external devices. On the contrary, in the case of Linux® and Raspbian OSs, Bluetooth communication is implemented exploiting an integrated antenna.

The control platform provides different services, implemented as a method of the object *System* and accessible from the GUI. They allow the user to configure the system settings and realize controlled FES sessions:

**System connection and configuration:** This function is implemented with the method *connect*, which connects the computer to external devices, enabling the serial communication with the electrical stimulator and the BLE dongle, if present. Furthermore, the system starts the scanning process, looking for Bluetooth acquisition devices. The user can therefore select the list of scanned devices with which he wants to establish the connection, instantiating and configuring the respective objects in the low layer of the software architecture.

The user can select the stimulation channels, associating each channel to a different acquisition device.

**Threshold calibration:** The implementation of the ATC processing technique relies on the setting of a proper voltage threshold, which allows the system to distinguish the effective muscle activity from the baseline signal generated by background electrical events. In order to adapt the ATC method to the variable subject conditions, the threshold calibration has to be performed. The user can trigger the calibration process using the control platform, which delivers a Bluetooth notification to the connected physical devices. The threshold calibration is conducted by a proper firmware routine of the device, implementing a finite state machine which modifies the threshold value starting from the power supply level (1.8 V) and gradually decreasing the voltage until the baseline is detected.

**System calibration:** The FES control mechanism is based on the relation between the ATC data acquisition unit and the stimulation unit. The modulation

of FES, in particular, is conducted by adjusting the stimulation intensity, which can be either obtained by modifying the pulse width or amplitude in order to produce the variation of the number of recruited motor units. As reported in [60], the conversion from ATC data to FES intensity values is achieved by exploiting a Look-Up Table (LUT), which reduces the computational cost of the stimulation intensity definition. Specifically, the LUT creates a one-by-one association between ATC values, ranging from 0 to a maximum value which varies among different subjects and current values. Two calibration processes are needed to define both the maximum ATC value that the voluntary action can produce and the proper current intensity that must be set to induce a successful and comfortable stimulation of the patient.

Considering the ATC maximum calibration ( $ATC_{max}$  calibration), the acquisition is performed during repetitive movement execution, and the maximum ATC value is statistically extracted from the collection peak values generated during the acquisition. The  $ATC_{max}$  calibration can also be called therapist calibration when it is performed in a master-slave FES configuration. The second calibration phase searches the proper stimulation intensity, and is described in the section 2.4.4.

**FES Training:** The FES Training represents the primary function of the ATC-FES system, in which the patient stimulation is driven by the voluntary movements of the therapist or the contralateral part of the patient body. The LUT, generated after the system calibrations, is exploited to convert ATC sequences provided by acquisition devices into modulated stimulation patterns delivered to the patient through the respective stimulator channels. The latency which separates the voluntary actions of the master and the patient stimulation represents a critical factor that must be minimized to enhance the system responsiveness.

### 2.4.3 Electrical stimulator

The current version of the system exploits an external electrical stimulator for performing the FES task, which is the RehaStim2, made by HASOMED GmbH [35]. The stimulator is classified as a IIa medical device and consists of 8 stimulation channels, organized in two groups made of 4 channels and controlled separately by two independent current generators. The power supply is provided by an internal battery, keeping the user connected to the device isolated from the power line interference, hence resulting compatible with the acquisition of bio-signals in parallel to the stimulation process. In order to ensure user safety, the stimulator is equipped with an emergency button, which can be used for manually stopping the stimulation process.

The RehaStim2 generates biphasic current pulses (Figure 2.9), characterized by adjustable intensity and a fixed pause of 100  $\mu$ s between the two phases of the

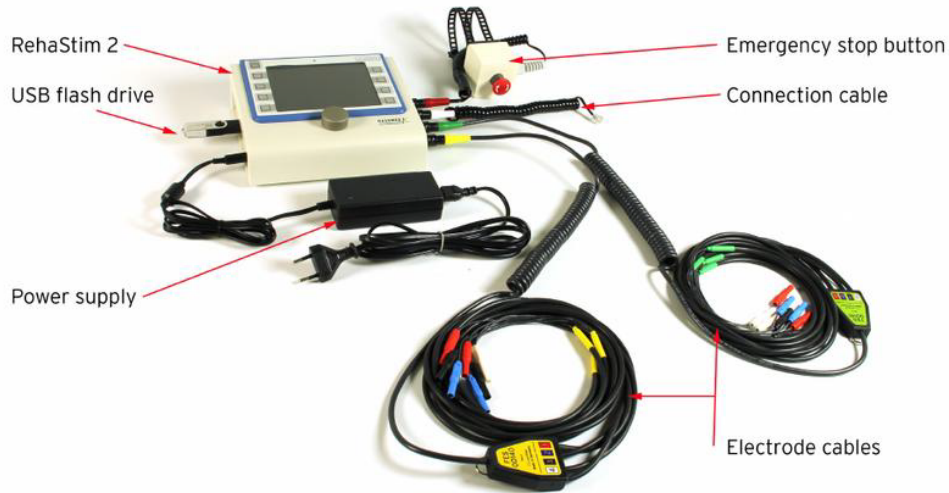


Figure 2.8: RehaStim2 electrical stimulator ready for use [35].

pulse. At the end of the pulse, the remaining charge on the electrodes and skin is actively removed. In order to deliver electrical pulses in safety conditions, the stimulator checks the impedance between the two active electrodes, sending a small test impulse before each stimulation pulse. If the impedance value is not included inside a reference range, then the electrical stimulation is blocked.

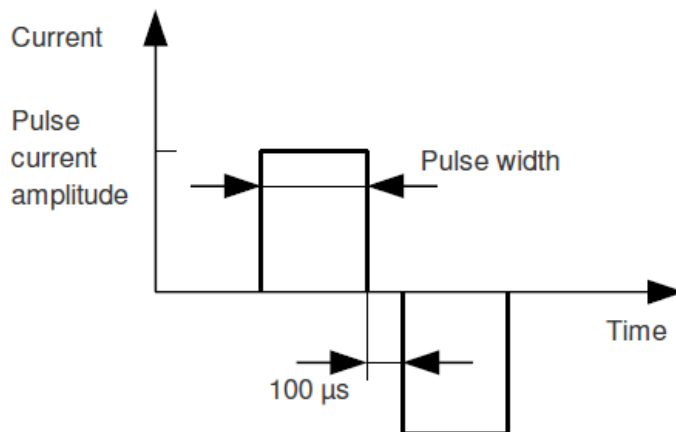


Figure 2.9: Representation of the biphasic current pulse generated by the RehaStim2 during the stimulation [43].

The control of the stimulation mode and the FES parameters setting can be achieved either accessing through a display interface integrated into the device or connecting the stimulator to a PC via USB connection.

The second control strategy is based on the ScienceMode2 communication protocol, enabling bidirectional communication between a PC and the functional electrical stimulator RehaStim2. The ScienceMode2 allows the user to implement custom made software solutions for creating complex stimulation patterns and training protocols, extending the stimulator application to a wide range of research scenarios [43].

The FES parameters which can be modified by the user are the following:

- Current intensity (I): 0 - 130 mA
- Pulse width (PW): 0 - 500  $\mu$ s
- Stimulation frequency: 1 - 50 Hz for 8 channels

Additionally, the RehaStim2 allows the user to intensify the stimulation in selected channels, sending in the same main stimulation period ( $t_1$ ) repeated pulses grouped in doublets or triplets, properly spaced with an interpulse interval ( $t_2$ ).

The pulse generator is controlled by selecting a stimulation mode among three different possibilities:

- The Continuous Channel List Mode (CCLM) simplifies the generation of complex stimulation patterns: A list of stimulation channels has to be specified, defining the respective stimulation parameters and the pulse group mode (single, doublets, or triplets). Electrical pulses, or pulse groups, are repeatedly generated in each specified channel according to  $t_1$ . A command is used to initialize or update the CCLM with current, pulse width, and pulse group mode parameters for each activated channel. After the initialization, the channel list is repeatedly processed according to the specified intervals. The CCLM can be stopped with the appropriate command.
- Using the One Shot Channel List mode (OSCL), the stimuli generation must be triggered by the start/update command sent by the user, allowing the PC, or other external devices, to control the main stimulation frequency, while the  $t_2$  time inside doublets and triplets is still managed by the stimulator.
- The Single Pulse command triggers the instantaneous generation of a single stimulation pulse, specifying the operating channel, the current intensity, and pulse width parameter.

In the ATC-FES system, the stimulator is mainly used in the CCLM mode since the stimulation frequency is managed directly by the RehaStim2, maximizing the stimulation reliability. Therefore, the control system is only responsible for sending commands through the ScienceMode2 protocol to start, update, or stop the electrical stimulation.

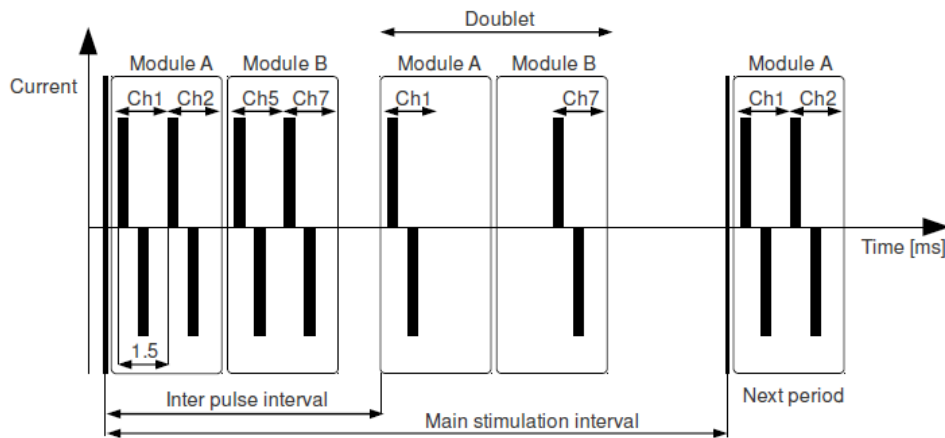
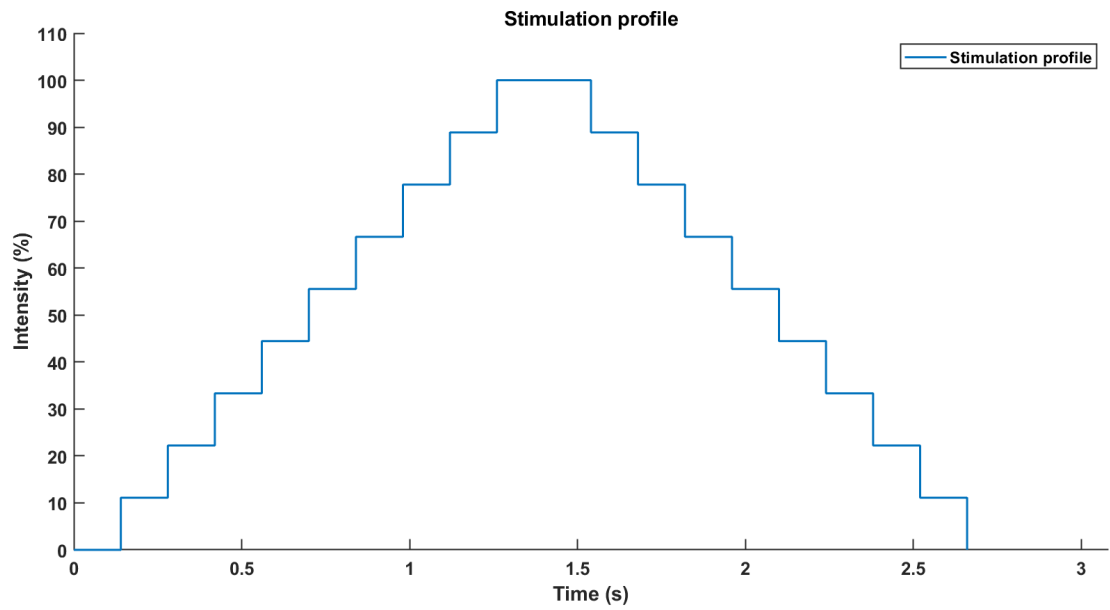


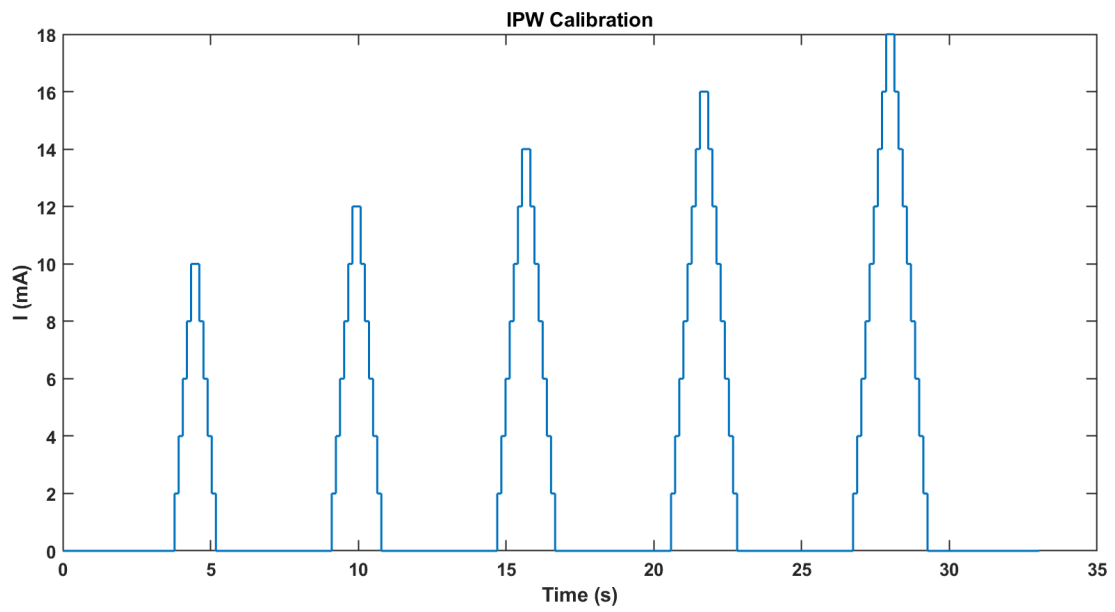
Figure 2.10: Example of the Continuous Channel List Mode [43]

#### 2.4.4 FES Calibration

In the ATC-FES system, the FES calibration process is crucial to define the limit intensity that can be employed to perform effective and tolerable electrical stimulations. The proper current intensity is set, delivering repetitive stimulation patterns to the patient at intervals of 4 seconds (Figure 2.11b), increasing the maximum pulse intensity from one stimulation to the next. A general pyramidal-shaped pattern (Figure 2.11a) is used for ramping up and down the current gradually, allowing a gradual excitation of nerves fibers [11]. The calibration is done when the stimulation is effective, without inducing discomfort in the patient. This calibration strategy can involve a single channel at a time, requiring a calibration repetition for each muscle investigated. The system allows the possibility of modulating the pulse width (PW) instead of the amplitude.



(a)



(b)

Figure 2.11: FES Calibration: (a) The pyramidal-shaped pattern employed for modulating the current intensity during the FES calibration. (b) Example of the calibration process, in which repetitive stimulation is delivered, increasing the maximum intensity. The acronym IPW refers to the possibility to calibrate either the current or the pulse width.

## Chapter 3

# Profile extraction algorithm

In the previous version of the ATC-FES system, presented in section 2.4, the two calibration phases were limited since they could not manage more than a single channel at a time. This approach increases the calibration time with the number of channels and prevents the calibration of complex multichannel movements. Moreover, as introduced in the section 2.4.4, the stimulation profile used for setting the FES parameter presents a symmetrical pyramidal shape, which did not represent the complexity of physiological muscle activation. On this basis, a different calibration approach was needed to extend the system application range and cope with higher-level functional movements.

Since daily life movements, such as the reaching and gait, involve the synergic activation of multiple muscle groups selectively recruited by the CNS, the FES calibration phase must be tailored to those specific activation patterns to induce the correct execution of the functional movement. In this project, the Profile Extraction algorithm (PE) has been proposed to extend the calibration to functional movements based on the synergic multichannel activation: The idea behind this method is to exploit the  $ATC_{max}$  calibration phase for extracting a multichannel ATC profile highly correlated to the muscle activation pattern generated during the voluntary movement. The resulting profile consists of a set of ATC sequences, representing the activation pattern of each channel expressed during a specific movement.

This information provides ATC maximum values produced by acquisition channels and a stimulation pattern to be used during the patient-side calibration. Reminding the purpose of the ATC-controlled FES system, it aims to improve FES results by modulating the electrical stimulation with a biomimetic pattern derived from the muscle activity. In the same way, this principle can also be applied to the FES calibration thanks to the extracted profile, improving the selection of the proper parameters. Furthermore, extracted profiles can be stored and used to deliver fully automated FES therapies that no longer require the simultaneous action of the therapist.

### 3.1 Processing pipeline

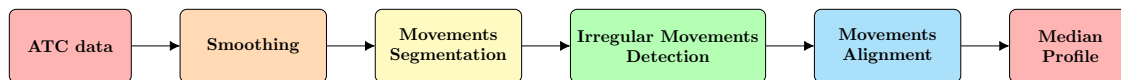


Figure 3.1: Schematic diagram of the Profile Extraction Pipeline.

The PE algorithm is structured in a processing pipeline, implemented into the ATC maximum calibration phase: The therapist has to perform a series of movement repetitions. At the same time, the muscle activity is collected using the wireless acquisition devices described previously in section 2.4.1. The pipeline takes the ATC values coming from acquisition channels and performs a series of processing stages that lead to the extraction of the final profile. Firstly, ATC sequences undergo a smoothing stage (Section 3.1.1), reducing the influence of background noise on ATC acquisitions. Then, regularized data sequences go through a segmentation step (Section 3.1.2), in which the algorithm detects ATC data segments that can be associated with an actual muscle contraction. The first two pipeline steps are performed in real-time during the data acquisition, working on all the investigating channels at the same time: ATC segments, generally called *movements*, are 2-D arrays in which rows correspond to ATC sequences of multiple investigating channels.

Once the user stops the acquisition, segmented *movements* undergo a selection step (Section 3.1.3), where they are compared to each other, and only those that show higher similarity are preserved. In the fourth step, the remaining data segments are aligned into a 3-D array, maximizing the cross-correlation (Section 3.1.4). The last processing step is responsible for the extraction of the final profile from the stack of movements.

#### 3.1.1 Smoothing

Despite the intrinsic robustness of the ATC technique to several noise alterations (Section 2.2), raw ATC data transmitted by acquisition channels must be regularized to smooth ATC sequences and reduce the number of spurious TC events which affect the baseline. In each channel, incoming ATC data are appended to a sliding window containing the previous values. The smoothing is achieved performing the median operation inside each window line.

The window width (WW) is an operating parameter that defines the number of ATC data involved in the median and consequently the level of smoothing: a higher window width value intensifies the smoothing effect but takes to an information loss, expressed as reduction of the maximum intensity of ATC sequences and their temporal resolution. The setting of the WW depends on the ATC sequences length and

the time interval length in which the ATC is computed. Considering a sequence of ATC values computed every 130 ms and a contraction duration which range from 2s to 7s, the WW parameter can range from 3 to 5 consecutive samples, but it can be further increased in case of persistent background noise.

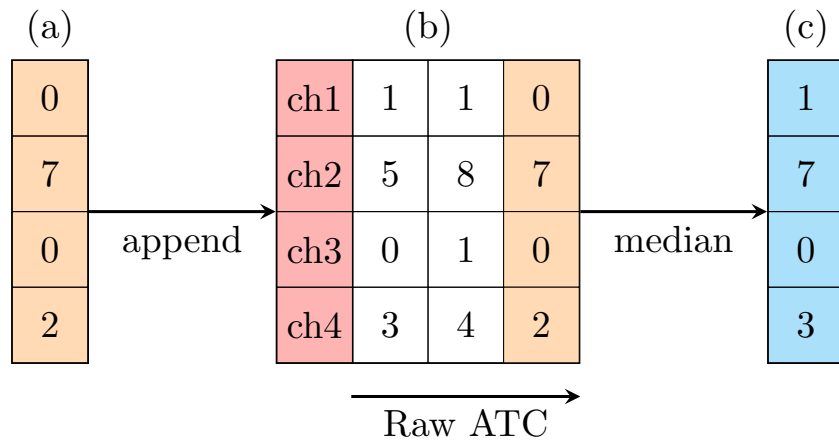


Figure 3.2: Example of the ATC smoothing process: Four acquisition channels send the lastly computed ATC data, organized in a column vector (a). The (a) vector is appended to the sliding window (b), which also stores the two previous ATC values of each channel ( $WW = 3$ ). Then, the median is performed along each row of the sliding window, generating a new column vector containing regularized ATC values (c).

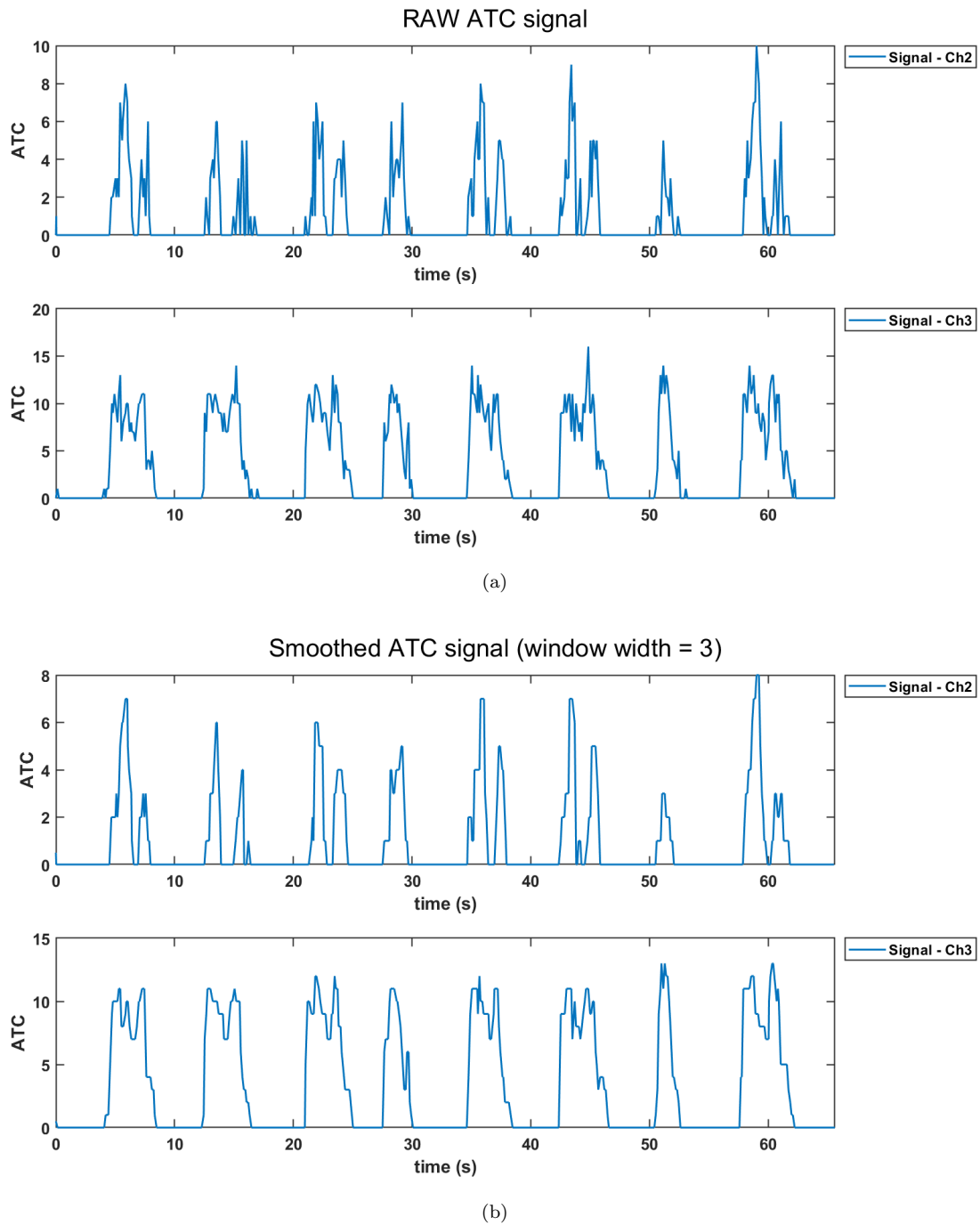


Figure 3.3: ATC smoothing example: (a) shows two raw ATC sequences recorded from two respective channels (*Ch2*, *Ch3*) during the repetitive execution of the drinking task (Figure 4.1). *Ch2* refers to the Biceps Brachii (BB), whereas *Ch3* represents the muscle activity of the Anterior Deltoid (AD). (b) shows the result of the smoothing process applied to both acquisition channels. The regularization effect of the smoothing on ATC sequences is clear.

### 3.1.2 Movements Segmentation

The Movements Segmentation process detects ongoing muscle contractions by checking the ATC data received from the Smoothing stage. Even though non-zero ATC values can be typically associated with muscle activity, sometimes even the background noise can produce spurious ATC spikes. Moreover, in the presence of persistent noise interference and the case of the wrong calibration of the ATC threshold, neither the smoothing can adequately prevent noisy ATC activations. In order to make the algorithm resilient to these alterations, two criteria have been introduced to determine if ATC sequences are part of a voluntary contraction or not:

**Channels activity:** The first criterion considers acquisition channels individually. It fundamentally assesses if channels exhibit an individual activity compatible with the voluntary contraction, classifying channels inactive or silent. The actual voluntary activity can be distinguished from the background noise considering sequences duration and peak intensities since the latter typically produces shorter and lower activation sequences. So, the channel is active when the sequence of last  $N$  ATC data contains non-zero elements (eq. 3.1) and a peak value higher than 2 ATC (eq. 3.2). The parameter  $N$  represents the minimum length of channel activation in terms of ATC samples and must be set according to the typical movement duration.

$$ATC_j \neq 0, \forall ATC_j \in ch_i \quad (3.1)$$

$$\max(ch_i) = ATC_{peak} > 2 \quad (3.2)$$

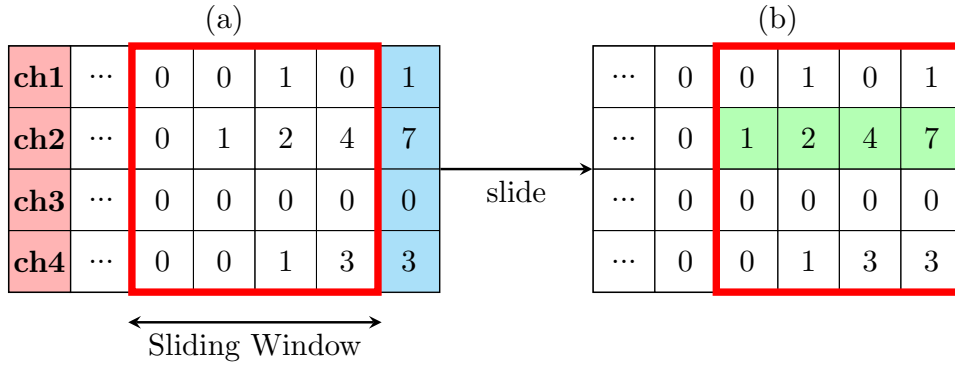


Figure 3.4: Example of channel activation: The channel activity is assessed considering the last  $N=4$  ATC values. Thus, a sliding window progressively checks the last 4 data verifying the satisfaction of activity conditions (eq. 3.1, 3.2). In (a), no channels are active since all sequences contain at least a zero value. On the contrary, in (b) the channel 2, marked in green, changes its status, becoming active.



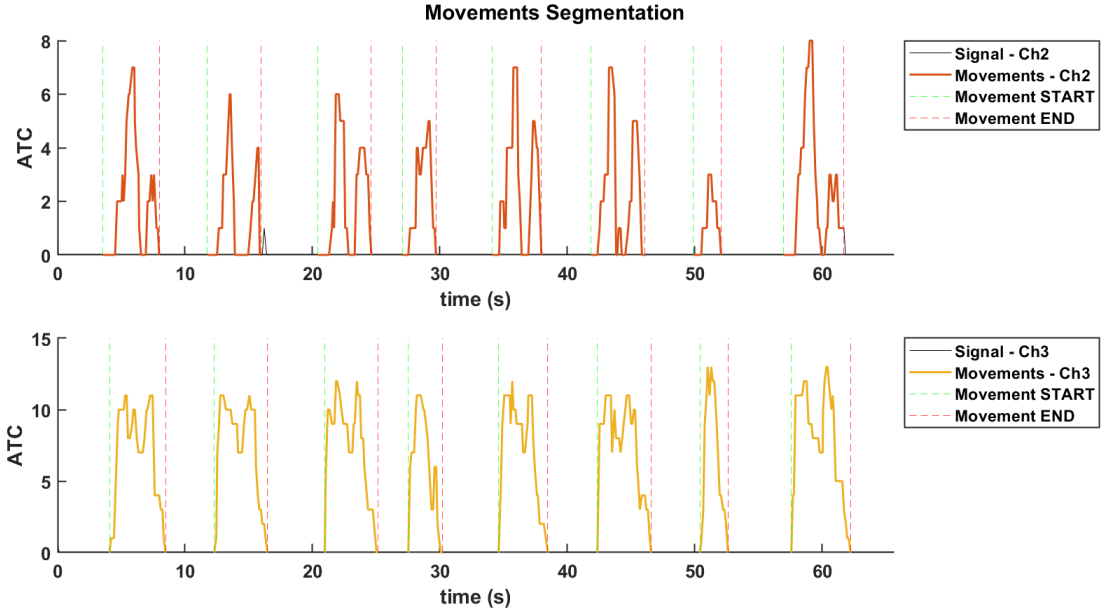


Figure 3.6: Movements Segmentation example: smoothed ATC sequences (3.3b) undergo the Movements Segmentation process, producing a collection of eight movements. As it can be noticed that the fourth and seventh activation sequences are different in shape, intensity, and duration from the others since they come from improper movement executions.

### 3.1.3 Irregular Movements Detection (IMD)

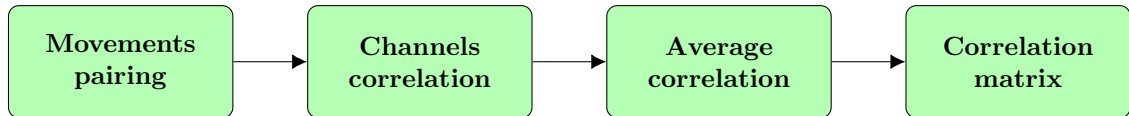


Figure 3.7: Schematic diagram of the Irregular Movements Detection process.

The IMD technique is performed at the end of the ATC acquisition and takes the collection of Movement matrices provided by the Segmentation stage. The algorithm selects the group of segments that exhibit the higher mutual similarity, starting from the assumption that most of the collection is made of regular and highly similar sequences. In the selection, Movement matrices are compared, extracting from each cross-check a Correlation Index ( $CI$ ), which quantifies the overall similarity between movement patterns and ranges from 0 to 1. The process outlined in figure 3.7 takes movement segments, expressed as multichannel 2-D arrays, and leads to the computation of the  $CI$ .

**1) Movements pairing:** Firstly, the system generates the list of all the possible combinations of segments included in the collection in order to compare each movement with the others (figure 3.8). Starting from a collection of  $N$  movements,  $\frac{N^2-N}{2}$  combinations are compared.

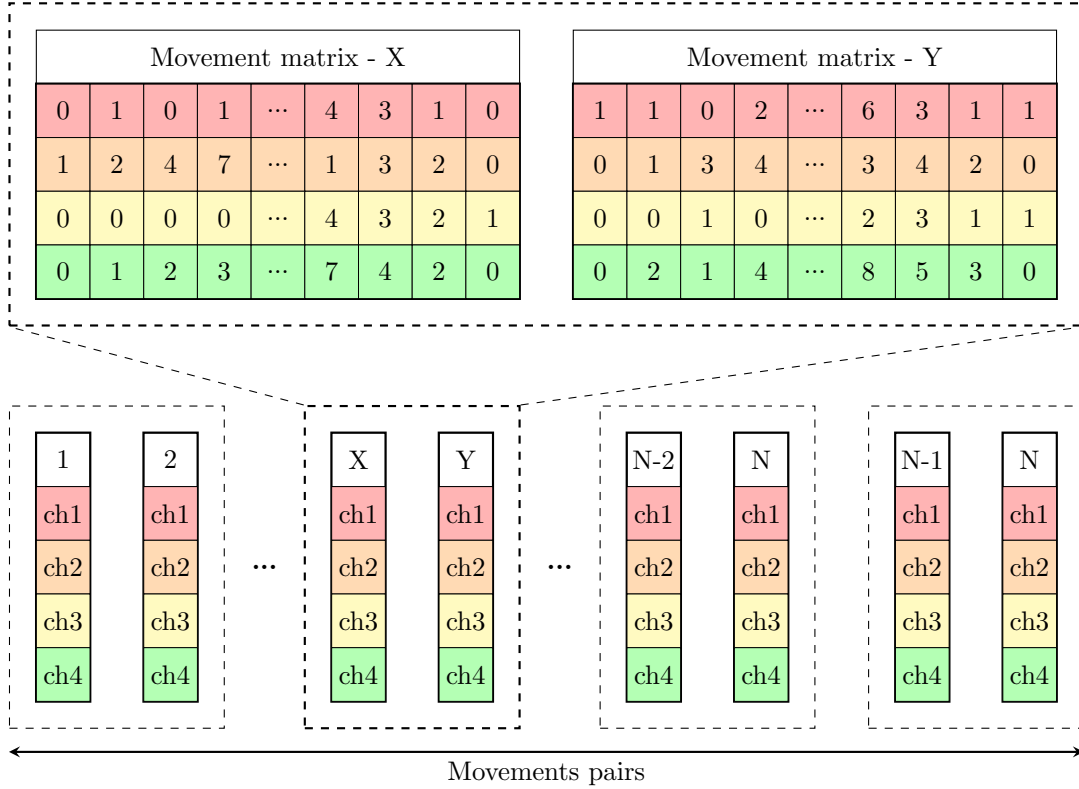


Figure 3.8: Paired Movement matrices: The figure zooms in on a generic pair of movements X and Y.

**2) Channels correlation:** The first step to compare two generic multichannel movements, X and Y, involves the computation of the cross-correlation ( $CC$ ) channel-by-channel (eq. 3.4): The operation returns a row vectors composed of  $L_x + L_y - 1$  elements, where  $L_x$  and  $L_y$  are the size of X and Y rows respectively. The  $CC$  vector estimates the similarity of two channel sequences as a function of their relative displacement. Thanks to the normalization factor, the function expressed by the equation 3.4 is sensitive to both pattern and intensity differences, returning the maximum value ( $CC = 1$ ) only if the two sequences are identical. The  $CC$  vectors are grouped in the  $CC_{xy}$  matrix (figure 3.9). The  $Lags_{xy}$  vector (eq. 3.5) contains values of relative displacement of Y channels respect to X channels,

which can be directly associated to each column of  $CC_{xy}$ .

$$CC_{xy}[ch, m] = \frac{\sum_{n=A}^B X_{ch}[n + m - L_y] \cdot Y_{ch}[n]}{\max(|X_{ch}|_2^2, |Y_{ch}|_2^2)} \quad (3.4)$$

$$Lags_{xy}[m] = m - L_y \quad (3.5)$$

$$m = 1, \dots, L_x + L_y - 1$$

$$A = \max(1, 1 - m + L_y)$$

$$B = \min(L_y, L_x + L_y - m)$$

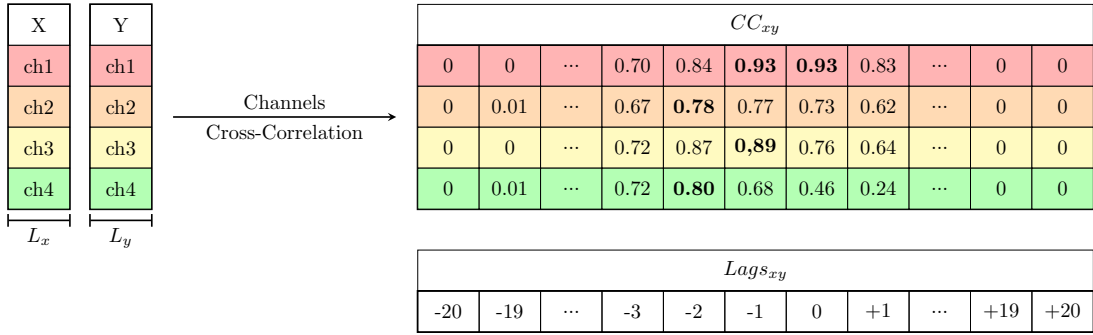


Figure 3.9: Channels Cross-Correlation computed between two different Movement matrices (X, Y)

**3) Average correlation:** A weighted mean of  $CC_{xy}$  rows is performed for merging channels similarities in an average correlation vector  $\overline{CC}_{xy}$  (figure 3.10). Weights are computed by quantifying the individual contribution of each channel proportionally to the activity. Specifically, the vector of weights is computed by integrating each channel sequence and averaging over the two movements involved (eq. 3.6a). Then, the resulting vector  $w_{xy}$  is eventually normalized (eq. 3.6b). Once the final weights vector  $W_{xy}$  is generated, the weighted mean is computed performing the inner product between  $W_{xy}$  and the matrix  $CC_{xy}$ .

$$w_{xy}[ch] = \frac{\sum_n X[ch, n] + \sum_m Y[ch, m]}{2} \quad (3.6a)$$

$$W_{xy}[ch] = \frac{w_{xy}[ch]}{\sum_{ch} w_{xy}[ch]} \quad (3.6b)$$

The Correlation index  $CI_{xy}$  is the maximum of the average correlation vector  $\overline{CC}_{xy}$  (eq. 3.7) and expresses the overall similarity between movement X and Y in a single parameter. The relative displacement between the two movement matrices is

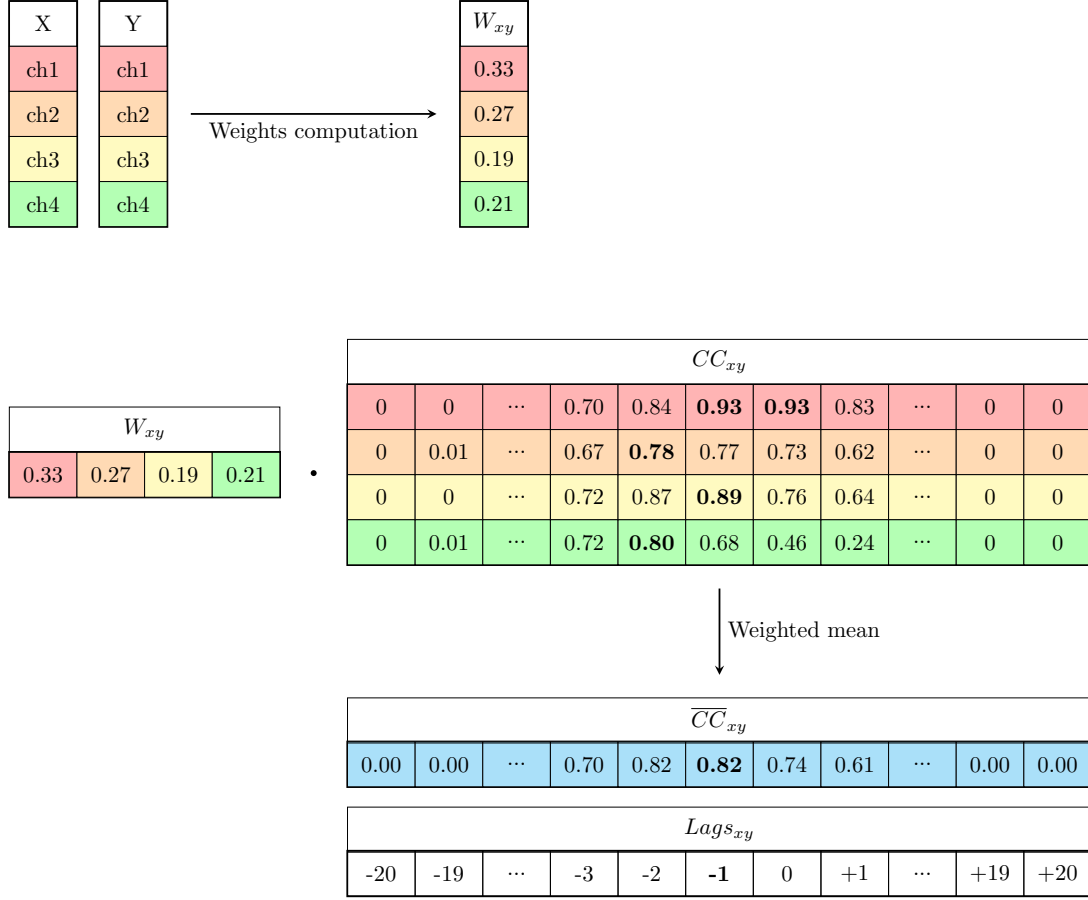


Figure 3.10: Computation of the Average correlation vector ( $\overline{CC}_{xy}$ ).

extracted from the  $Lags_{xy}$  vector.

$$CI_{xy} = \max(\overline{CC}_{xy}) \quad (3.7)$$

**4) Correlation matrix:** In the last step, the Correlation matrix is built by processing all the movement combinations. In this symmetrical matrix, rows and columns are associated with different movements, and each set of coordinates points to the Correlation Index of a specific movements combination (figure 3.11). The displacements associated with  $CI$  values are stored into an anti-symmetrical matrix, called Displacement matrix, where values represent lags between movements indexed by matrix columns and movements indexed by rows.

The Correlation matrix is then used for detecting irregular movements: indices contained into the matrix are compared with a fixed threshold value  $CC_{lim}$ . Two movements are similar if their  $CI$  is higher or equal to  $CC_{lim}$ , otherwise, they are

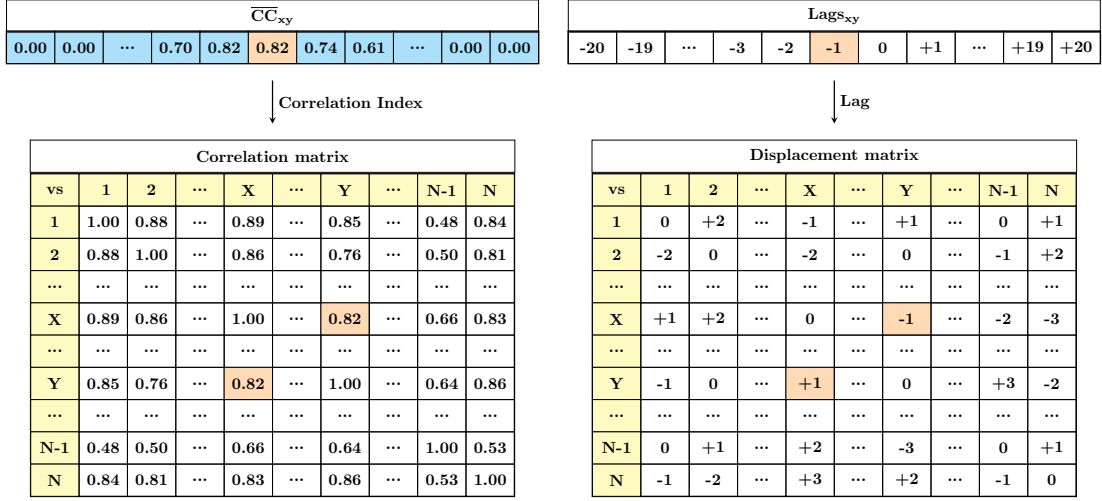


Figure 3.11: The Correlation matrix (left) and Displacement matrix (right) are built by processing all the movement combinations.

different (eq. 3.8a). Increasing the threshold level, both the similarity of regular movements and the process selectivity increase as well. During the project, a  $CC_{lim}$  equal to 0.7 has been used since it allows to discriminate regular movements in both single-channel and multi-channel applications flexibly.

If a movement shows a low similarity with most of the others (eq. 3.8b), it is considered irregular, and it is neglected from the movements collection. The removal of irregular movements is repeated iteratively until regular movements only remain in the collection. Even the Correlation matrix and Displacement matrix are corrected during the process, removing rows and columns related to irregular movements.

$$Low\ CI := \{CI \mid CI < CC_{lim}\} \quad (3.8a)$$

$$Irregular\ movement : \#Low\ CI \geq \frac{N^\circ\ Channels - 1}{2} \quad (3.8b)$$

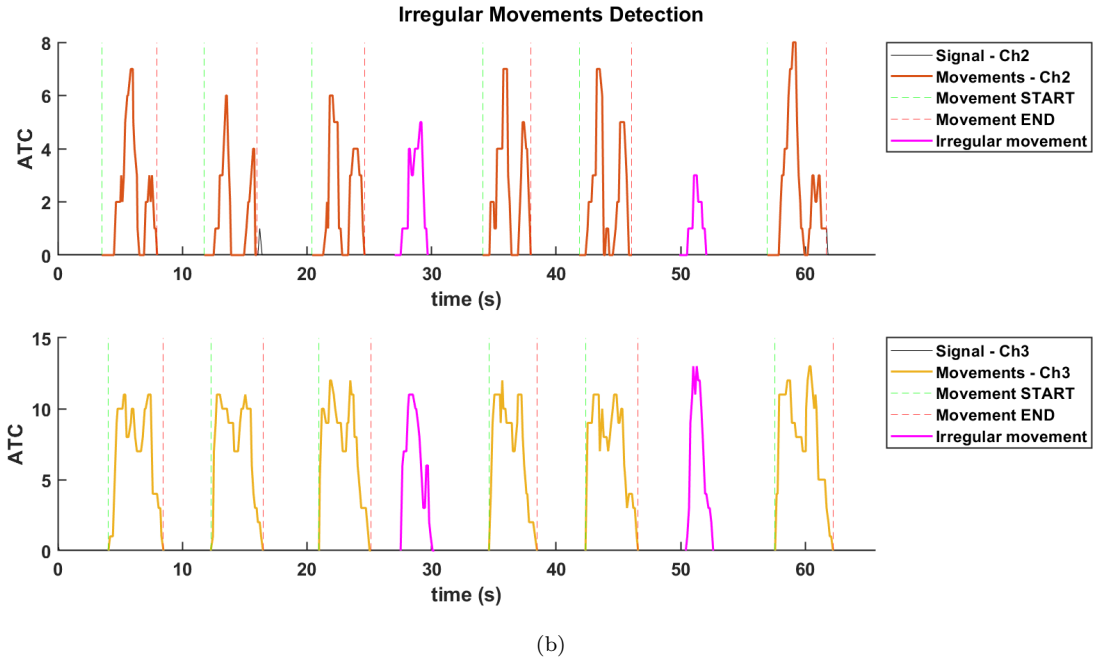
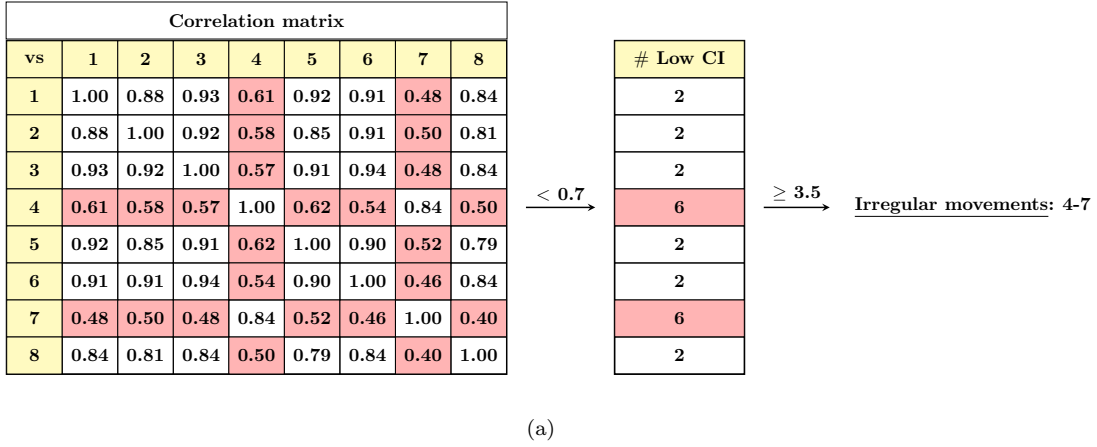


Figure 3.12: The collection of movements segmented in 3.6 are compared extracting the above Correlation matrix (a). Here, Correlation indexes lower than  $CC_{lim}=0.7$  are highlighted in red. If the number of low correlation values in a row is higher or equal to most movements, the respective movement is identified as irregular. The IMD algorithm has detected two irregular movements indexed by 4 and 7. (b) shows the result of the IMD process, which has identified the two irregular sequences.

### 3.1.4 Movements alignment and Profile extraction

After the IMD selection process, the remaining movements exhibit a high mutual correlation. Among them, the movement with the higher correlation values is selected as the reference. Before extracting the final profile, all the movements are



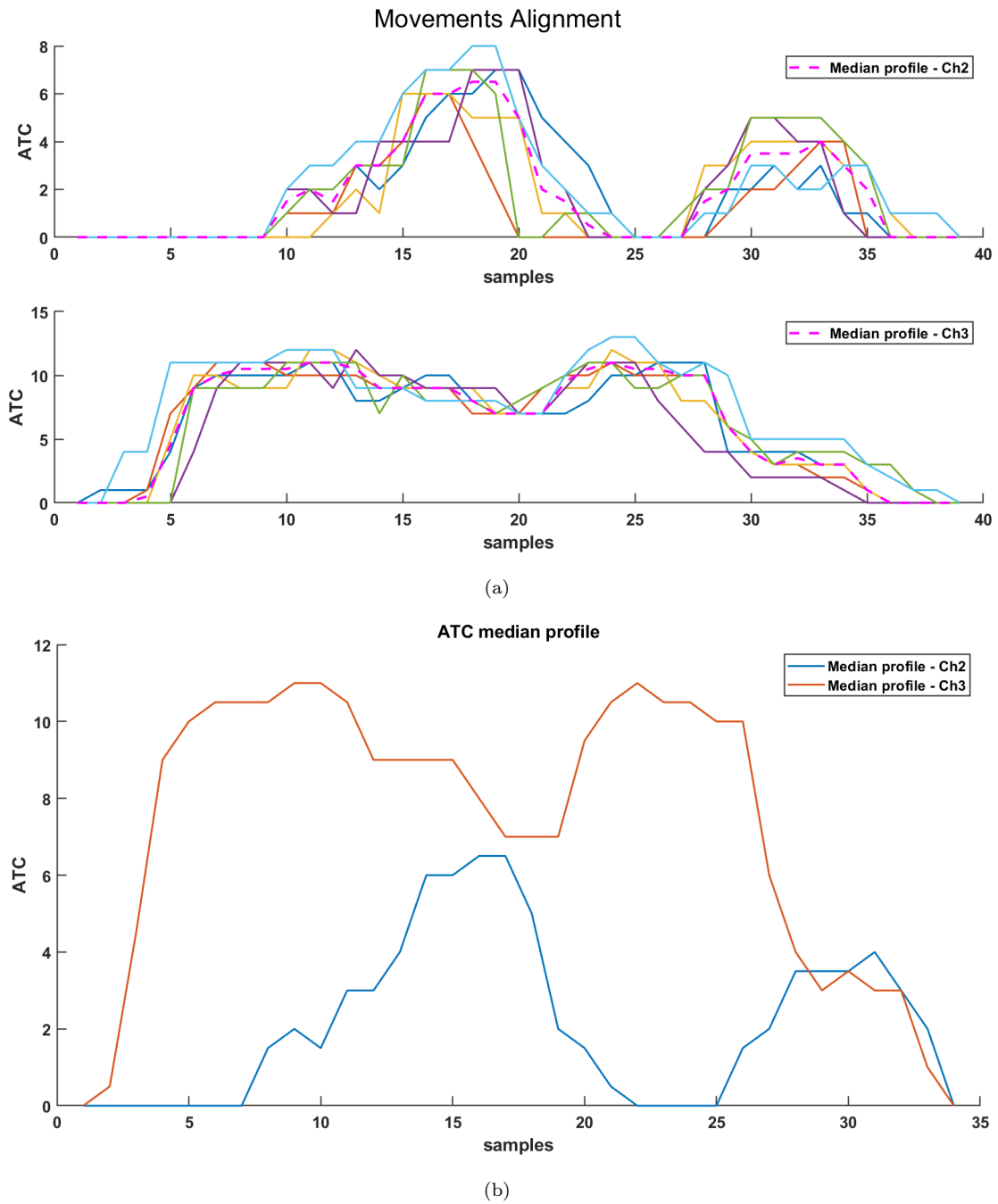


Figure 3.14: After the IMD, the resulting list of movements (3.12a) contains only those sequences which show high similarity. These movements are then aligned, maximizing their cross-correlations (a), and the median operation is performed across aligned movements generating the final activation profile. The profile is a multichannel ATC array in which each row is associated with a specific channel (b).

## 3.2 Algorithm development and system integration

The Profile Extraction algorithm has been firstly developed in Matlab for testing extraction performances on multichannel data recordings. Later, the algorithm was implemented in Python to integrate the Profile Extraction technique into the ATC-FES system. The implementation is based on two main classes: *ProfileGenerator* and *MovementSegmentation*. Since the Profile extraction algorithm involves the manipulation of multidimensional data, the classes exploit the NumPy library to organize data in array objects and easily perform operations with specific routines [10].

### 3.2.1 *ProfileGenerator*

This class is instantiated inside the object *System* each time that the  $ATC_{max}$  calibration is started and contains a set of methods which allow the execution of each stage of the Profile Extraction pipeline, except the movements segmentation, which is performed by a dedicated class, called *MovementSegmentation*.

#### Main attributes

- **window\_width**: It defines the width of the sliding window used in the smoothing of raw ATC events
- **cc\_lim**: It refers to the threshold value of Correlation Index used in the Irregular Movements Detection process.

#### Class methods

- **add\_channel(channelName)**: When the  $ATC_{max}$  calibration is started, the wireless communication with all the selected acquisition channels is progressively opened. This method is called for each channel that successfully responds, initializing internal data structures of the class according to the current number of channels.
- **start\_acquisition()**: After that all the selected channels are started, this method is called instantiating the object *MovementSegmentation* (Section 3.2.2) and enabling the acquisition of ATC data from *System*.
- **new\_atc(channel\_name, atc\_raw)**: Each time that the object *system* receives a Bluetooth notification from an acquisition device, this method is called to submit the ATC value to the *ProfileGenerator* object, specifying the channel of origin. Then inside the object, the raw ATC undergoes a smoothing process

by calling the method *raw\_atc\_smoothing*. Since the PE algorithm works on all channels synchronously, processed ATC data are appended to an input buffer, ensuring data synchronization without losing information. The buffer consists of a dictionary of lists indexed by channel names. When all the buffer channels contain at least an ATC value, first arrived data are grouped into a vector and are sent to the segmentation object.

- *raw\_atc\_smoothing*(atc\_raw, channel\_name): This method implements the smoothing process, described in section 3.1.1. A sliding window, represented by a dictionary of lists, is used for regularizing the raw ATC value with the previous data. Specifically, the method appends the last received ATC event to the end of the respective channel list and removes the first element in order to maintain the number of elements in the list equal to **window\_width**. Then, the median operation is performed in the list, returning the smoothed ATC value.
- *end\_acquisition*(): This method is called at the end of the calibration and triggers the interruption of the segmentation and the progression to the next pipeline steps. The method retrieves the list of movements sequences from the segmentation object, and then calls *irregular\_movement\_detection* and *movements\_alignment* to extract the final multichannel profile, expressed as a 2-D array.
- *max\_cross\_correlation*(): This method takes the list of segmented movements and computes the Correlation Index for each pair of movements, and provides the set of Correlation and Displacement matrices to the Irregular Movements Detection.
- *irregular\_movement\_detection*(): This method implements the Irregular Movements Detection process (Section 3.1.3), detecting and removing irregular sequences from the list of movements.
- *movements\_alignment*(): This method organizes movements matrices 3-D alignment array (Figure 3.13). It firstly selects the reference movement associated with the row of the Correlation matrix, which shows higher values. Other movements are mutually shifted using values of the Displacement matrix related to the reference row and concatenated, equalizing the dimensions by zero-padding.
- *get*(channel\_name): This method allow the object *System* to interact with *ProfileGenerator* and retrieve the ATC profile of a specified channel. If the channel name provided as input is *None*, the method returns a zero vector with the same length of the extracted profiles.

### 3.2.2 *MovementSegmentation*

This class is responsible for the segmentation of multichannel ATC sequences, and it is instantiated inside the *ProfileGenerator* object when the *start\_acquisition* method is called. The movement segmentation process outlined in section 3.1.2 is based on the assumption that acquisition channels are linked, producing coordinated activations. This statement cannot be true for muscle groups located in a different part of the body, i.e., muscles in opposite limbs. The main advantage of implementing segmentation in a separated class is the possibility of performing the profile extraction on different muscle groups that activate interdependently by instantiating a segmentation object for each group investigated.

#### Main attributes

- **min\_len**: The minimum number of consecutive ATC values checked to determine the channel activation in the movements segmentation process.
- **delay\_min**: It defines the minimum distance, expressed as the number of consecutive ATC samples, between two different movements. It is crucial in discontinuous channels activation, where a movement can contain a temporary simultaneous inactivation in all acquisition channels.
- **GF**: This attribute refers to the Group Factor, which plays a crucial role in the definition of the movement.

#### Class methods

- **update(atc)**: This method is called by *ProfileGenerator* whenever it has a new set of ATC values from all recording channels, updating the segmentation object. ATC data are organized in a column vector provided as input and appended to the ATC buffer. The buffer behaves like a sliding window with a fixed dimension (**min\_len**) and is used to progressively check the activity of channels and then the presence of an ongoing movement each time that a new set of ATC data is received. The Group Factor is used to stabilize the movement detection when many recording channels are employed, fixing a minimum number of active channels to define a movement activation and reducing the influence of noisy channels. When a movement is detected, incoming ATC values are concatenated to a Movement matrix until the conditions introduced in section 3.1.2 are no more satisfied. Here, the attribute **delay\_min** is used to check if the movement is definitively concluded, counting the number of consecutive iterations in which no relevant activity is detected. Once the movement is terminated, the matrix is appended to the list of movements, and the object is ready to detect a new movement.

- **stop()**: This method stops the segmentation process and returns the complete list of movements as output.

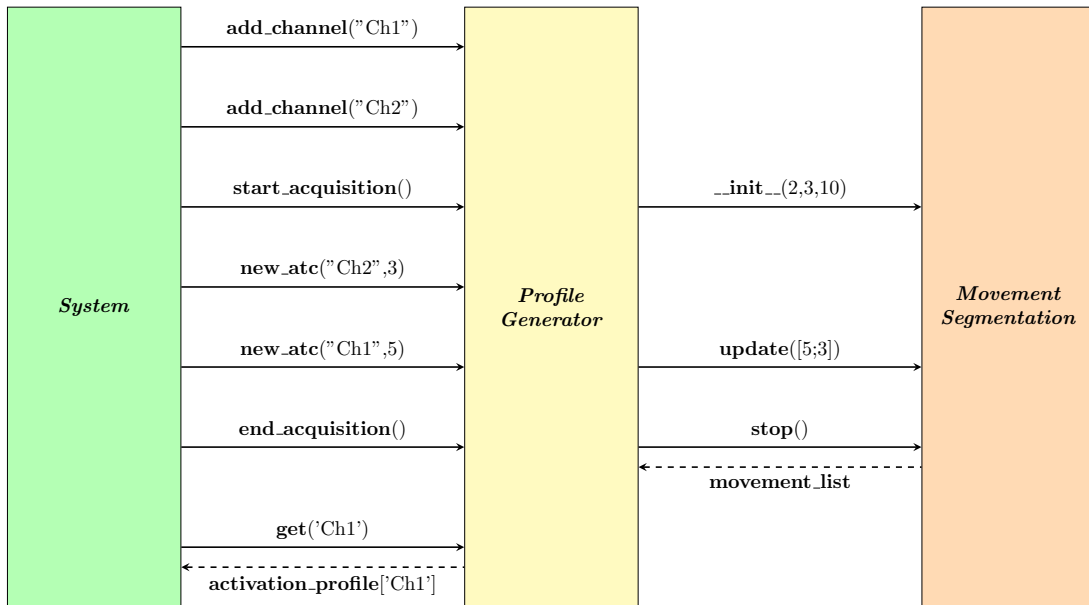


Figure 3.15: Example of communication between PE objects: the object *System* receives data from 2 acquisition channels ('Ch1' and 'Ch2'), so *ProfileGenerator* must collect data from both of them before updating the segmentation object. The *MovementSegmentation* is instantiated by setting the number of channels (2), the minimum length of a movement (3 consecutive ATC values), and the minimum distance between movements (10 ATC values). Thick lines represent the method calls, whereas dashed lines refer to the method response.

### 3.3 Preliminary tests

In order to test the segmentation and selection performances of the Profile Extraction algorithm, a preliminary investigating was conducted. Two healthy subjects were involved in a series of experimental sessions consisting of the repetitive execution of 4 daily life tasks. In each session, the muscle activity was measured exploiting the g.HIamp system [32] made by g.tec GmbH, which is a professional acquisition device designed explicitly for invasive and non-invasive biosignal recordings (figure 3.16). This system allowed the bipolar acquisition of the EMG signal from 28 different channels.



Figure 3.16: g.HIAMP: high performance biosignal amplifier [32].

The movements involved the upper and lower parts of the body separately: Two reaching movements were studied, measuring the right arm’s muscle activity and the torso. The former task is called *Drinking* (Section 4.1) and is represented by the action of grabbing a glass and simulating the drinking action. The latter is named *Shoulder Scratching* and is performed reaching the contralateral shoulder with the right hand and reproducing the scratching movement. Regarding lower limbs, they are involved in two basic exercises, standing up from the sit position and later climbing a step with the right leg. Each session is composed of 5 movements repetitions, separated by 10 seconds of rest. During a session recording, the EMG signal was manually segmented in real-time by an operator, placing markers at the beginning and the end of the movement execution. For each task, 4 sessions were performed, for a total of 16 experimental trials per subject. Later, experimental data were processed on Matlab, performing the ATC technique via software and applying the Profile Extraction algorithm on resulting multichannel sequences. Since the number of ATC sequences processed simultaneously is

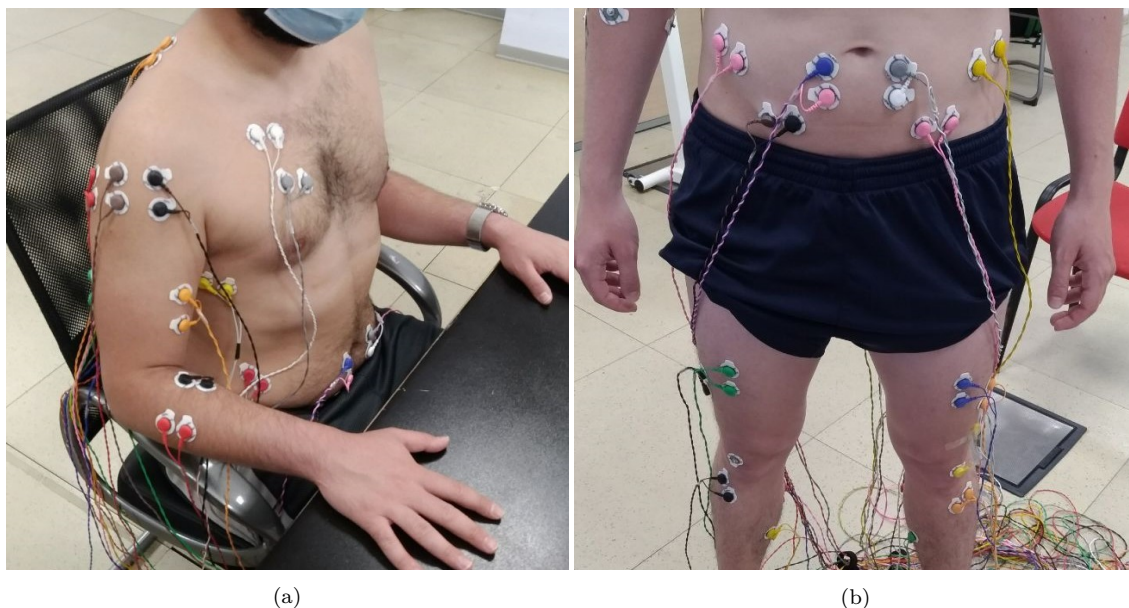


Figure 3.17: Preliminary tests: sEMG Electrodes placement configurations. (a) the upper body configuration. (b) the lower body configuration.

relatively high, at least one noisy channel can compromise the segmentation process. The Group Factor (GF) parameter, described in section 3.1.2, was introduced to increase the overall resistance of the PE algorithm to the presents of background noise. So three different trials were performed to validate the use of the GF parameter and the IMD selection process: Firstly, the PE was run disabling both the GF and IMD process (GF=0 - IMD=0). Then, the Group Factor was introduced in the second trial, determining sequences segmentations if more than 2 out of the total 28 channels were simultaneously active (GF=0.1 - IMD=0). In the last trial, even the selection process was enabled to remove irregular segments (GF=0.1 - IMD=1). Three main parameters were computed in each trial to assess the performances of the algorithm:

- Segmentation Lag: A segment is defined by two timing indices: the movement's beginning (onset) and ending (ending). This parameter is computed by subtracting the algorithm's segmentation to the closest manual segmentation, considered as the ground truth. The time lag is expressed in seconds and is computed individually for the onset and ending indices. It is positive if the index of the PE segmentation anticipates the respective of the manual one.
- Median Correlation (CC): This parameter measures the median similarity among movements of the same experimental session. It is computed performing the median on the Correlation matrix (Section 3.1.3) of the session.
- Movements Difference: This parameter is the subtraction between the actual

number of movements in each session and the number of segmented movements, corrected by the IMD process if enabled. Positive values can be due either to low segmentation performances or low inter-movements correlations. On the other hand, this parameter is negative when the segmentation algorithm shows poor selectivity, detecting additional spurious activations.

Results prove that the algorithm performances, in terms of segmentation accuracy and segments similarity, can be increased by employing the Group Factor and the Irregular Movements Detection. In the figure 3.18, the first trial (GF=0, IMD=0) shows a lack of segmentation accuracy, since many outliers are present. The second and especially the third (GF=0.1, IMD=1) exhibit a remarkable improvement, reaching a median value of -0.91 s for the onset and 0.39 s for the lag for the ending index. This result indicates that statistically, the automatic segmentation is included inside the manual one. The figure 3.19 shows the progressive increase of the similarity of the movements, starting from the median value of 0.68 and reaching 0.79 after the introduction of the IMD. The Movement Difference in all the three trials is equal to zero (Figure 3.20), but increasing of the algorithm selectivity negative values are removed, which means that the number of spurious activations is mostly reduced. At the same time, the number of positive differences has increased since the introduction of the IMD causes the general removal of low correlated activations.

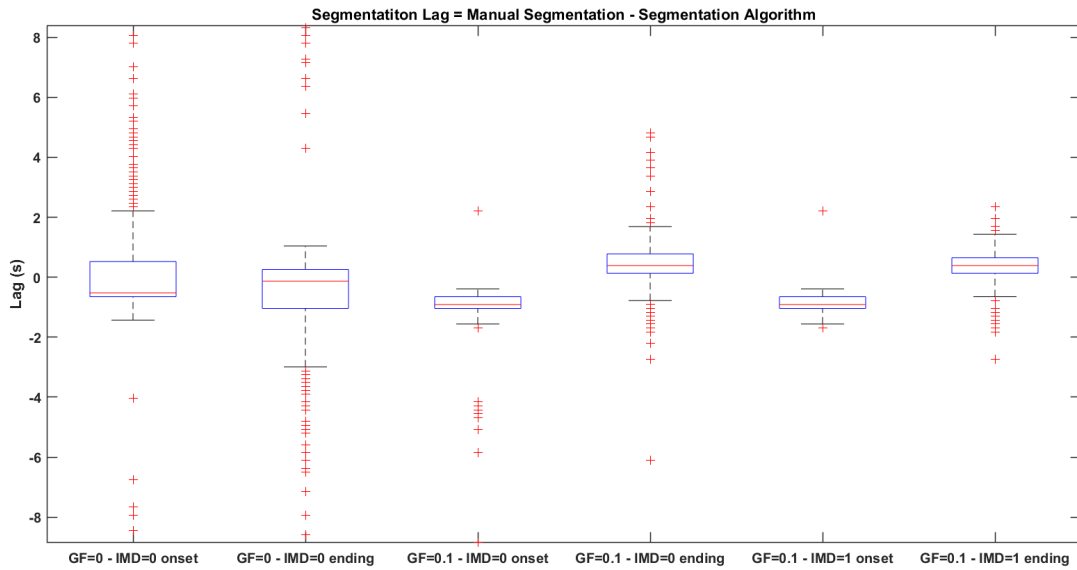


Figure 3.18: Profile Extraction validation: Segmentation Lags

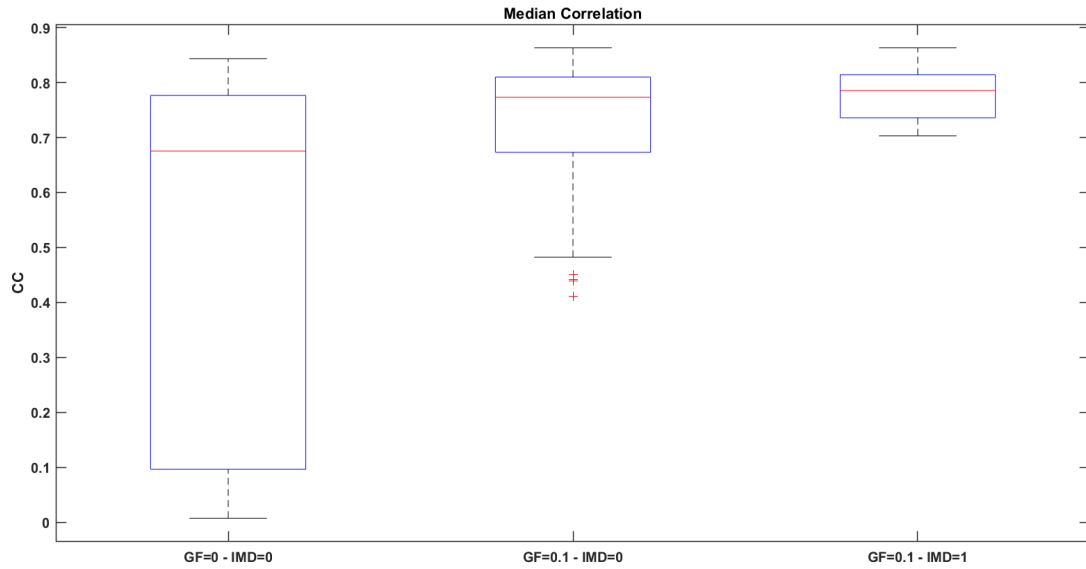


Figure 3.19: Profile Extraction validation: Median Correlations

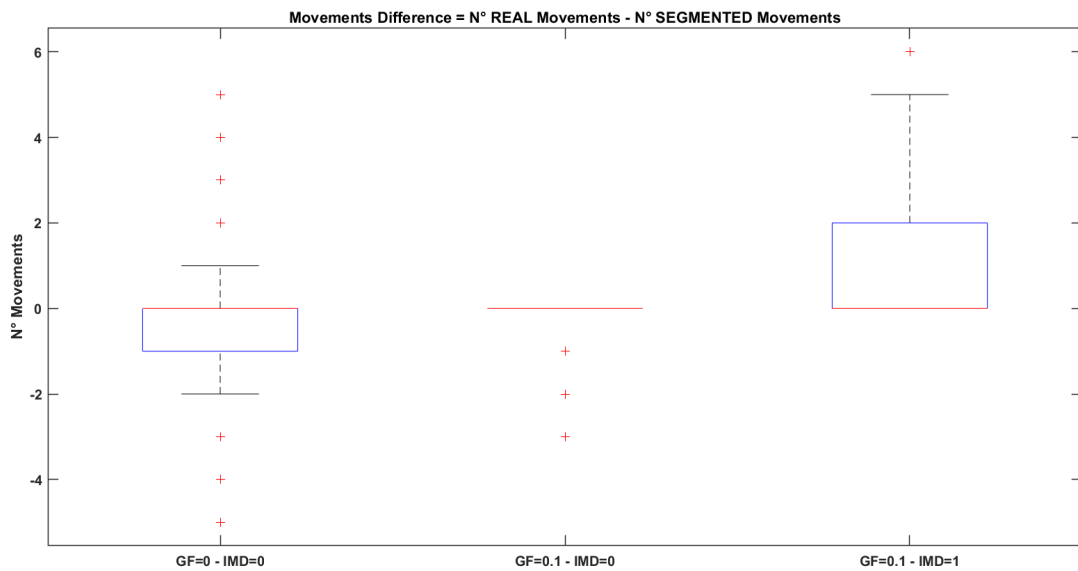


Figure 3.20: Profile Extraction validation: Movements Difference

## Chapter 4

# Multichannel ATC-FES: Calibration validation

The experimental validation was conducted to prove the effectiveness of the optimization introduced in the ATC-FES system. Specifically, the test aims to demonstrate that the employment of the Profile Extraction algorithm in the system calibration phase can successfully stimulate a multichannel functional task. The validation is organized in sessions, in which a couple composed of a therapist and patient performs the whole ATC-FES process, starting from system calibrations and ending with the training phase. The training follows the master-slave approach, in which the sequence of ATC events produced by the therapist during the execution of the target movement is used to modulate the electrical stimulation of the patient. The validation involved eight healthy subjects, four males and four females, aged between 24 and 27. Subjects are organized into eight therapist-patient couples, where two subjects were identified as therapists, whereas the others were divided into two groups of patients associated with respective therapists. The study involved two types of FES calibrations: the former exploited the activation profile generated by the Profile Extraction and was identified by the acronym PE. The latter was based on the less specific pyramidal-shaped pattern (PYR).

Two exercises were selected to assess the system's performances in both single-channel and multichannel configurations. Thus, the Elbow Flexion was selected as the single-channel reference movement, involving the contraction of the Biceps Brachii. The second exercise was a reproduction of daily living multichannel movement identified with the name of *Drinking* task. This exercise begins with the subject sitting in front of a table on which a bottle is positioned. Then, the subject grabs the bottle by extending an arm and bringing the object to the mouth, simulating the drinking action. The exercise ends with the return step, in which the subject puts the bottle back on the table, returning to the initial rest position (Figure 4.1). This task involves the action of two main muscles: The Anterior

Deltoid (AD) controls the rotation of the glenohumeral joint, producing the elbow elevation with its contraction. The Biceps Brachii (BB) is the second main muscle responsible for the elbow joint's flexion.



Figure 4.1: The *Drinking* task is composed of 4 main movement phases: the subject starts in a rest phase, with both hands leaned on the table. Then, the activation of the Anterior Deltoid supports the reaching of the bottle. After the bottle grabbing, the subject lifts the bottle until it reaches the mouth. During this phase, both the Anterior Deltoid and Biceps Brachii operate together. The drinking action ends by laying down the bottle and returning to the starting position.

## 4.1 Materials

The validation was conducted employing the Vicon Motion Capture System [72] for tracing movement trajectories of therapist and patient during the FES training execution. This tool is based on 12 cameras placed in a room in different positions to provide multiple views of the internal space. Cameras detect the movements in the 3-D space of specific reflective markers disposed on subjects in specific body locations. Through a labeling process performed manually by an operator, the Vicon system connects markers generating digital reproductions of the subjects' body segments. Then, the system computes trajectories data from the relative movement of segments and joints. In order to obtain reliable information from Vicon recordings, reflective markers must be applied to subjects' bodies following the Plug-in Gait Reference Guide indications [71].

The ATC acquisition is performed employing a set of two devices, described in detail previously (Section 2.4.1), equipped with Kendall™ H124SG pre-gelled Ag/AgCl electrodes with a 24 mm diameter, produced by Covidien [50]. The two devices are placed on the two muscles investigated, following the indications of the SENIAM project [65] in order to ensure proper skin preparation.

The stimulation electrodes employed in this study are the re-usable PG470W model, produced by Fiab [28], characterized by a contact area of a  $3.5 \times 4.5$  cm size. Before any electrodes application, a thin layer of conductive gel is applied on the active surface to enhance the stimulation effect.



Figure 4.2: Validation setup: Electrodes placement. Two stimulation channel were applied on patient.

## 4.2 Methods

Each test session is organized in three main steps:

- $ATC_{max}$  calibration: The therapist performs a series of 7 executions of a specific task, separated by a few seconds of rest. The system exploits the Profile Extraction algorithm for generating the activation profile, representative of the therapist's muscle activity, and calibrating the maximum ATC level that the therapist can produce.
- FES calibration: The patient is stimulated iteratively with a specific pattern, selected between PE and PYR, increasing the maximal current intensity of 2 mA each time a new stimulation is delivered. A rest interval of 5 seconds separates consecutive stimulations, allowing the patient to recover before the subsequent stimulation and reducing muscle fatigue. In the case of multichannel stimulation, the two channels are stimulated simultaneously with respective patterns, and current peak intensities can be selectively maintained or increased according to the patient response. When all stimulated channels

seem to produce an effective stimulation, the calibration is stopped without causing the patient discomfort, setting the current intensity limits.

- Training phase: The therapist is asked to perform 3 series of 10 movement repetitions, separated by 10s of rest, and the patient is stimulated according to the therapist’s muscle activity. A rest interval of 5 minutes separates two consecutive training series.

Using two different FES calibration strategies, differences in training performances are expected since using a biomimetic stimulation pattern is supposed to provide a stimulation similar to that generated by the therapist during the training execution. In order to prove the optimization involved by using the Profile Extraction technique, each couple was asked to perform 4 sessions, differing in the task performed and FES calibration type: the table 4.1 shows the different combinations of task and calibration. In order to avoid that the execution order of sessions might cause a bias in the results, PE and PYR sessions were performed on different days.

Session_ID	Task	FES Calibration type
MCH_PE	Multichannel (MCH)	Profile Extraction (PE)
MCH_PYR	Multichannel (MCH)	Pyramidal stimulation (PYR)
SCH_PE	Single channel (SCH)	Profile Extraction (PE)
SCH_PYR	Single channel (SCH)	Pyramidal stimulation (PYR)

Table 4.1: Validation sessions: Each session is characterized by the execution of a specific task (MCH=Drinking, SCH=ELbow flexion) and the use of a stimulation profile type, selected between PE and PYR, for performing the FES calibration. Sessions that employ different calibrations were performed on different days.

Vicon trajectories represent the time evolution of joint angles and segments positions in the 3-D space. It is possible to verify the effectiveness of the FES, and consequently the calibration performances, by comparing angular and position data of therapist and patient during the training sessions.

In order to evaluate the ability of the FES system to induce a correct movement execution, two main trajectories are studied: The angle between the forearm and the humerus segment was used for evaluating the elbow flexion execution, while the translation of the elbow joint along the vertical z-axis was used for assessing the activity of the anterior deltoid.

The data processing was performed in the Matlab environment and started with the segmentation of trajectories to compare one-by-one movements of therapist and patient. Thus, for each couple of movements, the shape similarity between their trajectory segments is checked by computing the maximum of the normalized

cross-correlation coefficient ( $\rho$ ) 4.1.

$$\rho[m] = \frac{\hat{R}_{x,y}[m]}{\sqrt{\hat{R}_{x,x}[0]\hat{R}_{y,y}[0]}} \quad (4.1)$$

The delay between the therapist and patient movement represented a further evaluation parameter and was computed exploiting the trajectories segmentation, subtracting the beginning timestamps of the two movement segments.

### 4.3 Results

The study of movement similarity has highlighted that the employment of a biomimetic stimulation pattern in the patient calibration phase involves an overall improvement in both the considered trajectories (Figures 4.5a, 4.5b).

In multichannel sessions, elbow angles generally showed a low correlation between therapist and patient (Figure 4.5a), with a median value of 0.58 for PE sessions and 0.51 for PYR. This outcome can be explained considering that the therapist's trajectory is the result of the complex cooperation of multiple muscle groups and cannot be easily reproduced, stimulating only two muscles by FES (Figure 4.3). Moreover, the stimulation is performed without any voluntary intervention of the patient. Nevertheless, median correlation values higher than 0.93 were achieved through the stimulation of the anterior deltoid, producing vertical elevations trajectories of the elbow comparable to those of the therapist (Figures 4.5b, 4.4). The boxplot in figure 4.7a shows the results of the similarity analysis in the case of the single-channel task: the simplicity of the task performed is reflected by the high correlation between therapist and patient, which was additionally increased employing PE calibration strategy reaching a median value of 0.98.

As regards stimulation delays, their median values were not affected by the adoption of the PE calibration technique and did not overcome 0.7 seconds (Figures 4.6a, 4.6b). PE sessions showed slightly higher time delays than PYR cases performing the multichannel task, whereas the stimulation of the single-channel task produced the opposite result (Figure 4.7b).

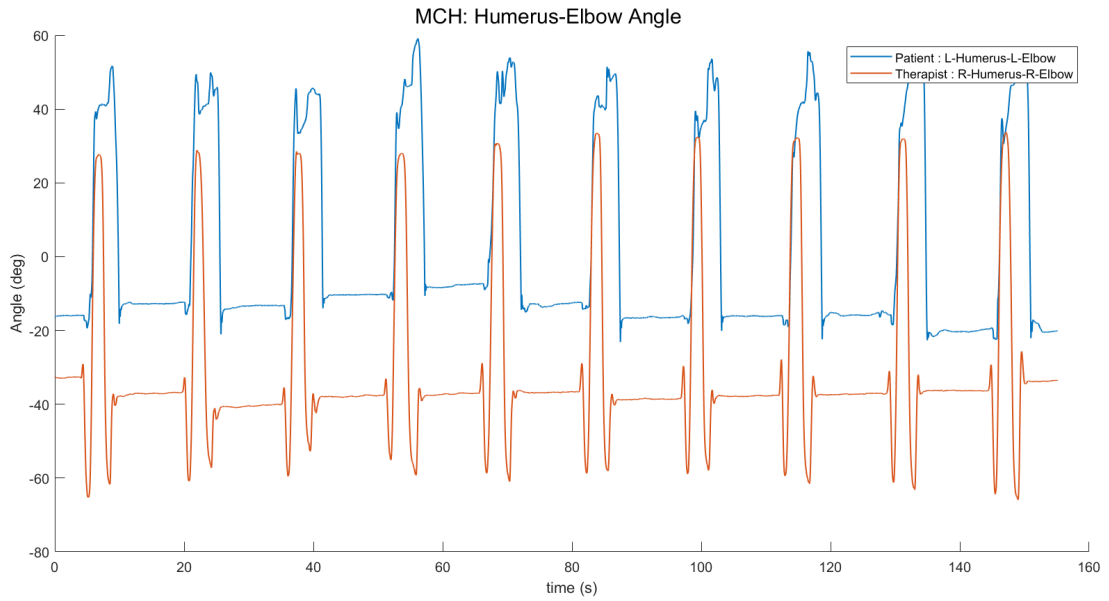


Figure 4.3: Elbow Flexion angle: Multichannel task. The positive angle variations represent the flexion movements. During each movement cycle, the therapist performs two low extensions associated with the reaching movement, whereas high-intensity peaks correspond to the bottle lifting phase.

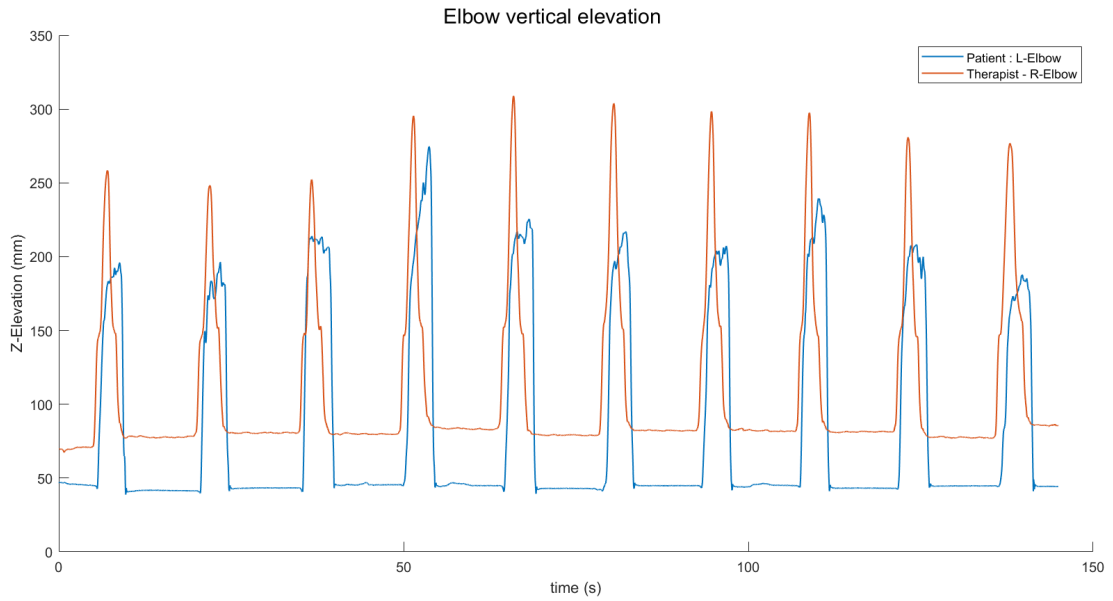
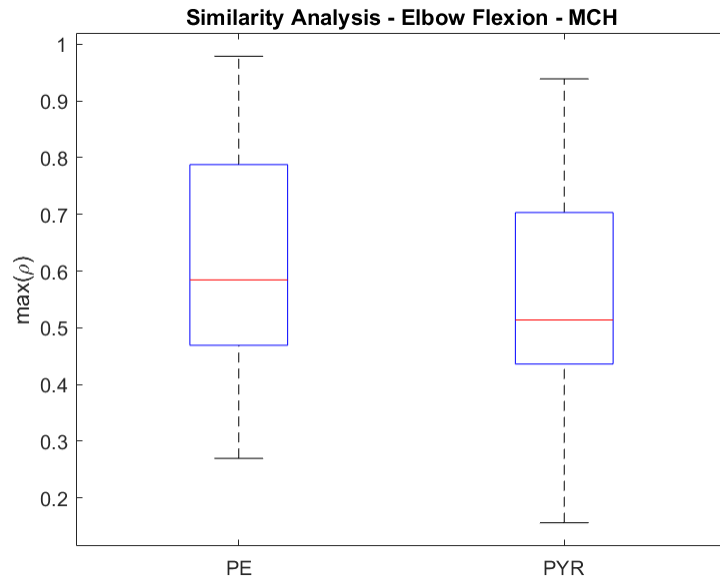
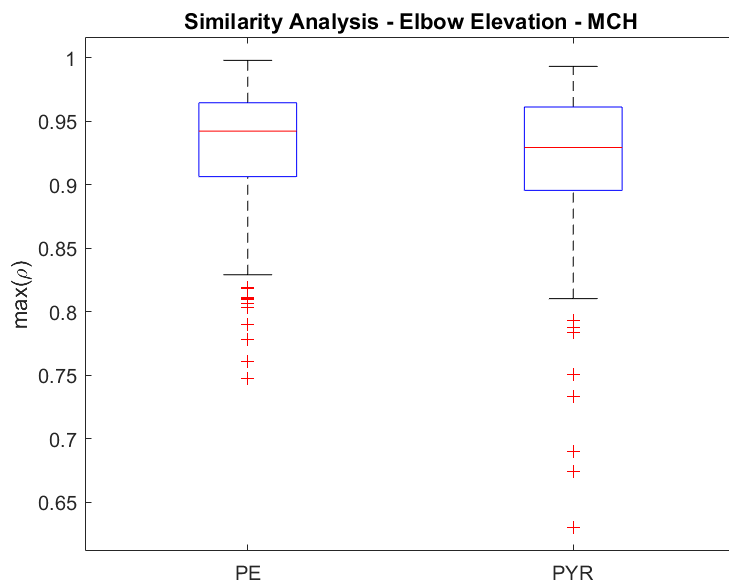


Figure 4.4: Elbow vertical elevation: Multichannel task.

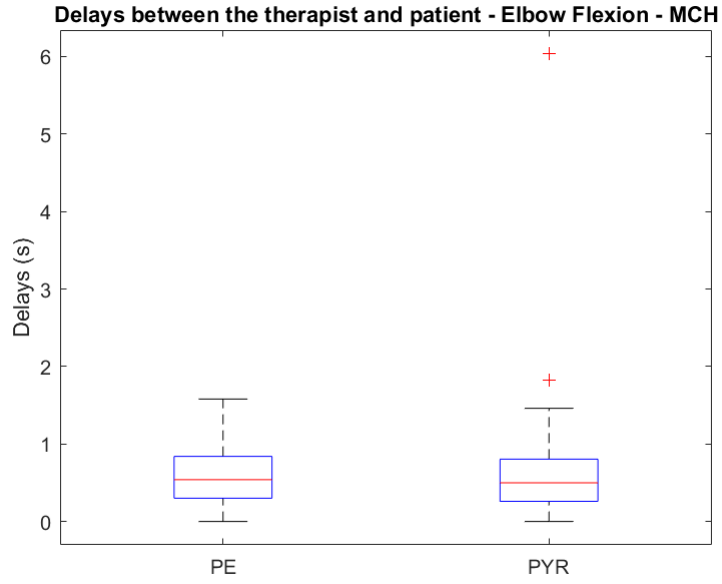


(a)

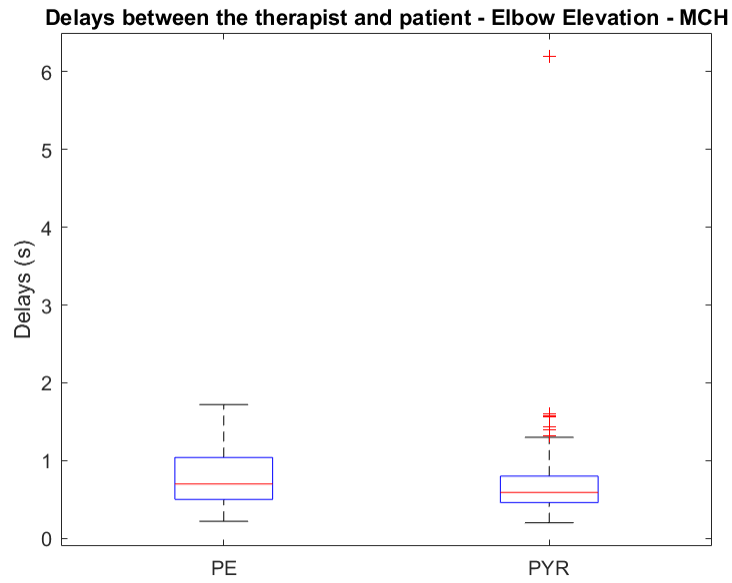


(b)

Figure 4.5: Similarity analysis boxplots: Multichannel task. (a) median values: PE = 0.58, PYR = 0.51; (b) median values: PE = 0.94, PYR = 0.93.

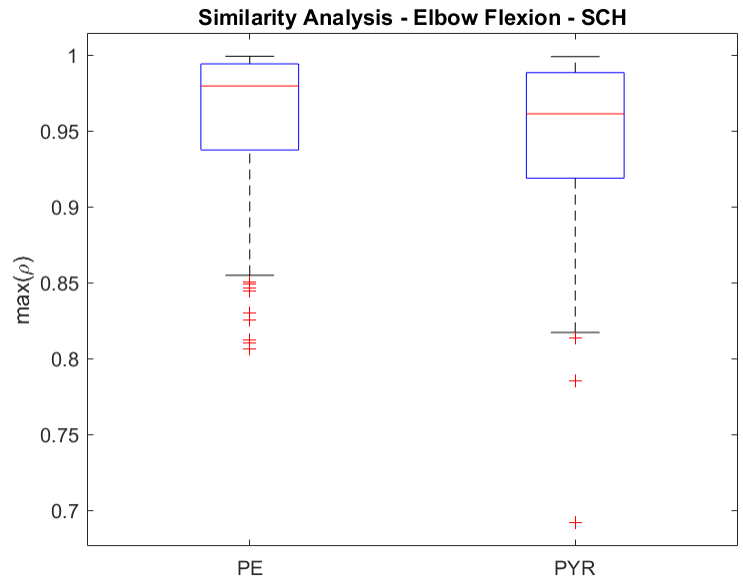


(a)

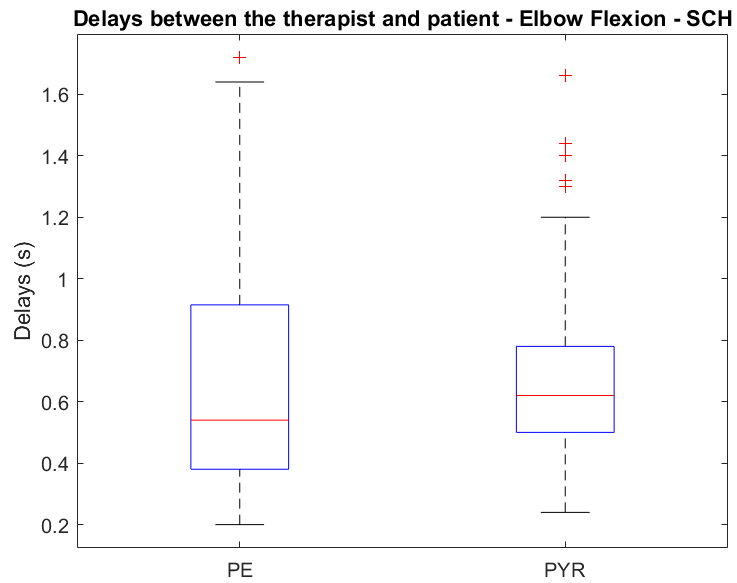


(b)

Figure 4.6: Movement delays boxplots: Multichannel task. (a) median values: PE = 0.54, PYR = 0.5; (b) median values: PE = 0.7, PYR = 0.59.



(a)



(b)

Figure 4.7: Single channel boxplots: Analysis of the similarity and delays. (a)  $\max(\rho)$  median values: PE = 0.98, PYR = 0.96; (b) Delays median values: PE = 0.54, PYR = 0.62.



# Chapter 5

## Conclusion

In an ATC-controlled FES system, the conversion of the muscle activity, expressed as Average Threshold Crossing values, into proper stimulation parameter represents the crucial step for effectively modulating the functional electrical stimulation. In a master-slave stimulation approach, the system calibration plays a crucial role, adapting the maximum stimulation intensity to the peak of muscle activity that the therapist can produce during the execution of a specific movement. The calibration is divided into two processes that operate individually: The ATC calibration process is oriented to the input stage of the system, analyzing the therapist's muscle activity and extracting max ATC value. The FES calibration works on the output stage and allows the operator to find the most effective stimulation settings. In the previous version of the ATC-FES system, calibration phases were limited since it could not manage more than a single channel at a time, and the stimulation profile used for setting the FES parameter did not represent the physiological muscle activation. Moreover, daily functional tasks are often the result of complex activation patterns involving different muscle groups. Hence, for extending the application scope of the ATC-FES system to the rehabilitation of functional tasks, an optimization of the whole calibration phase was necessary.

In this context, this thesis project aims to optimize an embedded ATC-controlled FES system, starting to approach new multichannel applications. A new calibration approach based on the custom-designed Profile Extraction algorithm has been proposed. This process allows the simultaneous calibration of multiple acquisition/stimulation channels, extending the system application to functional movements based on the synergic activation of multiple muscles. Moreover, the algorithm allows the extraction of a multichannel ATC sequence highly correlated with the voluntary activation pattern of the therapist's muscles. This information is then used to calibrate the maximum ATC value of each channel and to produce a biomimetic stimulation of the patient even during the FES calibration. Moreover, extracted profiles can be stored and used to deliver fully automated FES therapies, performing offline training sessions.

The Profile Extraction (PE) algorithm is implemented inside the ATC calibration phase. ATC sequences associated with the therapist action are segmented in real-time and undergo a processing pipeline during the signal acquisition, which removes irregular segments and extracts the statistical profile. The designing phase was followed by preliminary tests, which proved the effectiveness of the main blocks of the processing pipeline applying the algorithm to signal generated during the execution of four different tasks.

In the last part of the project, an experimental protocol was designed to validate the optimization solution introduced during this work. Specifically, eight therapist-patient couples were involved in structured experimental trials, in which whole ATC-FES sessions were conducted. Two different tasks involving one and two channels were analyzed to validate the system performances with different channel configurations. The second validation target was the comparison between the new FES calibration strategy, based on the Profile Extraction technique, and a second based on the generic pyramidal stimulation. Movement trajectories were used to assess stimulation performances and are collected using the Vicon motion tracking system.

Even though experimental trails differ only for the calibration strategy employed, the similarity comparison highlighted higher median cross-correlation in those trails which exploited the PE technique. In the multichannel task, median correlation values higher than 0.93 were achieved through the stimulation of the Anterior Deltoid, producing vertical elevations trajectories of the elbow comparable to those of the therapist. The simplicity of the Elbow Flexion task is reflected by the high correlation between therapist and patient, which was additionally increased employing PE calibration strategy reaching a median value of 0.98. The analysis of time delays between patient and therapist movements showed similar median values that were not affected by the adoption of the PE calibration technique and did not overcome 0.7 seconds. These results prove the effectiveness of the Profile Extraction algorithm applied to the calibration phase of an embedded ATC-FES system.

Starting from this work, it takes to further multichannel application: The Profile Extraction algorithm proved to successfully manage the processing of up to 28 channels simultaneously, offering the possibility to increase the number of controlled channels further. Future works should also focus on studying the co-modulation of multiple stimulation parameters to improve the stimulation response and manage the fatigue occurrence.

# Bibliography

- [1] Cc2540 - bluetooth® low energy wireless mcu with usb. <https://www.ti.com/product/CC2540>.
- [2] Cometa systems. <https://www.cometasystems.com/>.
- [3] Functional electrical stimulation. [https://en.wikipedia.org/wiki/Functional\\_electrical\\_stimulation](https://en.wikipedia.org/wiki/Functional_electrical_stimulation).
- [4] General principles - skeletal muscle anatomy. [https://www.brainkart.com/article/General-Principles---Skeletal-Muscle-Anatomy\\_21798/](https://www.brainkart.com/article/General-Principles---Skeletal-Muscle-Anatomy_21798/).
- [5] Instrumentation amplifier. [https://en.wikipedia.org/wiki/Instrumentation\\_amplifier](https://en.wikipedia.org/wiki/Instrumentation_amplifier).
- [6] Kivy - programming guide. <https://kivy.org/doc/stable/guide-index.html>.
- [7] Muscle fiber excitation, contraction, and relaxation. <https://open.oregonstate.education/aandp/chapter/10-3-muscle-fiber-excitation-contraction-and-relaxation/>.
- [8] Ou human physiology: Nervous system control of muscle tension. [https://cnx.org/contents/SNnPNNz9@1.9:5PgE7BA\\_@1/OU-Human-Physiology-Nervous-System-Control-of-Muscle-Tension](https://cnx.org/contents/SNnPNNz9@1.9:5PgE7BA_@1/OU-Human-Physiology-Nervous-System-Control-of-Muscle-Tension).
- [9] Surface emg sensor. <https://www.biometricsltd.com/surface-emg-sensor.htm>.
- [10] What is numpy? <https://numpy.org/doc/stable/user/whatisnumpy.html>.
- [11] K. Allen and C. Goodman. Functional electrical stimulation. [https://aci.health.nsw.gov.au/\\_\\_data/assets/pdf\\_file/0004/211819/Using-Electrical-Stimulation-January-2014.pdf](https://aci.health.nsw.gov.au/__data/assets/pdf_file/0004/211819/Using-Electrical-Stimulation-January-2014.pdf).
- [12] Giorgio Biagetti, Paolo Crippa, Laura Falaschetti, and Claudio Turchetti. A multi-channel electromyography, electrocardiography and inertial wireless sensor module using bluetooth low-energy. *Electronics*, 9(6):934, 2020.
- [13] Reza Boostani and Mohammad Hassan Moradi. Evaluation of the forearm emg signal features for the control of a prosthetic hand. *Physiological measurement*, 24(2):309, 2003.
- [14] Adrian Burden. Surface electromyography. *Biomechanical evaluation of movement in sport and exercise*, 01 2008.

- [15] Juan C. Calderón, Pura Bolaños, and Carlo Caputo. The excitation–contraction coupling mechanism in skeletal muscle. *Biophysical Reviews*, 6:133, 2014.
- [16] Enrique Mena Camilo, Jorge Airy Mercado Gutiérrez, Omar Piña Ramírez, Josefina Gutiérrez Martínez, Arturo Vera Hernández, and Lorenzo Leija Salas. A functional electrical stimulation controller for contralateral hand movements based on emg signals. In *2020 17th International Conference on Electrical Engineering, Computing Science and Automatic Control (CCE)*, pages 1–6, 2020.
- [17] Rubana H Chowdhury, Mamun BI Reaz, Mohd Alauddin Bin Mohd Ali, Ashrif AA Bakar, Kalaivani Chellappan, and Tae G Chang. Surface electromyography signal processing and classification techniques. *Sensors*, 13(9):12431–12466, 2013.
- [18] Mario Cifrek, Vladimir Medved, Stanko Tonković, and Saša Ostojić. Surface emg based muscle fatigue evaluation in biomechanics. *Clinical Biomechanics*, 24(4):327–340, 2009.
- [19] Marco Crepaldi, Marco Paleari, Alberto Bonanno, Alessandro Sanginario, Paolo Ariano, Duc Hoa Tran, and Danilo Demarchi. A quasi-digital radio system for muscle force transmission based on event-driven ir-uwb. In *2012 IEEE Biomedical Circuits and Systems Conference (BioCAS)*, pages 116–119, 2012.
- [20] Jasper R. Daube and Devon I. Rubin. Needle electromyography. *Muscle & Nerve*, 39(2):244–270, 2009.
- [21] Carlo J De Luca. Surface electromyography: Detection and recording. *DelSys Incorporated*, 10(2):1–10, 2002.
- [22] Carlo J De Luca, L Donald Gilmore, Mikhail Kuznetsov, and Serge H Roy. Filtering the surface emg signal: Movement artifact and baseline noise contamination. *Journal of biomechanics*, 43(8):1573–1579, 2010.
- [23] George V Dimitrov, Todor I Arabadzhiev, Katya N Mileva, Joanna L Bowtell, Nicola Crichton, and Nonna A Dimitrova. Muscle fatigue during dynamic contractions assessed by new spectral indices. *Medicine and science in sports and exercise*, 38(11):1971, 2006.
- [24] Catherine Disselhorst-Klug, Thomas Schmitz-Rode, and Günter Rau. Surface electromyography and muscle force: Limits in semg–force relationship and new approaches for applications. *Clinical Biomechanics*, 24(3):225–235, 2009.
- [25] Robert A Donatelli. *Sports-Specific Rehabilitation-E-Book*. Elsevier Health Sciences, 2006.
- [26] Barbara M Doucet, Amy Lam, and Lisa Griffin. Neuromuscular electrical stimulation for skeletal muscle function. *The Yale journal of biology and medicine*, 85(2):201, 2012.
- [27] Dario Farina, Roberto Merletti, Barbara Indino, Marisa Nazzaro, and Marco Pozzo. Surface emg crosstalk between knee extensor muscles: experimental and

- model results. *Muscle & Nerve: Official Journal of the American Association of Electrodiagnostic Medicine*, 26(5):681–695, 2002.
- [28] FIAB. Prodotti. <https://www.fiab.it/prodotti.php>.
- [29] Walter R Frontera and Julien Ochala. Skeletal muscle: a brief review of structure and function. *Calcified tissue international*, 96(3):183–195, March 2015.
- [30] S.K. Gollapudi, J.J. Michael, and M. Chandra. Striated muscle dynamics. In *Reference Module in Biomedical Sciences*. Elsevier, 2014.
- [31] Chris M Gregory and C Scott Bickel. Recruitment patterns in human skeletal muscle during electrical stimulation. *Physical therapy*, 85(4):358–364, 2005.
- [32] g.tec medical engineering GmbH. g.hiamp. [https://www.gtec.at/product/ghiamp/?gclid=CjwKCAiAqIKNBhAIEiwAu\\_ZLDtKRFEQ8F\\_TqZ7eLRWkMQGbT-rFqPcfuSHd5aHroMfqcsefvqBugnhoCEPYQAvD\\_BwE](https://www.gtec.at/product/ghiamp/?gclid=CjwKCAiAqIKNBhAIEiwAu_ZLDtKRFEQ8F_TqZ7eLRWkMQGbT-rFqPcfuSHd5aHroMfqcsefvqBugnhoCEPYQAvD_BwE).
- [33] David Alejandro Fernandez Guzman, Stefano Sapienza, Bianca Sereni, and Paolo Motto Ros. Very low power event-based surface emg acquisition system with off-the-shelf components. In *2017 IEEE Biomedical Circuits and Systems Conference (BioCAS)*, pages 1–4. IEEE, 2017.
- [34] Samar Hamid and Ray Hayek. Role of electrical stimulation for rehabilitation and regeneration after spinal cord injury: an overview. *European Spine Journal*, 17(9):1256–1269, 2008.
- [35] HASOMED GmbH. *Operation Manual RahStim2, RehaMove2*, 2012.
- [36] Stéphanie Hody, Jean-Louis Croisier, Thierry Bury, Bernard Rogister, and Pierre Leprince. Eccentric muscle contractions: Risks and benefits. *Frontiers in Physiology*, 10:536, 2019.
- [37] Morufu Olusola Ibitoye, Nur Azah Hamzaid, Nazirah Hasnan, Ahmad Khairi Abdul Wahab, and Glen M Davis. Strategies for rapid muscle fatigue reduction during fes exercise in individuals with spinal cord injury: a systematic review. *PloS one*, 11(2):e0149024, 2016.
- [38] Woohyoung Jeon and Lisa Griffin. Effects of pulse duration on muscle fatigue during electrical stimulation inducing moderate-level contraction. *Muscle & nerve*, 57(4):642–649, 2018.
- [39] Maikutlo B Kebaetse, Samuel C Lee, Therese E Johnston, and Stuart A Binder-Macleod. Strategies that improve paralyzed human quadriceps femoris muscle performance during repetitive, nonisometric contractions. *Archives of physical medicine and rehabilitation*, 86(11):2157–2164, 2005.
- [40] R Benjamin Keeton and Stuart A Binder-Macleod. Low-frequency fatigue. *Physical therapy*, 86(8):1146–1150, 2006.
- [41] Trisha Kesar and Stuart Binder-Macleod. Effect of frequency and pulse duration on human muscle fatigue during repetitive electrical stimulation. *Experimental physiology*, 91(6):967–976, 2006.
- [42] A.M. King, D.S. Loiselle, and P. Kohl. Force generation for locomotion of vertebrates: skeletal muscle overview. *IEEE Journal of Oceanic Engineering*, 29(3):684–691, 2004.

- [43] Bjoern Kuberski. *ScienceMode2, RehaStim2 Stimulation Device, Description and Protocol*. HASOMED GmbH, 2012.
- [44] Ganhui Lan and Sean X. Sun. Dynamics of myosin-driven skeletal muscle contraction: I. steady-state force generation. *Biophysical Journal*, 88(6):4107–4117, 2005.
- [45] Zuo Zheng Lou, Peng Yao, and Dingguo Zhang. Wireless master-slave fes rehabilitation system using semg control. In *International Conference on Intelligent Robotics and Applications*, pages 1–10. Springer, 2012.
- [46] P. J. Mansfield and D. A. Neumann. *Essentials of Kinesiology for the Physical Therapist Assistant*. Elsevier Health Sciences, 2014.
- [47] Hamid Reza Marateb, Mislav Jordanic, Monica Rojas-Martínez, Joan Francesc Alonso, Leidy Yanet Serna, Mehdi Shirzadi, Marjan Nosouhi, Miguel Ángel Mañanas, and Kevin C McGill. Reliable and accurate information extraction from surface electromyographic signals. In *Modelling and Analysis of Active Biopotential Signals in Healthcare, Volume 1*, 2053-2563, pages 7–1 to 7–18. IOP Publishing, 2020.
- [48] Frederic Martini et al. *Anatomy and Physiology'2007 Ed*. Rex Bookstore, Inc., 2006.
- [49] Kei Masani and Milos R Popovic. Functional electrical stimulation in rehabilitation and neurorehabilitation. In *Springer handbook of medical technology*, pages 877–896. Springer, 2011.
- [50] Medtronic. Covidien products. <https://www.medtronic.com/covidien/en-us/products.html>.
- [51] George Z. Mentis. Chapter 28 - the spinal and peripheral motor system. In Larry R. Squire, Darwin Berg, Floyd E. Bloom, Sascha du Lac, Anirvan Ghosh, and Nicholas C. Spitzer, editors, *Fundamental Neuroscience (Fourth Edition)*, pages 613–630. Academic Press, San Diego, fourth edition edition, 2013.
- [52] R. Merletti and S. Muceli. Tutorial. surface emg detection in space and time: Best practices. *Journal of Electromyography and Kinesiology*, 49:102363, 2019.
- [53] Roberto Merletti, Alberto Botter, Amedeo Troiano, Enrico Merlo, and Marco Alessandro Minetto. Technology and instrumentation for detection and conditioning of the surface electromyographic signal: State of the art. *Clinical Biomechanics*, 24(2):122–134, 2009.
- [54] Bojan Milosevic, Simone Benatti, and Elisabetta Farella. Design challenges for wearable emg applications. In *Design, Automation & Test in Europe Conference & Exhibition (DATE), 2017*, pages 1432–1437. IEEE, 2017.
- [55] Andrea Mongardi, Paolo Motto Ros, Fabio Rossi, Massimo Ruo Roch, Maurizio Martina, and Danilo Demarchi. A low-power embedded system for real-time semg based event-driven gesture recognition. In *2019 26th IEEE International Conference on Electronics, Circuits and Systems (ICECS)*, pages 65–68. IEEE, 2019.
- [56] Bethel AC Osuagwu, Emily Whicher, and Rebecca Shirley. Active proportional

- electromyogram controlled functional electrical stimulation system. *Scientific reports*, 10(1):1–15, 2020.
- [57] Andrea Prestia. Design and integration of an event-driven rehabilitation system for functional electrical stimulation, 2020.
- [58] Paolo Motto Ros, Marco Paleari, Nicolás Celadon, Alessandro Sanginario, Alberto Bonanno, Marco Crepaldi, Paolo Ariano, and Danilo Demarchi. A wireless address-event representation system for atc-based multi-channel force wireless transmission. In *5th IEEE International Workshop on Advances in Sensors and Interfaces IWASI*, pages 51–56. IEEE, 2013.
- [59] Fabio Rossi, Andrea Mongardi, Paolo Motto Ros, Massimo Ruo Roch, Maurizio Martina, and Danilo Demarchi. Tutorial: A versatile bio-inspired system for processing and transmission of muscular information. *IEEE Sensors Journal*, 2021.
- [60] Fabio Rossi, Paolo Motto Ros, Ricardo Maximiliano Rosales, and Danilo Demarchi. Embedded bio-mimetic system for functional electrical stimulation controlled by event-driven semg. *Sensors*, 20(5):1535, 2020.
- [61] Fabio Rossi, Paolo Motto Ros, Sofia Cecchini, Andrea Crema, Silvestro Micera, and Danilo Demarchi. An event-driven closed-loop system for real-time fes control. In *2019 26th IEEE International Conference on Electronics, Circuits and Systems (ICECS)*, pages 867–870. IEEE, 2019.
- [62] Fabio Rossi, Paolo Motto Ros, Stefano Sapienza, Paolo Bonato, Emilio Bizzi, and Danilo Demarchi. Wireless low energy system architecture for event-driven surface electromyography. In *International Conference on Applications in Electronics Pervading Industry, Environment and Society*, pages 179–185. Springer, 2018.
- [63] Stefano Sapienza, Marco Crepaldi, Paolo Motto Ros, Alberto Bonanno, and Danilo Demarchi. On integration and validation of a very low complexity atc uwb system for muscle force transmission. *IEEE transactions on biomedical circuits and systems*, 10(2):497–506, 2015.
- [64] Stefano Sapienza, Paolo Motto Ros, David Alejandro Fernandez Guzman, Fabio Rossi, Rossana Terracciano, Elisa Cordedda, and Danilo Demarchi. Online event-driven hand gesture recognition based on surface electromyographic signals. In *2018 IEEE international symposium on circuits and systems (IS-CAS)*, pages 1–5. IEEE, 2018.
- [65] SENIAM. Recommendations. <http://www.seniam.org/>.
- [66] Amirhossein Shahshahani, Masoud Shahshahani, Paolo Motto Ros, Alberto Bonanno, Marco Crepaldi, Maurizio Martina, Danilo Demarchi, and Guido Masera. An all-digital spike-based ultra-low-power ir-uwb dynamic average threshold crossing scheme for muscle force wireless transmission. In *2015 Design, Automation Test in Europe Conference Exhibition (DATE)*, pages 1479–1484, 2015.
- [67] Christopher Spiewak, M Islam, A Zaman, and Mohammad Habibur Rahman.

- A comprehensive study on emg feature extraction and classifiers. *Open Access Journal of Biomedical Engineering and Biosciences*, 1(1):1–10, 2018.
- [68] Didier Staudenmann, Karin Roeleveld, Dick F. Stegeman, and Jaap H. van Dieën. Methodological aspects of semg recordings for force estimation – a tutorial and review. *Journal of Electromyography and Kinesiology*, 20(3):375–387, 2010.
- [69] Mingxu Sun, Christine Smith, David Howard, Laurence Kenney, Helen Luckie, Karen Waring, Paul Taylor, Earl Merson, and Stacey Finn. Fes-upp: A flexible functional electrical stimulation system to support upper limb functional activity practice. *Frontiers in Neuroscience*, 12:449, 2018.
- [70] H Lee Sweeney and W Hammers David. Muscle contraction. *10.1101/cshperspect.a023200*, 10(2)(3), February 2018.
- [71] Vicon Motion Systems. Plug-in gait reference guide. <https://docs.vicon.com/display/Nexus211/Plug-in+Gait+Reference+Guide>.
- [72] Vicon Motion Systems. Vicon nexus user guide. <https://docs.vicon.com/display/Nexus211/Vicon+Nexus+User+Guide>.
- [73] Jacopo Tosi, Fabrizio Taffoni, Marco Santacatterina, Roberto Sannino, and Domenico Formica. Performance evaluation of bluetooth low energy: A systematic review. *Sensors*, 17(12):2898, 2017.
- [74] Hayder A Yousif, Ammar Zakaria, Norasmadi Abdul Rahim, Ahmad Faizal Bin Salleh, Mustafa Mahmood, Khudhur A Alfarhan, Latifah Munirah Kamarudin, Syed Muhammad Mamduh, Ali Majid Hasan, and Moaid K Hussain. Assessment of muscles fatigue based on surface emg signals using machine learning and statistical approaches: a review. In *IOP Conference Series: Materials Science and Engineering*, page 012010. IOP Publishing, 2019.
- [75] Yu Zhou, Yinfeng Fang, Kai Gui, Kairu Li, Dingguo Zhang, and Honghai Liu. semg bias-driven functional electrical stimulation system for upper-limb stroke rehabilitation. *IEEE Sensors Journal*, 18(16):6812–6821, 2018.
- [76] Yu Zhou, Jia Zeng, Kairu Li, Levi J Hargrove, and Honghai Liu. semg-driven functional electrical stimulation tuning via muscle force. *IEEE Transactions on Industrial Electronics*, 2020.
- [77] Tanja Zidarič, Marko Milojević, Jernej Vajda, Bostjan Vihar, and Uroš Maver. Cultured meat: Meat industry hand in hand with biomedical production methods. *Food Engineering Reviews*, 12, 12 2020.